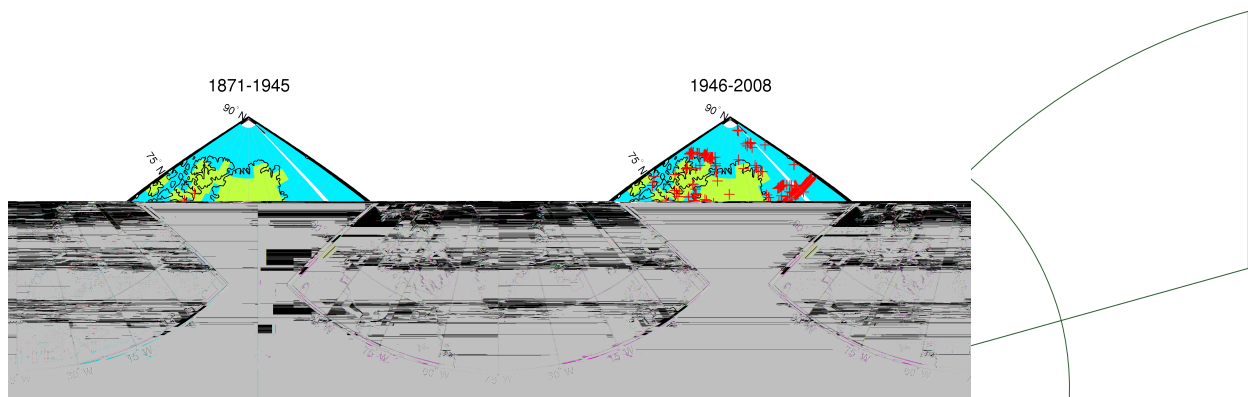




M. Sc. Thesis, August 17th, 2012

Evaluation of the 20th Century Reanalysis for the Greenland area

- using meteorological observations and ice core data



Majbritt W. Sørensen

*Centre for Ice and Climate, Niels Bohr Institute,
University of Copenhagen, Denmark*

Supervisor:

*Bo M. Vinther, Centre for Ice and Climate, Niels Bohr Institute,
University of Copenhagen, Denmark*



Preface

The following thesis marks the completion of the master's degree in geophysics, conducted in the period 2009-2012, by Majbritt W. Sørensen at Niels Bohr Institute, University of Copenhagen.

The thesis was carried out in the time frame of one year, corresponding to 60 ECTS point.

University: University of Copenhagen
Institute: Niels Bohr Institute
Department: Centre for Ice and Climate

Author: Majbritt W. Sørensen

Signature: _____

Email: majbrittws@gmail.com

Academic advisor: Bo M. Vinther

Submission date: July 27, 2012

Front page figure: Map of meteorological stations providing pressure data for the 20th Century Reanalysis Project (20CR) for the Greenland area. Land (green) and water (blue) grid cells being used within the 20CR can be seen. Red crosses denote pressure observation stations. The black circles denote the only ten stations operational up until 1921. Right: The period from 1871-1945 (period 1), left: the period from 1946-2008 (period 2).

Acknowledgement

First of all I would like to thank the Centre for Ice and Climate. It has been a great experience to be part of a science group where research as well as the social relations are put in absolute priority. Never have I heard so many interesting talks, gotten to know so many inspiring people and eaten so much cake as I have done for the past year.

A special thank must go to my supervisor, Bo M. Vinther, whose expertise within his field of research helped me develop a good understanding of the subject. He understood my way of working and gave me room to discover and explore new things on my own. He was very good at keeping the aim of the thesis on a realistic level and his wide knowledge of climate science was highly appreciated, especially during the final months of the project.

A special thank must, without doubt, be pointed at my best friend and office mate Anne W. Petersen. She helped me tremendously during the entire process of programming, analysing and writing. Especially during the end of the thesis, where she volunteered for proof-reading and gave a lot of advice and suggestions in connection to that. Also her stock of tea, liquorice and muslibars helped me through some otherwise long and hungry nights.

Jakob Wrigley, Sune Rasmussen and Aslak Grinsted were of great help when I had a MATLAB, L^AT_EX, or printer related problem, which happened not so seldom.

Also a thank to Lisbeth Nielsen who agreed to proof-read parts of the thesis, even though she had her own deadline to worry about.

Finally I will mention my father who, in his own Knud-Sørensen way, kept me focused on the task ahead and the importance of finishing on time by weekly calls from the countryside.

Thank you, everyone. I could not have done this without you!



And we're off!! [Pers. photo, 2010]

Abstract

The 20th Century Reanalysis Project (20CR) is the first project to have produced an atmospheric reanalysis covering the time period all the way back to 1871. It assimilates surface pressure observations and uses sea surface temperatures and the sea ice distribution as boundary conditions. The spatial and temporal resolution is $2^\circ \times 2^\circ$ and 6 hours, respectively.

The 20CR has been globally tested against previous reanalyses covering the post World War II era and meteorological observations, and is evaluated to perform at the same level as those previous reanalysis products. But when zooming in on the Arctic area no evaluation has been conducted specifically for this area all the way back to 1871. Thus evaluating the 20CR for the Greenland area for the entire time span will be the aim of this thesis.

A comparison between reanalysis output and observations of temperature and precipitation, in annual mean, around the coast of Greenland will be conducted along with a comparison of the accumulation at NGRIP¹ and the precipitation rate obtained from the 20CR. The accumulation at NGRIP will be obtained from six cores drilled in the years 1996-2004 (five shallow cores and one deep core). A noise level analysis will be conducted on the ice cores beforehand to discover whether or not a common signal is present. Finally the reanalysis output will be used to explain the variations measured for the isotopic composition of stable water measured in the shallow cores at NGRIP.

Problemformulering

Reanalyseprojektet, kaldet The 20th Century Reanalysis Project (20CR), er det første projekt, som har produceret en atmosfærisk reanalyse dækkende helt tilbage til 1871. Den assimilerer overfladetryk, og bruger havoverfladetemperaturer og havisudbredelse som grænsebetingelser. Den rumlige og tidlige opløsning er henholdsvis $2^\circ \times 2^\circ$ og 6 timer.

20CR er på globalt plan blevet afprøvet mod tidligere reanalyser, dækkende perioden efter anden verdenskrig, og er evalueret til at være lige så god som disse tidligere reanalyser. Men hvis man zoomer ind på det arktiske område er der ikke foretaget en lignende evaluering for hele tidsperioden tilbage til 1871. Det vil være specialets mål at opnå en sådan evaluering.

En sammenligning mellem reanalysens output og temperatur- og nedbørsobservationer vil blive udført for årsmidler fra stationer langs den grønlandske kyst. Fra fem korte kerner og en dyb kerne, boret på NGRIP i årene 1996-2004, vil akkumulationen her blive sammenlignet med nedbørsmængderne fra reanalysen. Desuden vil der blive udført en støjanalyse på kernerne, for at afdække om der findes et fælles signal i kernerne. Slutteligt vil reanalysens output blive brugt til at forklare de stabile vandisotopers variation, der er blevet målt på de korte kerner.

¹North Greenland Ice Core Project

Contents

1	Introduction	8
2	Scientific background	11
2.1	A brief introduction to reanalyses	11
2.2	The 20th Century Reanalysis Project	12
2.2.1	The production of the 20CR	12
2.2.2	Evaluation of the performance of the 20CR	12
2.2.3	Data from the Greenland area	14
2.3	Meteorological observations	15
2.3.1	Platforms for meteorological observations	15
2.3.2	Temperature observations	17
2.3.3	Precipitation observations	17
2.4	Ice core analysis	18
2.4.1	Stable isotopes	19
2.4.2	Accumulation	22
2.4.3	Noise	23
2.5	Correlation and significance	24
3	Presentation of the data used in this study	27
3.1	Meteorological data from DMI	27
3.2	Reanalysis data	29
3.3	Mathematical approach	30
3.4	Glaciological data	32
3.4.1	Stable isotope measurements - $\delta^{18}\text{O}$	32
3.4.2	Accumulation calculation	34
4	Temperature analysis - observational data from Greenland	36
4.1	Results	36
4.1.1	Comparison of the 20CR with coastal stations	36
4.1.2	Correlation tables	36
4.1.3	Large scale correlation maps	40
4.2	Discussion	42
4.2.1	Comparison of the 20CR with coastal stations	42
4.2.2	Correlation tables	43
4.2.3	Large scale correlation maps	44
4.2.4	The influence on correlations of a warming of the Arctic	45
4.3	Summary	46
5	Precipitation analysis - observational data from Greenland	47
5.1	Results	47

5.1.1	Comparison of the 20CR with coastal stations	47
5.1.2	Correlation tables	47
5.1.3	Large scale correlation maps	50
5.2	Discussion	51
5.2.1	Comparison of the 20CR with coastal stations	51
5.2.2	Correlation tables	56
5.2.3	Large scale correlation maps	57
5.3	Summary	58
6	Ice core analysis - measurements from NGRIP	59
6.1	Noise level analysis	60
6.2	Results	62
6.2.1	Comparison of the 20CR with accumulation at NGRIP	62
6.2.2	Correlation tables	63
6.2.3	Large scale correlation maps	63
6.3	Discussion	64
6.3.1	Comparison of the 20CR with accumulation at NGRIP	64
6.3.2	Correlation tables	64
6.3.3	Large scale correlation maps	65
6.4	Summary	65
7	Using the 20CR for comparison with ice core proxy data	66
7.1	Temperature vs. isotope profiles	66
7.1.1	Results	66
7.1.2	Discussion	67
7.2	Precipitation-weighted temperature vs. isotope profiles	69
7.2.1	Results	69
7.2.2	Discussion	69
7.3	Summary	71
8	Conclusion	73
9	Outlook	77
	Bibliography	78
	A Figures	85

Chapter 1

Introduction

For several decades the Arctic area has been a central theme when discussing the study of climate changes for the Northern Hemisphere. This is at least to some extent because of the extensive effort put into retrieving deep ice cores from Greenland which have provided us with information on the climatic state of the atmosphere as far back as the Eemian period¹. Retrieving ice from the Eemian has been of high priority due to the present projections for the future climate, which most likely will approach the same levels of temperature as during the Eemian, being a global temperature rise of 2-7 °C by 2100, depending on the climate scenarios chosen (Stott and Kettleborough [2002]). By extensive investigation of the natural proxies for climatic variations and the mechanisms influencing them a better understanding of the mechanisms responsible for climatic changes will be reached, hopefully leading to an increase in the accuracy of climate predictions.

An area receiving attention at present is the melting of the ice sheets. Due to the present projections for the future it is of high interest to determine the mass balance of the Antarctic and Greenland ice sheets, since a large melting of these ice sheets will result in a considerable sea level rise which may have huge impacts on the low elevation areas of the world. To determine the stability of the ice sheets for the past century or more, observations of precipitation rate, runoff, temperature and so forth are necessary to develop methods capable of modelling the mass balance. Such observations are not possible to retrieve since only very few observational stations have been operational for an adequate amount of time and the location of them is often too far from the ice sheet to be able to represent the conditions at the ice sheet. The closest one gets to actual observational data sets spanning the polar area as well as the time period desired is reanalysis data. Reanalyses are coupled atmosphere-land models creating gridded meteorological parameters of high temporal resolution (six hours) by assimilating observational data (such as surface pressure fields) and using sea surface temperatures (SST) and sea ice distribution as boundary conditions when available.

Reanalysis data can be used in the creation of surface mass balance models to determine how the stability of the ice sheets has evolved back in time, and thus to project its future development. This has been done by E. Hanna et al. [2011] where calibrated near-surface air temperatures, precipitation, run-off and surface latent heat obtained from the most recent reanalysis, the 20th Century reanalysis Project (20CR), have been combined and used in a surface mass balance model of the Greenland ice sheet. The result showed a decreasing mass balance from the mid-Twentieth Century, even accelerating for the last ten years.

Another study using reanalysis data is the investigation of precipitation-weighting of temperature observations to better explain the variations seen in the proxy parameters found in ice cores (Persson et al. [2011]). Ice core data is only recorded during snowfall, thus precipitation-weighting is a reasonable approach and here reanalysis data are highly appreciated since the

¹The previous interglacial, called the Eemian, lasted approx. from 130000 to 110000 years before present (Hvidberg et al. [2007]).

alternative will be gridded observations which lack the physical aspect keeping data sets in mutual coherence. Gridded observational data sets do not guarantee that boundary conditions and physical properties are respected but since reanalyses are coupled atmosphere-land models, this is guaranteed here.

Reanalysis data can thus be used in a variety of projects, such as assessing the sensitivity of mass balance to climate changes, for instance when coming out of the the late 19th Century cold period, correlating proxy parameters to meteorological features and to put current day extreme events in context of past weather events, for instance to discover how storm tracks and intensities have varied back in time.

The 20th Century Reanalysis Project is to date the reanalysis extending furthest back in time, e.i. back to 1871. This is possible since the only assimilation data needed is surface pressure observations, and boundary conditions are determined by observations of SST and sea ice distributions. Those data are available back to the mid 19th Century in almost continuous records for several stations. The 20CR is globally evaluated to perform at the same level of accuracy as previous reanalyses (in the time of overlap, e.i. 1948-present). However, the reliability of the 20CR may be questioned when moving far back in time due to the sparse coverage of observational data available. Especially when considering the regions far north and south where difficult accessibility and harsh climate conditions have hindered the establishment of weather stations. The aim of this thesis is to evaluate the performance of the 20CR in the area surrounding Greenland. If proven to perform well for this area the 20CR will be a valuable tool for further climate research concerning Greenland.

The approach for the evaluation will be to correlate observational records of temperature and precipitation obtained from stations along the coast of Greenland to parameter output from the 20CR. To obtain a data series from the center of the Greenland Ice Sheet shallow cores drilled at the scientific deep drill site in Greenland called The North Greenland Ice Core Project (NGRIP) will be examined. The cores have been drilled and measured during the late 1990s and early 2000s but due to a lack of dating any analyses have not been performed yet. Recently the NGRIP shallow cores have been dated and in combination with the deep core hence represent the longest available records of ice core data at present. Therefore the largest overlap with the 20CR is aquired. The accumulation at NGRIP will be determined and compared to the 20CR and finally the 20CR parameter output will be used in explaining the variations measured for the isotopic profiles from the ice cores.

The thesis is structured in the following way:

Chapter 2: gives an introduction of the 20CR, how the reanalysis was constructed and the observations used in it, including a presentation of the surface pressure data from the Greenland area. This is followed by a historical overview of the development of meteorological observational methods, particularly temperature and precipitation measuring devices, since it is those observations that will be compared to the reanalysis output in the coming chapters. Furthermore a section is dedicated to the general ice core analysis, specifically the stable isotopes and the accumulation parameter, since these data also will be compared to the reanalysis output. Finally a section describing the methods and mathematical equations used for the statistical analysis is found.

Chapter 3: The specific meteorological and glaciological data used in the thesis will be presented here. First a description of the observational data obtained from DMI, then of the reanalysis data files used, will be examined. Corrections were made to make the reanalysis data comparable to the observational data, and the mathematical approach for doing so is mentioned here as well. Then the glaciological data is presented, being the stable isotope measurements and the resulting accumulation parameter.

Chapter 4: Now the comparison between observational temperature data along the coast of Greenland and the temperature obtained from the 20CR will be carried out. The results will be presented, followed by a discussion. It will be examined how the warming of the

Arctic observed for the 1980s and forward is affecting the correlation between the 20CR and observations.

Chapter 5: The precipitation data from the meteorological stations at the coast will also be correlated to the 20CR output in a similar way as for the temperature analysis.

Chapter 6: From the shallow cores drilled at NGRIP the isotopic profiles and hence the accumulation parameters can be extracted. The accumulation rate is a direct parameter and can thus be compared to the precipitation rate obtained from the 20CR. This is done here. A noise level analysis is conducted on the cores beforehand.

Chapter 7: As a further step the reanalysis parameter output is now being used in order to better understand the variations seen for the stable isotope profiles. A comparison between the proxy parameter $\delta^{18}\text{O}$ and the 2 m temperatures from the 20CR is being conducted. To improve the resultant correlations it is tested whether or not a precipitation-weighting of the temperatures from the 20CR will make a difference.

Chapter 8+9: Finally a conclusion and an outlook where recommendations for improvements of the 20CR and suggestions for possible directions of future research will be reviewed.

Chapter 2

Scientific background

In the following chapter I will describe the most commonly used reanalyses, and the 20th Century Reanalysis specifically. Hereafter I will account for the methods to obtain observational data to validate the reanalyses, primarily temperature and precipitation, and then I will present the ice core analysis process, focusing on measurements of stable water isotopes and accumulation. Finally the theory of correlation and significance will be examined.

2.1 A brief introduction to reanalyses

In order to understand the climatic changes that are currently happening and to relate the occurring events to previous incidences, long-term climatic data sets are necessary. Therefore the development of retrospective analyses, or reanalyses, to create such continuous and long-term data sets has been rapid over the last few decades.

The first steps on constructing a reanalysis, were done manually by Brandes in 1819. He produced 365 daily maps of pressure contours only by using barometric pressure observations from multiple European stations taken in 1783 (Compo et al. [2011]). Since then many attempts to develop an automatic reanalysis have been made, most commonly known are perhaps the NNR (The National Center for Atmospheric Research, NCAR, and The National Center for Environmental Prediction, NCEP, have collaborated in developing a reanalysis) and ERA-40 (European Centre for Medium-Range Weather Forecasts, ECMWF, has made a reanalysis ranging 40 years) reanalyses. Both reanalyses mentioned use an assimilation model to handle the input of observational data, such as surface pressure and temperature, wind speed and humidity. The models then use the large amount of data to obtain gridded data sets of a resolution of T159 (ERA-40) and T62 (NNR), which correspond to a grid cell length of $\sim 1.125^\circ \times 1.125^\circ$ and $\sim 2.81^\circ \times 2.81^\circ$, respectively [(Kistler et al. [2001]), (Uppala et al. [2005]), (2011a)]. An output of several parameters is obtained for 60 levels in the vertical for ERA-40 and 28 for NNR every 6 hours. The sea surface temperatures (SST) and sea-ice distribution was used as boundary conditions and forcing fields for ERA-40, along with a fixed geographical distribution of aerosol and a climatological ozone distribution (Uppala et al. [2005]). Besides SST and sea-ice cover the albedo, snow-cover, roughness length, soil wetness and vegetation resistance is used as boundary fields for NNR (Kalnay et al. [1996]). For both reanalyses, and any previous reanalyses not mentioned here, the period of coverage does not extend more than 60 years back at a maximum. The NNR is running from 1948-present while the ERA-40 covers the period from 1957-2002 (Compo et al. [2011]). A reanalysis covering a longer period would aid climate scientists in many cases, such as when comparing observational or proxy data to reanalysis output to discover how different data sets configure to each other.

2.2 The 20th Century Reanalysis Project

The most recent developed reanalysis is called the 20th Century Reanalysis Project (20CR) and is developed in an international collaboration of scientists and institutions from all over the globe, such as NOAA¹, MétéoFrance, Environment Canada, South African Weather Service, NCAR and CIRES² (Compo et al. [2011]). As an improvement to the earlier reanalyses it spans a period as far back as 1871-present at a temporal resolution of 6 hours and a spatial resolution of $2^\circ \times 2^\circ$. It uses monthly observed sea-ice distributions and SSTs as boundary conditions and newly compiled surface and sea level pressure (SLP) reports and observations as assimilation data, to produce the reanalysis data set. It produces a large variety of parameters such as surface temperature, precipitation, relative and specific humidity, geopotential heights and zonal and meridional wind in 24 pressure levels.

2.2.1 The production of the 20CR

A preliminary first version of the 20CR was computed in 2008. It spanned the period 1908 to 1958 and was done as a small scale test of the reanalysis. The second version completed the intended idea of a reanalysis spanning the period 1871-present. This is the final version referred to as 20CR.

The coupled atmosphere-land model used for calculating the 20CR data set is the April 2008 experimental version of the NCEP Global Forecast System (GFS). The SST and sea-ice fields were obtained from the UK Met Office HadISST1.1 dataset (Rayner et al. [2003]) and monthly mean data were interpolated to daily resolution. The pressure data were taken from the International Surface Pressure Databank (ISPD), (2012f), which is a collection of pressure observations obtained from national and international archives throughout the entire globe. It has been established through extensive international cooperation under the direction of the Atmospheric Circulation Reconstructions over the Earth (ACRE) (Compo et al. [2011]). The data assimilation method used with the surface observations is called the Ensemble Kalman filter. It is an algorithm which uses a series of measurements observed over time (containing noise and other inaccuracies) to produce a model estimate that tend to be more precise than an estimate based on any single measurement. The filter is named after Rudolf E. Kalman, one of the primary developers of its theory. For further details concerning the mathematical method used, see (Compo et al. [2011]), (Compo et al. [2008]) or (Compo et al. [2006]).

The 20CR was produced using a large number of different servers. This made the computation of the data set very fast since the calculations could then run in parallel modes. The entire period, 1871-present, was split into 5-year intervals which each had a spin-up period of 14 months. The same first-guess field was used for every 5-year period but the spin-up period made sure the observations and not the first-guess field was controlling the reanalysis output. The end of each period has been compared to the beginning of the following one, and the difference here was assessed to be negligible (Compo et al. [2011]). The 20CR will continuously get updated as new observation data are being available throughout the globe.

2.2.2 Evaluation of the performance of the 20CR

To determine the quality of the 20CR different approaches can be used. G.Compo et al. [2011] primarily compared the 20CR with the previously used reanalysis, ERA-40, which is highly trusted. Also comparisons with pressure observations in several height levels are evaluated by G.Compo et al. as a validation test of the reanalysis.

To investigate if the uncertainty of the 20CR is varying as expected and to show how much

¹National Oceanic and Atmospheric Administration, Asheville USA

²Cooperative Institute for Research in Environmental Sciences, Boulder USA

the reanalysis improves with rising numbers of observations, a plot of the first-guess root-mean-square (r.m.s.) difference from pressure observations (blue) vs. the expected r.m.s. difference (red) is seen in fig. 2.1, alongside the average number of observations from 1871 to 2008 (black). It is obvious how the number of observations heavily affects the error on the

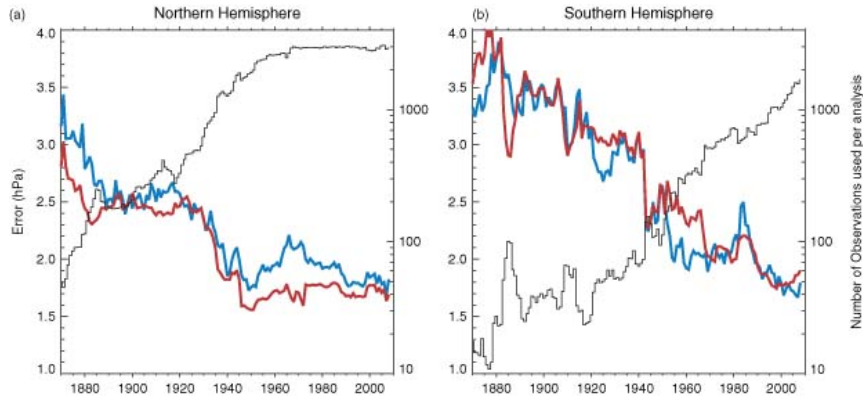


Figure 2.1: Time series of the 6-hourly first-guess r.m.s. difference from pressure observations (blue) and expected r.m.s. difference (red) calculated over individual years from 1870 to 2008 for the extratropical (a) Northern Hemisphere ($20^{\circ} \text{N} - 90^{\circ} \text{N}$) and (b) Southern Hemisphere ($20^{\circ} \text{S} - 90^{\circ} \text{S}$). The square root is calculated on the annual mean square values. The thin black curve shows the average number of pressure observations for each analysis in the indicated year (note the logarithmic scale) (figure from Compo et al. [2011]).

model. It is also interesting to see the boom in observations happening in the 1920s-1970s, especially in the Northern Hemisphere. The Southern Hemisphere lags behind in observational coverage but after the introduction of weather satellites during the 1960s (Uppala et al. [2005]) the number of observations is today at the same order of magnitude for the two hemispheres.

To determine the quality of the 20CR, a global assessment of the upper-air fields (in form of the geopotential heights) can be compared with other reanalyses which use upper-air observations as input such as ERA-40 (Uppala et al. [2005]) and NNR (Kalnay et al. [1996]). This was done by G. Compo et al. [2011] and the result indicated that the 20CR was in general of a very high standard throughout the entire period and especially when considering pressure field calculations. The 300 hPa geopotential height anomalies are a nice example of the high correlation obtained for the 20CR and ERA-40/NNR. Here the correlation of subdaily anomalies for the region poleward of approx. 20°N was everywhere higher than 0.9 for the period 1958-1978. The same was the case for the period 1979-2001 but now the Southern Hemisphere also showed correlations of more than 0.9 between $30^{\circ} \text{S} - 60^{\circ} \text{S}$.

The reanalysis was also capable of capturing meteorological features which have a strong SLP and SST forcing, such as the NAO index (Compo et al. [2011]). Also when considering the zonal mean precipitation rate averaged over 1980-2000, the 20CR was capable of capturing the rate quite precisely for the entire latitudinal span.

In general reanalyses tend to overestimate the precipitation rate at coastal areas and underestimate the precipitation rate inland (Hanna et al. [2006]), and for ECMWF-based models (ERA-40, for instance) especially the interior plateau of Greenland is too dry whilst the southern part is too wet. Whether or not this is the case for the 20CR as well, was not answered by G. Compo et al. [2011].

It is clear that the quality of the 20CR is highly dependent on the amount of pressure observations available, and ACRE and its partners estimate that millions of additional data from the nineteenth and early twentieth century is just waiting to be digitised and used in projects such as the 20CR.

2.2.3 Data from the Greenland area

Observations for the Northern Hemisphere is at present carried out in large numbers and have been so many decades back, as seen in fig. 2.1. But data from observation stations located in the Greenland area have not been available for the 20CR throughout all years back to 1871 (2012f) and this may be a problem affecting the output calculated from the 20CR. Analogous to fig. 2.1 I have produced a plot showing the station count for the Greenland area, here defined as 54°N - 90°N and 100°W - 10°E (fig. 2.2). Information of pressure stations used for the 20CR was retrieved (2012f) and from here an extract of the Greenland area was plotted. The pressure data set used for the 20CR is presented as a large combination of data sets originating from several different sources. Hence the count shown do not take into account when a station has changed name or is delivering several identical observations from different instruments. Therefore the number count is somewhat optimistic. However, it is seen that only ten stations are delivering pressure data up until 1921. Hereafter the number of observations increases significantly.

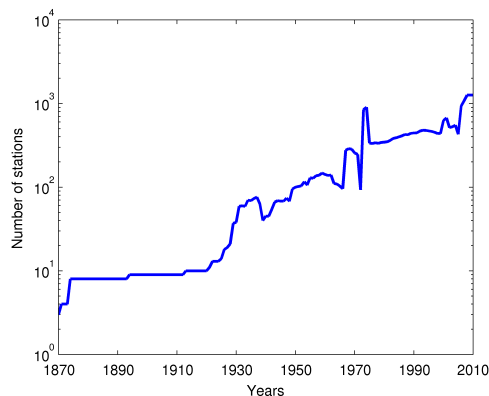


Figure 2.2: The blue curve shows the average number of pressure observations used within the 20CR in the indicated year (note the logarithmic scale).

The spatial distribution of the pressure data may be interesting, hence as seen on fig. 2.3 the locations of the stations providing pressure assimilation data are seen. The only ten stations providing data until 1921 is seen as black dots and the remaining stations are denoted by a red cross. The period from 1871 (one station in England delivered data from 1833, the subsequent observations began in 1868 or later) to 1945 was only represented by approx. 100 stations, none of which was located on the west side of Greenland until 1922 but as seen the number of stations and the spatial distribution of those have increased highly, especially for the European area (fig. 2.3 (right)). The 20CR is thus expected not to perform perfectly for the Greenland area since the assimilation data needed for the 20CR to keep touch with actual observation values is nonexistent for a large period of time where the 20CR is producing parameter output.

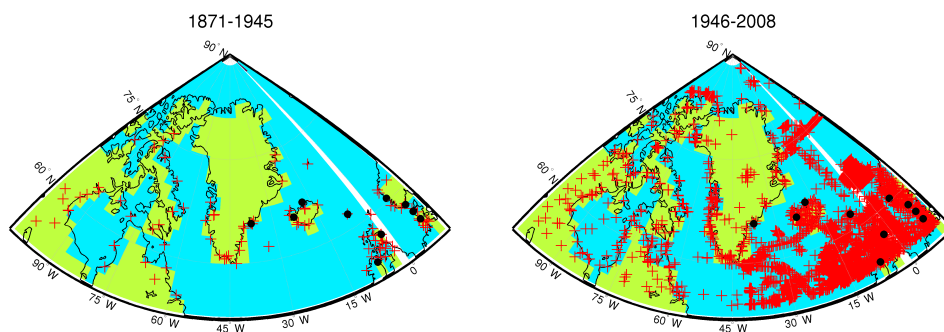


Figure 2.3: The spatial distribution of the pressure data used within the 20CR. Stations providing data prior to 1921 is denoted with black circles, the remaining stations is seen as red crosses. Left: The total number of stations for the period 1871-1945. Right: The total number of stations for the period 1946-2008

2.3 Meteorological observations

The boundary conditions and assimilation data used within the 20CR originates from meteorological observations of pressure and temperature done at the surface level. The meteorological state of the atmosphere have been observed and recorded since the invention of the thermometer in the middle of the sixteenth century. But the earliest temperature measurements are difficult to compare to modern scales due to the varying use of liquids (water, ethanol, other liquids which changes with temperature), fixpoints (body temperature, minimum temperature of Danzig in 1709, boiling and freezing points of water) and changing environment from measurement to measurement. Eventually the preferred temperature indicator became mercury and the tube containing it was sealed off from the surrounding atmosphere thus being independent of the atmospheric pressure. The fixpoint was chosen to be the boiling (100°C or 212°F) and freezing (0°C or 32°F) point of water after the Swedish astronomer Anders Celcius, albeit his denotation was the opposite (Strangeways [1999]).

In Denmark the first systematic temperature observations began in 1751 when P. Horrebow initiated three times daily observations at Rundetaarn, Copenhagen and for the next more than hundred years this was the only official meteorological station in Denmark (Closter et al. [2006]). During the 1870s a number of stations both in Denmark, Faroe Island and Greenland were established and several parameters such as temperature and precipitation were measured continuously (Cappelen [2011]).

In addition to the stationary meteorological stations measurements were also conducted from merchant vessels and during expeditions, and can be found in log books and diaries of the expedition members. Other historical documents contain more vague information of rivers freezing and lost harvest. Though such data are subjectively determined and biased when comparing to modern data, it is still a way of obtaining observed meteorological data or indications of climate changes far back in time (Jørgensen and Cappelen [2007]).

Over time the development of measuring devices have been rapid and the accuracy of the measured parameters have been enlarged significantly. Now the atmospheric condition is measured from almost every location and elevation, and the distribution of stations is covering the entire globe, both at land and sea. Below the most common measuring platforms are described, followed by a description of the measuring instruments and difficulties encountered when measuring temperature and precipitation.

2.3.1 Platforms for meteorological observations

Back in time collection of continuous meteorological data was a time consuming project and stations needed to be constantly manned. The measurements were only done at surface levels and thus both automatic methods as well as measurements from many layers of the atmosphere was the natural next step for the meteorological development:

Radiosondes

The first usable measurements of the atmosphere away from the surface of the Earth were done late in the nineteenth century where recording instruments were strapped to balloons or kites and were able to ascend and descend through the troposphere recording temperature, pressure, humidity and wind speed on a circular paper disc (Brettle and Galvin [2003]). By the 1920s the radiosondes were able to transmit the measurements using short-waved radio signals and after the Second World War the development of telemetry had become both inexpensive and light-weight and thus the amount of regular soundings of the atmosphere rose exponentially (Brettle and Galvin [2003]).

Today more than 800 sites all over the globe are launching radiosondes at a minimum of two times daily. The data are being collected and shared world wide to be used as input for weather-prediction models, air pollution models, to aid climate research, to support satellite

data and to assimilate observations for reanalyses (2009a). The launch and maintenance of radiosondes require a lot of manning and steps are being taken towards automatically preparing and launching the sondes but at present most radiosondes are being handled manually. In fig. 2.4 (left) a radiosonde is being launched.

Automatic weather stations - AWS

Due to the time consuming effort needed to operate a manual weather station the development of automatic weather stations have been of high priority. The first AWS was set up during the 1960s with the development of data loggers and telemetry (Strangeways [2003a]). This made it possible to record observations in remote areas of the Earth. AWS are capable of measuring many parameters, the most important being temperature, pressure, humidity and wind. But also solar radiation, precipitation and snow height (depending on station location) are measurable parameters. The AWS need power to conduct measurements and log them, thus solar panels are installed to provide the needed electricity. In fig. 2.4 (middle) an automatic weather station is seen.

AWS can be placed at land but also at sea, as bouys or onboard ships. The AWS for bouys measure almost the same parameters as on land, except radiation and precipitation. Instead the sea surface temperature (1 m below waterline) and wave height are being recorded (Strangeways [2003a]). The amount of AWS has increased significantly and today more than 37,000 daily observations are made and supplied for reanalyses data assimilations (Uppala et al. [2005]).

Weather satellites

Today the atmospheric condition of the Earth is mainly observed from satellite based platforms. Primarily two types are used for weather observations, the geostationary satellites and the polar-orbiting ones. The geostationary orbiting plane is coinciding with equator at an orbital distance of 35,790 km (Strangeways [2005]). The advantage of using geostationary satellites is that the satellite is situated above the exact same spot of the Earth at all times and thus the development of weather systems can be tracked continuously. The disadvantage is that the resolution of the satellite track is lower than what can be obtained from other satellite types due to the large distance from Earth and the polar regions are poorly covered due to the low angle of projection. Hence the polar-orbiting satellites are introduced; here the altitude can have any value but normally they are situated 800-900 km from Earth. This gives an orbital period of approx. 100 minutes and the poles are visited 14 times a day (Strangeways [2005]). Unlike the geostationary orbit, the polar orbit allows complete Earth coverage as the Earth turns beneath it. If several satellites are put in the same orbit but some distance apart, the temporal resolution for the polar satellites can be improved. Today each location of the polar area is scanned every sixth hour (2011c).

The satellites use radiometers to measure the Earth's atmosphere. They detect within the electromagnetic spectrum from microwave to ultraviolet radiation and from this a wide range of information can be obtained from the measurements such as sea surface temperature, humidity profiles, cloud height and cover, wind direction and velocity, snow cover, sea ice distribution (used in reanalyses) and so on, all obtained by measuring the radiance in various wavelength bands (Brugge and Stuttard [2003]).

The use of satellite data is extensive. From the launch of the first successful weather satellite in 1960 the amount of data measurements being used every day have gone from zero to more than 180,000 (Uppala et al. [2005]).

Many countries have launched weather satellites, such as USA, Japan and Russia, and also Europe has contributed with the development of project Meteosat. A drawing of the satellite can be seen in fig. 2.4 (right). The latest launch of a European weather satellite happened July 5 2012 and when successfully operating it will be called Meteosat-10 (2012e).

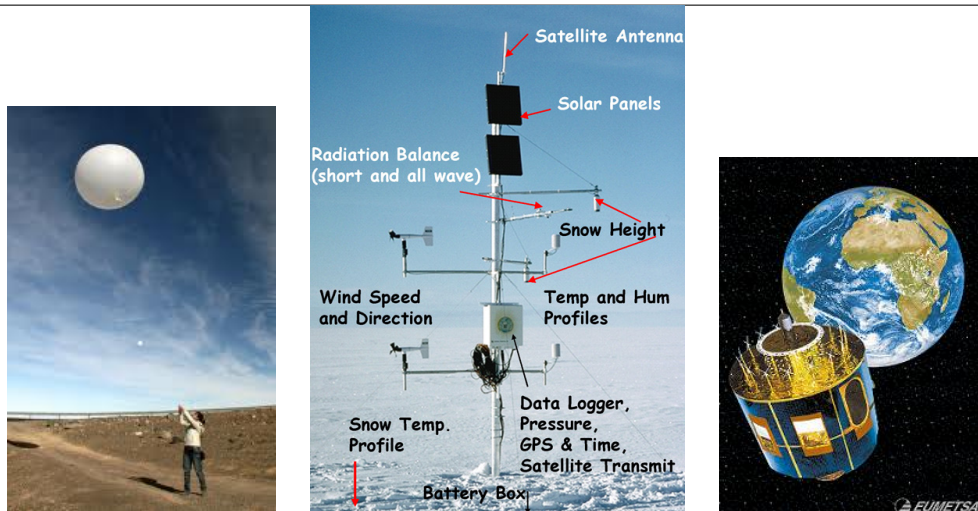


Figure 2.4: The most widely used observational platforms of today. Left: Radiosonde being launched (2012d), Middle: AWS with indication of instruments (2011b) and right: Meteosat weather satellite (2005c).

2.3.2 Temperature observations

Observations of the temperature have been carried out for many decades, as earlier mentioned. But due to the lack of standardised observation conditions data sets from different sites can be difficult to compare. For instance was the thermometer situated inside a small room at the top of the tower for the first 16 years of observation at Rundetaarn in Copenhagen. Subsequently it was moved outside which made comparison with the older data impossible. Today standardised conditions have been defined by the World Meteorological Organization (WMO) and include the thermometer being situated at an altitude of 1.25-2 m above ground level inside a well-ventilated wooden box, called a Stevenson screen. The observation should be done quickly to avoid direct solar radiation and body heat to influence the temperature, and preferable it should be taken continuously every 3 hours (Strangeways [1999]). Apart from the thermometers using liquids as indicator, also electrical thermometers are used, primarily at AWS. Here the electrical resistance change with temperature and thus various metals, mostly platinum and nickel, can be used as thermometers (Strangeways [2003a]).

When measuring temperature (or any other meteorological parameter) a variety of circumstances can affect the measurements and must be taken into consideration when interpreting the temperature profiles. Such circumstances could be either **apparent**; station relocation, change in observing times, changes in averaging methods, changes in design or colour of the screens, replacement of instruments, or **real**; urbanisation or vegetation changes surrounding the station, albedo changes, changes in atmospheric circulation, changes in atmospheric transparency, such as CO₂ or aerosols, changes in solar forcing and so forth (Frich et al. [1996]). The apparent factors contribute to the noise of the measurements which may mask an actual change in climate and therefore it is critical to keep any induced noise as low as possible. Therefore the standards for temperature measurements must be complied with at every station all over the world.

2.3.3 Precipitation observations

Precipitation rate is a very difficult parameter to obtain due to the chaotic behavior of rain and snow when falling. It is, however, possible to measure precipitation fairly reliably by the

use of rain gauges. The most commonly used is the tipping-bucket rain gauge (Strangeways [2003b]) that collects precipitation, and when full it tips and is ready for the next filling. The number of tips is then logged. There are several sources of error for this kind of gauge, for instance is the water stuck on the side of the bucket between each tip not accounted for, and neither is the amount of rain left in the bucket after a rainfall. Another gauge used is the weighing gauge. Here the precipitation is being collected in a large container and the weight is gradually measured. But here the water may evaporate over time causing noise. Instead of a weighing gauge, a capacitance gauge can be used. The principle is the same but instead of weighing the container the capacitance can be measured using the water as a dielectric. From here the amount of water can be deduced. Another approach is to use an optical gauge where raindrops and snowflakes are being detected by their effect on a horizontal beam of infrared light. This is, however, a very expensive method that needs large amounts of electricity to keep condensation away from the beam head (Strangeways [2003b]). For AWS at buoys, in addition to the mentioned gauges, attempts have been made to use hydrophones to record the sound generated by precipitation at sea but unfortunately not yet successful (Quartly et al. [2002]). Any truly reliable instrument for recording precipitation is yet to be invented. When measuring precipitation in the form of snow the same gauges mentioned above can be used, however with a larger uncertainty due to the fact that snow, because of its low density, is more affected by local wind conditions and the surrounding environment and may thus blow off the gauge before measurement. Snow is also capable of clustering together under certain conditions which can make measurements by rain gauges impossible. A nice example of this is seen in fig. 2.5.



Figure 2.5: Rain gauge with clustered snow blocking the top.

2.4 Ice core analysis

Since the completion of the first deep drilled ice core at Camp Century in Greenland in 1966 it has been evident that ice cores are capable of containing large amounts of information concerning past climatic conditions (2012b). Both temperature, precipitation amounts, atmospheric content of CO_2 , CH_4 , dust and so forth, and many other parameters can be inferred from ice core data. But to obtain the valuable parameters a huge analysing and measuring project must be completed.

As the core has been pulled up from the depth it is logged, that is the length is measured and the core is being divided into pieces of 1.65 m in length, called a "run". Hereafter the full core is being analysed, first a dielectric profile (DEP) is recorded, then the core is cut vertically in half and an electric conductivity measurement (ECM) is conducted on one of the half pieces. A line scanning is carried out on the other half of the core, whereafter the core pieces are being cut horizontally into three parts (bags) of 55 cm each. The bags are subsequently cut into several parts as illustrated in fig. 2.6. The upper part being analyzed in order to obtain information on the physical properties (crystal size, shape and so forth) and another part is used for gas measurements. A third part is used for the continuous flow analysis (CFA) and finally the stable water isotopes are being measured from

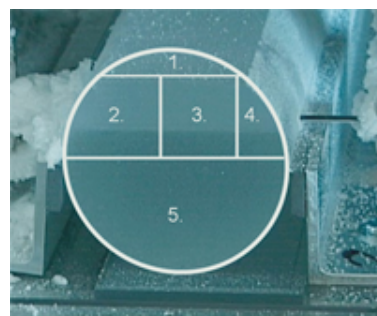


Figure 2.6: Cutting plan for the NGRIP deep drill ice core: 1; physical properties of the ice, 2; gas content of the ice, 3; CFA (impurities), 4; isotopic composition, 5; ECM and storage (2012b).

another small part of the core. The remaining section of the core is being stored for later use (2012b).

The measurements analysed for this thesis are the stable water isotope values. Based on the annual cycle of the isotopes the annual accumulation can be derived also.

2.4.1 Stable isotopes

The inland ice is build up by many thousand years of snowfall. The snow is compressed by the subsequent snowfall and eventually the density has increased until reaching $917 \frac{kg}{m^3}$ being the density of solid ice (2012b). From this point on the annual layers get thinner due to ice flow stretching the layers, an illustration of this is seen in fig. 2.7. But how is it possible to distinguish one year of snowfall from the other? The answer lies within the isotopic composition of the stable isotopes of water.

When water, H_2O , evaporates from the ocean several hundreds to thousands of kilometers from Greenland [(Johnsen et al. [1989]), (Charles et al. [1994])] a journey begins for the water in which it gets lifted and transported via the atmospheric wind patterns and ends up as precipitating snow at the Greenland inland ice. During the transport the water is

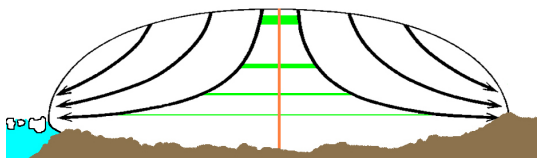


Figure 2.7: Ice flow of an ice sheet. Arrows indicate the flow direction, green layers indicate an annual accumulation year that gets compressed due to overlying weight and stretched due to the flow of the ice (2012b).

affected by temperature and pressure changes which influences the isotopic composition of the water along the path of transport. The most abundant isotopes in natural water are ^{16}O , ^{18}O , H and D; in the forms of $H_2^{16}O$, $H_2^{18}O$ and $HD^{16}O$. The ratios of these isotopic compositions in the present ocean water are 0.9977:0.0020:0.0003, respectively (Johnsen [1986]). The ^{16}O isotope is lighter than the ^{18}O , which constitutes of two extra neutrons compared to

^{16}O . The same is the case for D, which carries an extra neutron than the H. From here on the heavy isotopes correspond to ^{18}O or D.

A standard approach when measuring the isotopic composition of a water sample is to measure the ratio of the heavy isotope to the lighter one with a mass spectrometer, that is

$$R_i = \begin{cases} \frac{[^{18}O]}{[^{16}O]} = \frac{[H_2^{18}O]}{[H_2^{16}O]} & \text{for } i = ^{18}O \\ \frac{[D]}{[H]} = 2 \cdot \frac{[HDO]}{[H_2O]} & \text{for } i = D \end{cases}$$

Since it is more precise to obtain relative values, compared to absolute ones, a sample is always measured as the deviation from the ratio of a standard, usually the Standard Mean Ocean Water, *SMOW*. The parameter one obtains is the δ value of a given isotope:

$$\delta_i = \frac{R_{i_{sa}} - R_{i_{SMOW}}}{R_{i_{SMOW}}} = \frac{R_{i_{sa}}}{R_{i_{SMOW}}} - 1$$

Here the i subscript refers to the heavy isotope, *sa* stands for sample and *SMOW* is the standard used.

Since the lighter isotopes have a higher vapour pressure than the heavier components, they evaporate and condensate more rapidly than the heavy ones (Paterson [1994]). Hence there will be a lower amount of heavy isotopes in the evaporated water cell compared to the ocean. The δ value in the present ocean are zero or quite close to that. It is not exactly zero since this requires the isotopic ratio of the ocean to be the same as the standard value, and that is practically impossible since the surface layer of the ocean is constantly changing δ value due to evaporation, mixing and precipitation or other water input to the ocean. As the water evaporates from the ocean surface a fractionation in heavy and light isotopes occur and the δ value for the evaporated water will be negative, perhaps around -10 ‰ for O^{18} just above

the ocean surface. As the air mass moves north it gets cooled down and the vapour starts to condensate. The heavy isotopes condensate out first and therefore the precipitation will gradually become more and more negative. When reaching Greenland the precipitation will have values around -30 to -40 ‰ depending on site, elevation and season.

Dansgaard et al. [1973] determined that the most dominating factor of the δ values is the temperature difference from the main source area to the deposition site. That is, the amount of cooling affecting the air mass during the transport. Since the sea surface temperatures are much more stable than the air temperatures, the δ values are highly dependent on the temperature at deposition site (Paterson [1994]). For that reason the δ values follow an an-

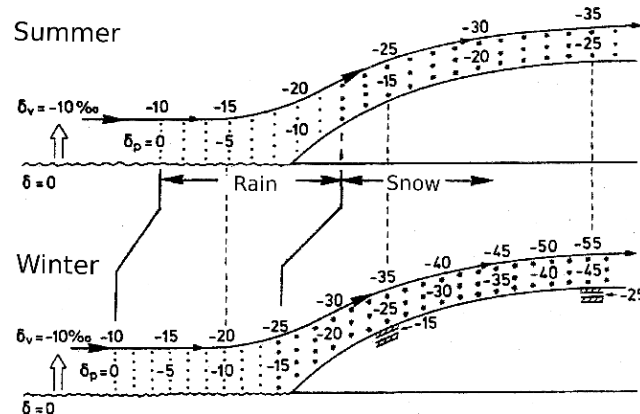


Figure 2.8: Simplified model depicting the fractionation of the isotopic composition of water (Dansgaard et al. [1973]). Top: The water evaporates from the ocean surface and is transported north. The heavy isotopes are continuously removed by rainfall causing the δ values of the precipitation to drop. When reaching Greenland the snow will have a δ value of -25‰ (hypothetically). Bottom: The same transport path but occurring in winter. Due to the lower temperature of the atmosphere the water vapour condensate out at an earlier point and the δ values will thus become more negative before reaching Greenland.

nual cycle due to the annual cycle of site temperature, which is sketched in fig. 2.8. Since the summer temperatures at deposition site are higher than the winter temperatures, the isotopic profiles of the ice will follow a sinusoidal curve where it is possible to determine the summer maximum and winter minimum. This profile is often used for dating the core along with other annually cycled profiles (eg. Ca^{2+} , Na^{+} and other chemical impurities) (Rasmussen et al. [2006]). In fig. 2.9 the $\delta^{18}\text{O}$ cycle from a shallow core drilled at NGRIP can be seen. The data is raw $\delta^{18}\text{O}$ data from the core called NG97S2 (details on the shallow cores are found in sec. 3.4). The annual cycle is seen and the annual layer thickness is about 0.5 m for the top part of the ice core. When moving down the annual cycle get smoothed out and the layer thickness decreases (see sec. 3.4.1).

There are several mechanisms influencing the isotopic composition of the precipitation, both during evaporation from source area, transport and precipitation at site. Those have to be taken into account when interpreting isotope data:

The source region temperature influences the isotopes, since a simultaneous rise of temperature at both source and deposition site will give a smaller variation in δ values than if only the site temperature rose. Additionally, if the strength of the evaporation increases (for instance at nearby ocean areas) compared to precipitation then the δ values increase. This is mostly relevant for coastal areas. The isotopic composition of the source will of course also have an impact on the δ values in the ice cores but mostly on a very long time scale (glacial -

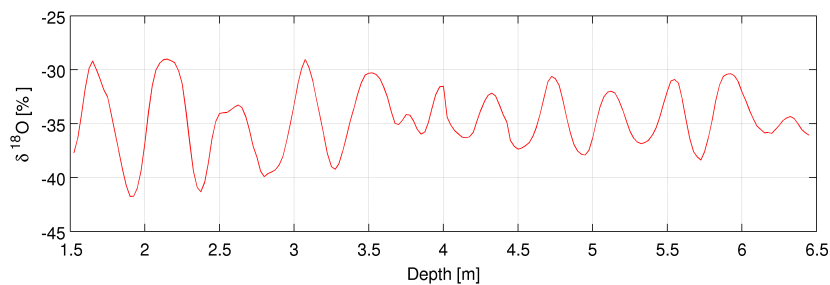


Figure 2.9: Raw $\delta^{18}\text{O}$ cycle from the top of an ice core at NGRIP (core name: NG97S2) [present study].

interglacial) will it be possible to detect any changes (Ruddiman [2008]).

During transport the evaporated water is affected by the properties within the cloud, such as the degree of supersaturation of water vapour and whether the vapour condensate into liquid droplets or ice crystals (Cuffey and Paterson [2010]). Also the attributes of the cyclones transporting the water vapour from the ocean surface up and into the higher atmospheric levels and ultimately to the deposition site in Greenland might affect the isotopic fractionation significantly if patterns or mixing of air masses change. These changes are also only relevant for large climate changes, such as glacial vs. interglacial changes.

Finally the conditions during the precipitation events and physical changes at the deposition site may disturb the perception of the isotopic profiles. The largest problem when using δ values as a proxy parameter is the fact that the temperature is only being recorded when a snow fall occurs. This means that the coldest temperature is uncaptured since it requires a clear sky in wintertime, whereas the warmer temperatures are heavily represented and thus contribute to rise the annual δ values which makes the impression that the temperature at deposition site is higher than reality (Cuffey and Paterson [2010]). This can be taken into account by precipitation-weighting the temperature profiles when comparing temperature observations and isotope profiles (this is described in sec. 7.2). Another problem in connection with the seasonal timing of the precipitation events is the fact that for most of Greenland the precipitation typically occur during warm weather. If this has changed at some point, the δ values will also shift, which then can be confused with a shift in temperature rather than changing precipitation patterns. The same confusion may occur for elevation changes of the ice sheet. If the height of the ice sheet diminish the δ values will rise due to the natural lapse rate of the atmosphere ($\sim -0.6 \frac{\text{‰}}{100 \text{ m}}$ for Northern Greenland (Ambach et al. [1968])) and not due to a climatic change of the atmosphere (Paterson [1994]). The flow of the ice is also important to take into account before interpretation, since with increasing ice core depths the ice originates further inland and at progressively higher elevations (Paterson [1994]). This is solved by drilling at the ice divide where the flow is only vertical (see fig. 2.7). If the ice divide had moved back in time, this would then influence the record. Postdepositional alterations may also affect the isotopes since the snow is in contact with the atmosphere through pore channels as far down as 70 m (Schwander et al. [1993]) or more, and thus sublimation and condensation may occur which will alter the mean isotopic value. Diffusion within the ice core is also an effect which creates noise in the profile and smoothes out the true signal. This can be corrected for by back-diffusion of the measurements (Johnsen [1977]). As a final contributor to disturbing the simple picture of a linear δ -temperature relation is the cloud vs. ground temperature. Since the snow is formed within the clouds it is in reality the temperature at formation that is recorded in the precipitation and not the surface temperature (Cuffey and Paterson [2010]). Due to the temperature lapse rate this is typically the same as ground temperature, shifted some constant positive value, but occasionally inversion layers flip the image and the surface gets colder than at cloud level. This should not be a problem on longer time scales since the inversion layers do not tend to persist for significant periods of time. However it may be the case for climatic conditions other than for the Holocene

[(Ruddiman [2008]), (Paterson [1994]), (Cuffey and Paterson [2010])].

Despite all of the contributing factors the first order linear relationship between δ value and site temperature is found to be [(Dansgaard and Johnsen [1964]), (Johnsen et al. [1989])]

$$\delta^{18}O = 0.67T - 13.7\text{‰}$$

for the present day Greenland climate, which explains a large portion of the observed Greenland $\delta^{18}O$ signal but due to the reasons mentioned above the relation can not be assumed to hold for different climatic conditions and different ice sheet configurations (Vinther et al. [2009]).

2.4.2 Accumulation

The accumulation at Greenland is a very difficult parameter to measure since snow is an elusive medium. At one point one year the annual accumulation may be $20 \frac{cm_{ieq}}{yr}$ ³ and 10 meters away it may be only $10 \frac{cm_{ieq}}{yr}$ due to snow being moved by wind after deposition and settling in small surface irregularities. These undulations that occur on the surface of the ice are called sastrugi formations and are part of the reason why noise in ice cores are relatively high (see sec. 6.1). The accumulation, or annual layer thickness, can be done on the site of interest. A sequence of years measured by pit studies or ground-penetrating radar (defined by the δ_i seasonal cycle) are measured and corrected for density changes and a mean is obtained. For NGRIP the present day annual accumulation is found to be $0.186 \pm 0.01 \frac{m_{ieq}}{yr}$ according to D. Steinhage [2005], $0.19 \frac{m_{ieq}}{yr}$ according to D. Dahl-Jensen [1997], and $0.193 \frac{m_{ieq}}{yr}$ according to the present study (see sec. 3.4.2). The numbers are supported by a comprehensive study done by A. Ohmura and N. Reeh [1991], followed up by an updated study by R. Bales and others [2009], where the precipitation and accumulation for the entire Greenland has been measured from both meteorological stations along the coast and glaciological pit studies from the inland ice. The result from the latest paper can be seen in fig. 2.10. When referring to precipitation it is the total amount of rain/snow which precipitate on to the ground, (P). Accumulation, however, is the precipitation minus any evaporation, sublimation or drifting which may occur after deposition, (P-E). But when measuring the accumulation at one place, it is virtually always higher than the precipitation measured the same place, even though drifting and evaporation loss would cause accumulation to be smaller. The main reason for this is the difficulties in capturing snowflakes when measuring the precipitation. In fact the meteorological accumulation is on average 17% smaller than the glaciological precipitation (Ohmura and Reeh [1991]). Therefore an uncertainty of 20% must be assumed when considering any precipitation data.

A change in annual layer thickness, λ , could be a result of changing temperatures since warm

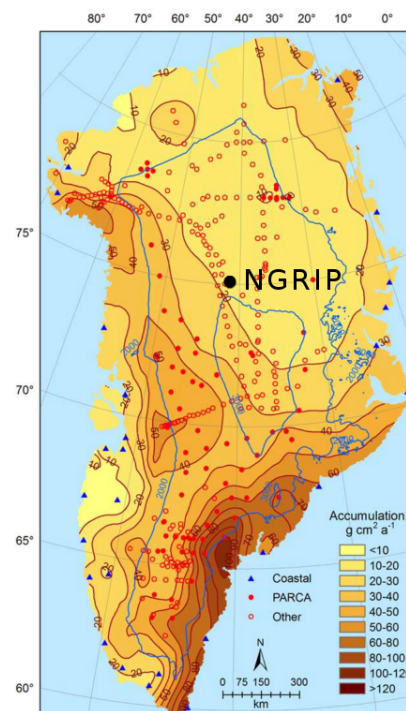


Figure 2.10: Annual accumulation and precipitation in $\frac{g}{cm^2 yr}$ for Greenland. Dots on glaciers indicate locations of cores and pits obtained by The Program for Arctic Regional Climate Assessment (PARCA), circles are cores and pits from other sources and triangles are meteorological stations (Bales et al. [2009]). NGRIP is sketched as well.

³*ieq* means ice equivalent

air can contain more water vapour compared to cold. It could also be a consequence of changing wind patterns. As mentioned in sec. 2.4.1 the precipitation events may occur at different times of the year depending on the site studied. This is a result of the prevailing wind pattern for that season. If discovering a significant and prolonged change in λ , it may be interpreted as a shift in dominating wind systems.

2.4.3 Noise

A continuing problem when analysing ice core data is the amount of noise that will be present either from wind drifting, diffusion within the ice or cutting of the ice. The most prominent source of error, however, when comparing shallow cores that are drilled relatively close to each other, is the sastrugi formations due to wind. At the surface of the ice sheet snow is regularly blown away from its original deposition site. And due to sublimation and recrystallization when the wind wears off, the snow will create a surface full of ridges and troughs, like sand dunes, but parallel to the prevailing wind direction. These sastrugi can cause large variations in the annual layer thickness from core to core, since one core may be situated in a sastrugi valley one year, causing the annual layer to be thin, and the following year the valley is filled up, creating a large annual layer thickness. Hence the intercorrelation between for instance shallow cores may not be as good as intuitively expected. When considering the deeper part of the ice cores (> 400 meters) other sources of noise become important, such as diffusion, but for the top part of an ice sheet the sastrugi formation is dominating the noise [(Wonders, W.C. [1971]), (Vinther et al. [2010])].

When only considering one core it is impossible to determine how much of the measured signal is noise and how much is actual signal. But when having several cores from the same location, the amount of noise can be identified, assuming that the signal for all cores are the same. The procedure for doing so is called the signal-to-noise ratio (SNR) and below the derivation for the calculation is described.

Following the approach of B. Vinther et al. [2006], assume we have N cores, each with a total variance, v_i , which is a combination of a signal variance, s_i , and a noise variance, n_i .

$$v_i = s_i + n_i$$

The mean variance of the noise and signal, respectively, is then

$$\bar{n} = \frac{1}{N} \sum_{i=1}^N n_i \quad \bar{s} = \frac{1}{N} \sum_{i=1}^N s_i$$

The mean variance of the cores can then be denoted as

$$\bar{v} = \frac{1}{N} \sum_{i=1}^N v_i = \frac{1}{N} \sum_{i=1}^N (s_i + n_i) = \bar{s} + \bar{n} \quad (2.1)$$

By stacking the cores, that is, averaging the total signal for all cores, a mean profile of the N cores appear. Since the signals in the individual cores are assumed identical and the noise is uncorrelated, the average variance for the stacked cores can be written as

$$v_A = \bar{s} + \frac{1}{N} \bar{n} \quad (2.2)$$

By using eq. (2.1) and eq. (2.2) the signal can be written as

$$\begin{aligned} \bar{s} &= v_A - \frac{1}{N} (\bar{v} - \bar{s}) \\ \Downarrow \\ \bar{s} - \frac{1}{N} \bar{s} &= v_A - \frac{1}{N} \bar{v} \\ \Downarrow \\ \bar{s} &= \frac{v_A - \frac{1}{N} \bar{v}}{1 - \frac{1}{N}} \end{aligned} \quad (2.3)$$

and by using the same equations the noise can be written as

$$\begin{aligned}
 \bar{n} &= N \cdot v_A - N \cdot \bar{s} \\
 \Downarrow \\
 \bar{n} - \frac{1}{N}\bar{n} &= \bar{v} - v_A \\
 \Downarrow \\
 \bar{n} &= \frac{\bar{v} - v_A}{1 - \frac{1}{N}}
 \end{aligned} \tag{2.4}$$

The *SNR* can now be written as follows, by dividing eq. (2.3) by eq. (2.4)

$$SNR = \frac{\bar{s}}{\bar{n}} = \frac{v_A - \frac{1}{N}\bar{v}}{\bar{v} - v_A} \tag{2.5}$$

and by knowing only variances of signal and noise for N cores, a parameter for the amount of noise in the measurements is found (Vinther et al. [2006]).

2.5 Correlation and significance

When comparing two data sets, for instance an observation profile and a model output, a very useful parameter can be computed to uncover how well the two data sets coincide. The parameter often used is the correlation, or Pearson's correlation coefficient, which can be calculated using eq. (2.6), assuming the data sets considered are independent.

$$r = \frac{cov(obs, model)}{\sigma_{obs} \cdot \sigma_{model}} \tag{2.6}$$

Here $cov(obs, model)$ is the covariance of the observations, *obs*, and the model data, *model*, and σ_{obs} and σ_{model} are the standard deviations of the observations and the model data, respectively. The covariance can be written as

$$cov(obs, model) = \frac{1}{N} \sum_{i=1}^N (obs_i - \overline{obs})(model_i - \overline{model})$$

where \overline{obs} and \overline{model} are the mean value of the vector variables *obs* and *model*, respectively and N is the number of data pairs considered (Taylor [1997]).

The standard deviation, σ , is the square root of the variance of the variable in question (Taylor [1997]). The denominator in eq. (2.6) can thus be written as

$$\sigma_{obs} \cdot \sigma_{model} = \sqrt{\frac{1}{N} \sum_{i=1}^N (obs_i - \overline{obs})^2 \cdot \frac{1}{N} \sum_{i=1}^N (model_i - \overline{model})^2}$$

The assumption of independence may not hold for meteorological parameters since subsequent years to some extent always are correlated due to the response lag within the climatic system.

The reason for using correlation instead of just covariance is that the correlation value is unitless and thus is a comparable parameter when considering different variables such as temperature and precipitation.

The correlation is a measure for the degree of linear relationship between two data sets. If the correlation is zero the two variables in question are entirely uncorrelated, whereas a correlation of 1 (-1) means the variables are completely correlated (anticorrelated) and express the same (directly opposite) pattern for the entire sample period, possibly with an arbitrary offset which can not be seen from the correlation [(Taylor [1997]), (2006a), (2005a)].

When the correlation value of two data sets have been found it is interesting to know whether the correlation obtained is significant, in statistical terms. That is, whether or not the correlation observed for the data sets occurred by chance. If the probability, p , that a calculated correlation is found by accident, is less than 5% then the correlation is denoted as significant. If p is less than 1% then the correlation is highly significant. The statistical significance can be looked up in tables found in nearly every statistical textbook and an extract of such is seen in table 2.1. The details concerning the correlation values in the table and the calculations

Table 2.1: Table of critical values for Pearson correlation. Both one-tailed and two-tailed statistical significance, p , are denoted. N is the number of measurements (2005b).

		One-tailed probabilities			
N	p	0.05	0.025	0.005	0.0005
		Two-tailed probabilities			
N	p	0.1	0.05	0.01	0.001
4		0.900	0.950	0.990	0.999
5		0.805	0.878	0.959	0.991
6		0.729	0.811	0.917	0.974
7		0.669	0.754	0.875	0.951
.	
.	
45		0.248	0.294	0.380	0.474
50		0.235	0.279	0.361	0.451
60		0.214	0.254	0.330	0.414
70		0.198	0.235	0.306	0.385
80		0.185	0.220	0.286	0.361

hereby can be found in (Taylor [1997]) and (Pugh and Winslow [1966]). As seen from the table the number of measurements of comparison has a huge impact on the required correlation for a given significance level. When considering only 5 data points a correlation of 0.878 is needed for the correlation to be significant. When considering ten times the amount of data points the correlation only needs to be ≥ 0.279 for the same level of significance. This makes sense since a high correlation between only five data points can easily occur and yet still be randomly grounded, but it is much harder to achieve the same correlation for 50 data points by accident.

Due to the auto-correlation of subsequent years when considering meteorological parameters the significance level is somewhat underestimated here. In reality the degrees of freedom for the time series examined are lower than assumed for meteorological parameters.

In table 2.1 the top bar is mentioning both a one-tailed and a two-tailed probability. This refers to the distribution of the probability and the correlation value one would expect to find. The probability distribution follows a gaussian curve with mean value zero. When considering the two-tailed test for a significance level you are seeking correlation values in both ends of the scale. That is, for a significance level of $p \leq 0.05$ half of the probability is for finding a significant positive correlation and the other half is for finding it in the negative end of the distribution. When using a one-tailed test you are testing for the possibility of a relationship in one direction and are completely disregarding the possibility of a relationship in the other direction. So when knowing a priori that the correlation to be found must lie in the positive end of the distribution, it is appropriate to denote the significance level as one-tailed probability levels (2012a).

By knowing the correlation, r , between two variables it is easy to calculate the portion of variance in variable 1 that can be accounted for by variable 2. It is done simply by squaring the correlation coefficient (Stockburger [2001]). For instance, if the correlation between variable 1, say the temperature at Nuuk for a period of 30 years, and variable 2, the NAO index for the same period, was $r=0.75$, then 56% of the variance in the temperature at Nuuk will be explained by the variance of the NAO. This can also be applied for the correlations mentioned in sec. 2.2.2 where ERA-40/NNR and the 20CR are producing correlation values above 0.9 for a large area of the globe. Here the same mechanisms determining the variance for ERA-40/NNR 300 hPa geopotential height anomalies is explaining more than 80% of the variance found for the same parameter in the 20CR even though the mathematical approach and the assimilation data used to produce the geopotential height are different for the two reanalyses.

Chapter 3

Presentation of the data used in this study

In the following chapter I will present the data used in the thesis. First the observational data from stations around the coast of Greenland will be introduced, then the model data obtained from the reanalysis will be presented, followed by the glaciological data found in ice cores.

3.1 Meteorological data from DMI

For the investigation of the reliability of the 20CR in the Greenland area a comparison with observational data has been conducted. Temperature and precipitation data from ten different locations around the coastline of Greenland has been selected (Cappelen [2011]). The ten stations are plotted in fig. 3.1 and their precise location specifications can be found in table 3.1. Thule and Station Nord only provide a temperature data set hence the most northern precipitation profile was obtained from Danmarkshavn. The meteorological stations in Greenland were initiated over a longer period of time by the Danish Meteorological Institute (DMI). The first temperature observations began on the more accessible west coast of Greenland in Upernavik, Ilulissat and Ivittuut in the year 1873, whilst the precipitation observations began later in 1890 at the same stations. On the northern east coast, however, there are no digitised daily data available until 1949. But in Tasiilaq, situated at the south east coast of Greenland, the first records of temperature and precipitation were taken in 1895 and in 1898, respectively. The latest station to begin observation was Narsarsuaq which produced its first data in January 1961, and in 1966 the meteorolog-

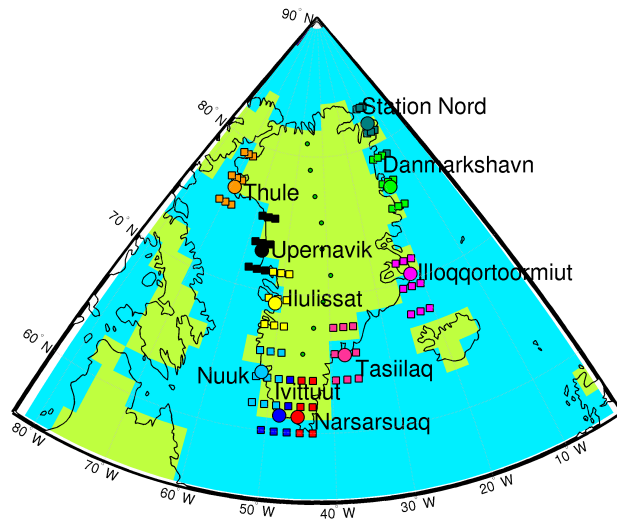


Figure 3.1: Map of Greenland and its observational stations. The 20CR land-sea mask is plotted, green being treated in the calculations as land and blue as water. For each station the center of the nine closest grid cells are marked, which are used to calculate the weighted parameter mean for all ten stations. The ice divide is marked (green dots) as well.

Table 3.1: Table of applied stations in Greenland. The World Meteorological Organization (WMO) designated station number, the name of the station, the geographical location and the elevation of the stations are seen [(Cappelen [2011]), (Boas and Wang [2011])].

Station no.	Name of station	Lat.	Lon.	Elevation [m]
04211	Upernavik	72°47' N	56°07' W	19
04221	Ilulissat	69°13' N	51°03' W	39
04250	Nuuk	64°10.5' N	51°43.5' W	20 ¹
34262	Ivittuut	61°12' N	48°11' W	30
04270	Narsarsuaq	61°10' N	45°25' W	34
04320	Danmarkshavn	76°46' N	18°40' W	11
04339	Illoqqortoormiut	70°25' N	21°58' W	42 ¹
04360	Tasiilaq	65°36' N	37°38' W	29 ¹
04310	Station Nord	81°36' N	16°39' W	36
04202	Thule	76°32' N	68°45' W	77

¹ The station have been moved, heights denoting the latest location

ical station in Ivittuut was closed (Cappelen [2011]). In table 3.2 the periods from where observations took place can be seen. The number of complete observational years for each station is seen. In table 3.3 the number of complete observational years is seen again, now the total observational period (1873-2008) is divided into two. Since the observation periods

Table 3.2: Years of operation at the Greenland meteorological stations. All denoted years begin January 1st and end December 31st (Cappelen [2011]). For each station the period for which temperature and precipitation have been recorded is shown along with the total number of years available for both parameters.

	Temp.	No. of obs. yr.	Prec.	No. of obs. yr.
Station Nord	1952-2011	30	No data	No data
Danmarkshavn	1949-2010	57	1949-2010	56
Thule	1946-1981	23	No data	No data
Upernavik	1873-2010	136	1890-1980	67
Illoqqortoormiut	1949-2010	57	1950-2010	56
Ilulissat	1873-2010	136	1890-1984	88
Tasiilaq	1895-2010	110	1898-2010	103
Nuuk	1890-2010	113	1890-2010	94
Ivittuut	1873-1960	88	1890-1960	66
Narsarsuaq	1961-2010	47	1961-2010	48

are of different length and generally commence in two steps, I have chosen to split the observational period into two, one prior to 1946 (called period 1) and one from 1946 and onwards (called period 2). This is primarily because of the four new stations being established after World War II (Station Nord, Danmarkshavn, Thule and Illoqqortoormiut) and the shift in location for the most southern observation station, from Ivittuut to Narsarsuaq, in 1961, and also because of the large coverage of observations being established after the war with larger coverage from radiosondes and AWS, and the beginning of the satellite era (Compo et al. [2011]). Hence a division of the time period into an old, less reliable period and a young, more trustworthy period is a reasonable decision. The second period is further split into two, when considering the temperature parameter, one prior to 1980 and one after. The reason for this is seen in sec 4.2.4.

The observation data from Thule and Station Nord was obtained from the NASA GISS¹

¹Goddard Institute for Space Studies

website and not directly from DMI. It is, however, DMI who owns the meteorological station at Station Nord but the US Air Force that controls the Thule station (Boas and Wang [2011]). This may have an effect on the comparability between the stations since the data from Thule most likely has been carried out by the American Military, who may have used different procedures when collecting the data. It is for instance important at which time of the day the measuring took place and whether it was done automatically or manually, see sec.2.3.2. None of these informations were available from NASA GISS and care must be taken when comparing data from the two institutions. The timeseries of the NASA GISS observations are also missing a lot of values which results in many years not being a part of the calculations, and that most certainly will have an impact on the results.

Table 3.3: For each station the period for which temperature and precipitation have been recorded is shown along with the total number of years available for both parameters. The parameters have been split up into two periods, one prior to 1946 (period 1) and one from 1946-present (period 2). Period 2 is further divided into two periods, one before 1980 and one after.

	No. of temp. obs. yr.				No. of prec. obs. yr.	
	1873 -1945	1946 -2008	1946 -1980	1980 -2008	1890 -1945	1946 -2008
Station Nord	0	30	17	13	No data	No data
Danmarkshavn	0	57	30	27	0	56
Thule	0	23	22	1	No data	No data
Upernavik	73	63	35	28	38	29
Illoqqortoormiut	0	57	30	27	0	56
Ilulissat	73	63	35	28	52	36
Tasiilaq	47	63	35	28	45	58
Nuuk	51	62	35	27	37	57
Ivittuut	73	15	15	0	51	15
Narsarsuaq	0	47	20	27	0	48

In fig. 3.1 the 20CR grid cells are defined, and it can be seen that some of the observational stations are situated in a cell denoted as water. This will affect the way temperature and precipitation is calculated within the specific cell and hence the comparison of the 20CR versus observations must take into account the land-sea distribution within the reanalysis.

3.2 Reanalysis data

Several date files have been provided by the NOAA/OAR/ESRL PSD, Boulder, Colorado, USA, from their web site at <http://www.esrl.noaa.gov/psd/> (2012c). The data used from the 20CR is the following:

- A land-sea mask (94x192)
- A topography grid (94x192), geopotential height, [m.a.s.l]
- A monthly temperature grid (192x94x1656), [K]
- A monthly precipitation rate grid (192x94x1656), [$kg/m^2/s$]
- Daily temperature grids, one for each year (192x94x365 or 192x94x366), [K]
- Daily precipitation rate grids, one for each year (192x94x365 or 192x94x366), [$kg/m^2/s$]

The data files were extensive and required a large amount of computing to handle, especially the daily grids. The files were provided in NetCDF format and consisted of a latitudinal, a longitudinal and a temporal component along with the actual requested parameter (temperature, precipitation rate, height or land/sea). The latitude and longitude vectors were combined into a matrix for which the requested parameters could get plotted as a function of, to obtain a gridded image of the globe.

The monthly data files were averaged over 12 months to acquire an annual mean for each grid cell. When considering the daily parameter grid, the same was done but here averaging over 365 days. February 29th was deleted for every leap year data file. When computing the precipitation-weighted temperature data set the daily temperature and precipitation rate files were combined and averaged over one year. In this way the temperatures of days with high precipitation were valued higher than days with little precipitation. The days with no precipitation at all were removed from the annual average calculations (see sec. 7.2 for further details).

3.3 Mathematical approach

The temperature and precipitation data from DMI and NASA GISS have been given as a monthly mean value for each station each month. From the monthly mean I have calculated an annual mean, both from January to January and also from July to July, the reason for this is mentioned in sec. 3.4.1. The correlation between the observational data sets and the 20CR data sets for both situations have been calculated as well using eq. (2.6). Unfortunately not all months are represented in every year for the observational data sets, thus the years with missing data, even for just a month, is disregarded in the calculation of the annual mean and hence also in the correlation.

Before any correlations can be calculated some corrections to the data sets must be made. The reanalysis data is given in a certain grid layout. These grid points do not intersect with the observational stations along the coast. This must be taken into account before comparison. Also the topography used in the 20CR is based on a model which spectral nature is

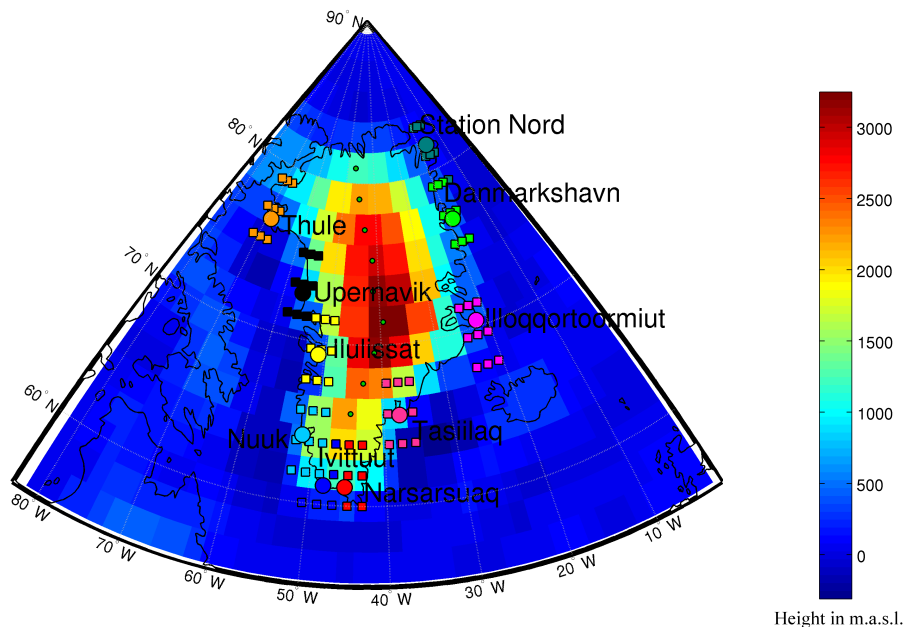


Figure 3.2: Map of Greenland and its observational stations. The 20CR topography used in calculating a lapse rate to height-correct the modelled data, is seen.

causing the heights to vary, even over sea areas. The geopotential heights should be zero above the ocean but as seen in fig. 3.2 this is not the case. The difference in height between reanalysis and observation stations must also be corrected for. The approaches for correcting the data sets are discussed below.

Height-correction of the 20CR data

To obtain a comparable set of data, the height of both the observational station and the model must be the same. From the model topography the geopotential heights of the grid points have been extracted and as expected they do not coincide with the station heights. Therefore I must correct the reanalysis data using a temperature lapse rate.

The topography plot in fig. 3.2 shows how the height of Greenland is defined. I have used

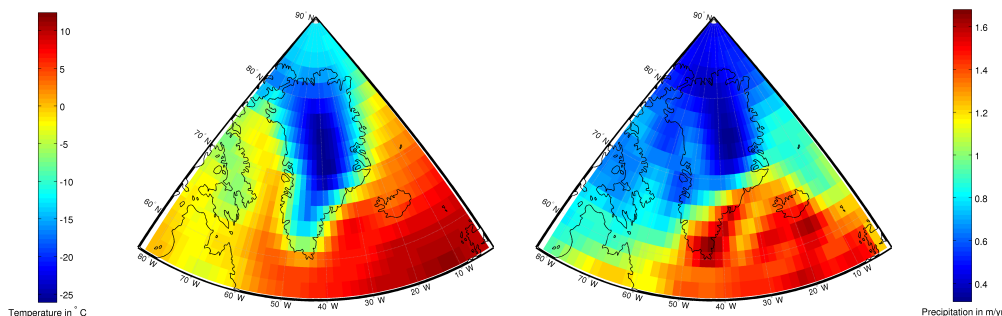


Figure 3.3: Map of Greenland. Left: Average temperature from the 20CR, 1873-2008. Right: Average precipitation from the 20CR 1873-2008. Blowup of figures can be found in the appendix (fig. A.1 and A.2).

this to determine a temperature lapse rate for each station by plotting the height versus temperature from the 20CR for each station along the latitude being closest to the station, beginning at the coast and ending at the middle of Greenland (denoted as the round green symbols in fig. 3.2). Then a linear regression has been made and the slope of the line is thus the lapse rate. The lapse rate values were found to be on average $-0.64 \frac{^{\circ}\text{C}}{\text{km}}$, lowest at Station Nord ($-0.45 \frac{^{\circ}\text{C}}{\text{km}}$) and highest at Illoqqortoormiut ($-0.75 \frac{^{\circ}\text{C}}{\text{km}}$).

In fig. 3.3 (left) it is clear why this is necessary since the temperature over the Greenland ice sheet is significantly lower than at the coast along the same latitude. This is thus because of the height of the ice sheet rather than a climatological signal. The same is not seen for precipitation (fig. 3.3 (right)) since other effects (in combination with orography) determine how much precipitation is formed, such as source areas and air mass patterns. Thus a height-corrections is only made for the temperature parameter.

Position-weighting the 20CR data

The gridpoints in 20CR unfortunately do not match the exact positions of the observational stations, and I have therefore calculated a weighted mean using the nine closest grid point values for each station mentioned in table 3.2. As seen in fig. 3.4 the grid point value is located at the center of a grid cell in which the value is valid for. I could have chosen to use just the cell wherein the station is located but to ensure

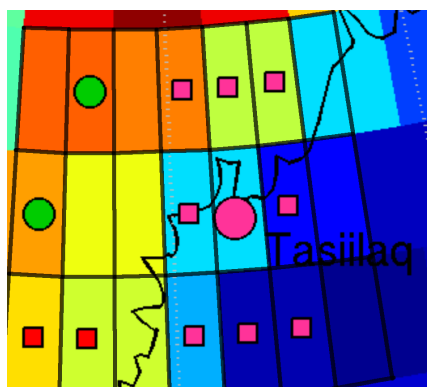


Figure 3.4: Indication of how the grid cells are defined. The grid value is the value representing the entire grid cell but designated to the center of the cell for coordinate-recognition. The figure here is a blowup of the topography of the 20CR surrounding Tasiilaq as seen in fig. 3.2.

that both a land and a water grid cell is represented and to smooth out any grid cell specific variations, I have used the cell wherein the station is located and the surrounding eight grid cells to calculate an average model value for each station site.

$$T_{weight} = \frac{\sum_{i=1}^9 \frac{T_i}{d_i}}{\sum_{i=1}^9 \frac{1}{d_i}} \quad (3.1)$$

The nine grid values are then weighted by distance using eq. (3.1) where T_i are the temperatures each year and d_i are the distances from the station in question to the nine surrounding gridpoints. The precipitation data has been treated the same way and a weighted mean has been calculated using the same equation.

3.4 Glaciological data

The glaciological data used are obtained from the Greenland inland ice, more precisely the scientific deep drill of NGRIP. It is situated at the ice divide approximately 1700 km from the southernmost tip of Greenland. Several cores have been drilled here, including two deep drill, one commencing in 1996 but unfortunately got stuck in the hole in 1997 in a depth of 1371.8 m. A new deep drill began in 1999 and after some difficulties it hit bottom in July 2003 at a depth of 3084.99 [(Dahl-Jensen and Buchardt [2001]), (Dahl-Jensen and Buchardt [2003])]. As parallel projects to the deep drilling also shallow cores were planned to be drilled during the years 1997-2003. Those were only approximately 100 m long and should cover the last ~350 years. The deep drilling began in 1996 and lasted until and including the season of

Table 3.4: *Drilling date and total length of cores used in the thesis.*

Name of core	Drilling date	Total length
NG04S1	July 31 - August 4 2004	110.5 m
NG03S1	June 8 - June 13 2003	110 m
NG03S2	July 22 - July 25 2003	100.5 m
NG97S1	July 14 - July 17 1997	98.57 m
NG97S2	July 24 - July 29 1997	138.71 m
NG96	May 1996 - July 1997	1371.8 m

2004. The deep drilling was scheduled to end in 2003 but due to some technical difficulties when reaching the bottom the project was extended for one season. This gave rise to the drilling of one extra shallow core in 2004, hence the total amount of shallow cores drilled at NGRIP is 5 [(Gundestrup [1997]), (Dahl-Jensen and Buchardt [2003]), (Dahl-Jensen and Buchardt [2004])]. In table 3.4 the cores used in the thesis are listed with information about the drilling period and length of cores. The NG96 refers to the first deep drilling of which I have used the top 100 m of the measurements. The rest are shallow cores drilled in the vicinity of the camp, see fig. 3.5.

3.4.1 Stable isotope measurements - $\delta^{18}\text{O}$

After returning to Denmark the $\delta^{18}\text{O}$ record of the cores have been measured. The isotopic data have been available for many years but only recently have the cores been dated and thus can be used for comparison with other climatic parameters. Therefore the cores have never been analysed due to the lack of a depth-age transformation. The dating of the cores have been done by Henrik B. Clausen at Centre for Ice and Climate by the use of the isotopic profile and reference horizons from ECM, for instance the Laki eruption in 1783 (Clausen and Hammer [1988]). This is a layer in the ice of high acidity originating from the volcanic ashes emitted from Laki and transported via the stratospheric wind systems to the polar

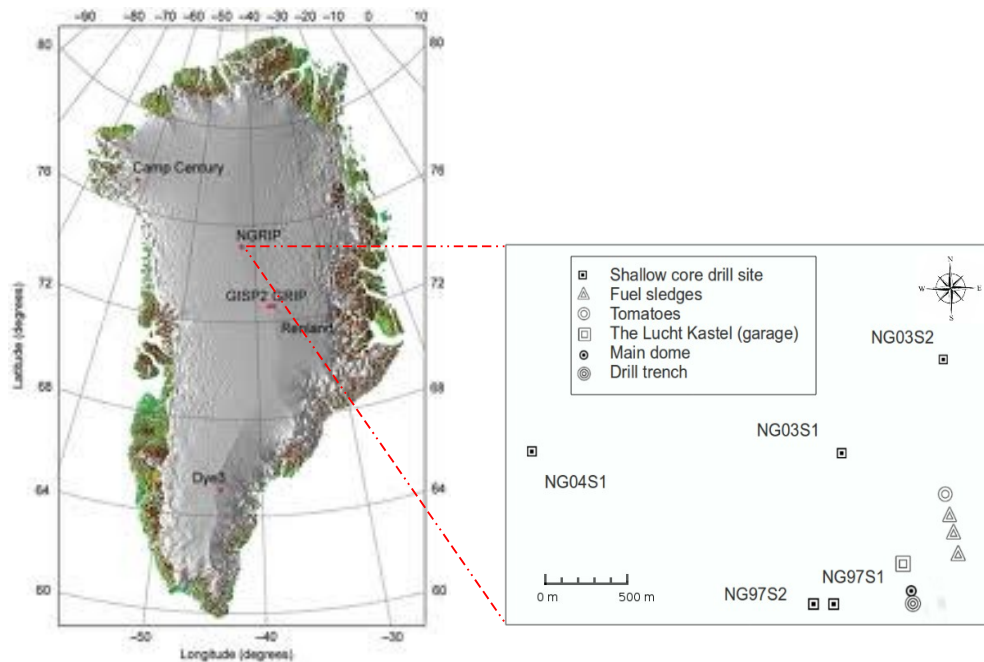


Figure 3.5: Left: Greenland and the main drill sites, excluding NEEM, Hans Tausen and Flade Isblink. Right: Blow-up of NGRIP field camp and the shallow core drill sites.

area where it precipitated and now can be found in every ice core from the Greenland area. The measurements of $\delta^{18}\text{O}$ had been done in increments of 2.5 cm for each core and with an annual accumulation of approx. 20 cm_{ieq} the resolution of the cores are adequate for analysing annual signals. If seasonal signals were investigated a resolution of 1 cm would be more appropriate to capture the subannual variations, as was done by B. Vinther et al. [2010].

To obtain an 'age vs. isotope' data set, I have used linear interpolation. The raw data was presented as an 'age vs. depth' file and a 'depth vs. isotope' file. Those have been combined to result in an 'age vs. isotope' profile, first by interpolating the depth profile to match the 'depth vs. isotope' file and then by extrapolating the resulting 'age vs. isotope' file to obtain an annual isotope record. The January-to-January time span of the year have been decided to run from minimum to minimum of the $\delta^{18}\text{O}$ values corresponding to the coldest time of the year. In reality the lowest temperatures in Greenland occur in late January/February and a more appropriate term would be to denote the annual mean to be a February-to-February annual mean [(Steffen and Box [2001]), (Persson et al. [2011]), (Vinther et al. [2010])].

Along with an annual mean splitting in winter, an annual mean from and to the warmest time of the year (high $\delta^{18}\text{O}$ values) has been calculated as well. This is called the July-to-July annual mean and is also based on interpolation. The reason for doing so is that the winter temperatures are the ones mainly determining if a year is relatively warm or cold, due to its higher variability than for the summer months (Persson et al. [2011]). If a winter experience very low temperatures the annual mean will also be low and vice versa for the relatively warm winters. Therefore an annual mean calculated from January to January splits the cold winter signal into two years and hence diffuses the signal.

In summary the data sets used henceforward are an 'age vs. $\delta^{18}\text{O}$ ' annual mean calculated both from January to January and also from July to July.

A problem occurring within the firn is diffusion of the stable isotopes. It implies that the isotopes move within the pores of the firn after deposition. This greatly dampens the seasonal cycle of the isotopic profiles and smooths out the high frequency oscillations [(Johnsen et al. [2000]), (Johnsen and Vinther [2007])]. However, when considering the annual cycle for the top 100 m of the cores, it is wasteful to backdiffuse the signal since the seasonal variations will get averaged out anyhow when calculating the annual mean. Therefore I have used the raw isotope data, only manipulated by interpolation.

3.4.2 Accumulation calculation

The accumulation is calculated on the basis of a density data set, the 'age vs. depth' data file and some constants such as the present day accumulation rate, the strain rate and the density of solid ice. The density data is measured on the second shallow ice core drilled in 1997. With a sample length of approx. 1.65 m the mean density for each sample has been measured and it is found that the density of newly precipitated snow is around $330 \frac{kg}{m^3}$ whilst the density increases downward until reaching $917 \frac{kg}{m^3}$ which is the density of solid

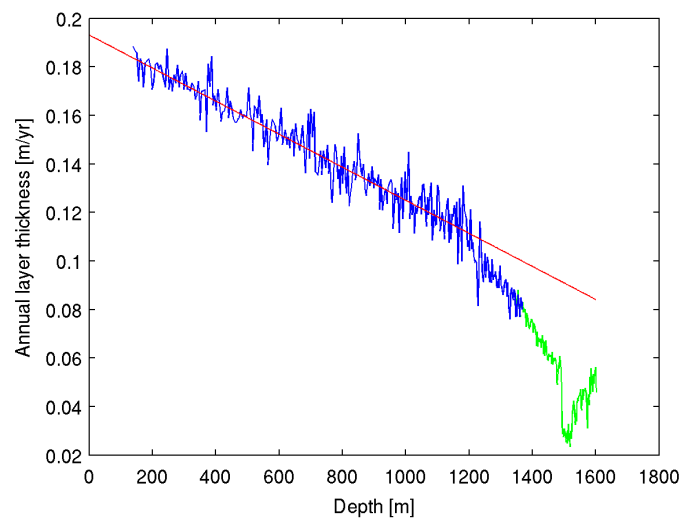


Figure 3.6: λ versus depth. NGRIP1 annual layer thicknesses (blue) and NGRIP2 annual layer thicknesses (green), both 30-year averages. Red line is a linear regression of the past 8000 years, with a slope of $-6.8 \cdot 10^{-5}$, being the strain, and an present day accumulation determined to be $0.193 \frac{m_{iceq}}{yr}$.

ice (2012b). The density profile is the same for all cores, since it is only dependent on the amount of overlying snow (the pressure) and have thus only been measured once. The 'age vs. depth' data set was found as described in sec. 3.4.1 and the present day accumulation is determined to be $0.193 m_{iceq}$ at NGRIP. The strain rate and the present day accumulation have been determined on the basis of the 'age vs. depth' data set. Since the accumulation during the Holocene has been relatively constant in Central Greenland (Dahl-Jensen et al. [1993]), averaged over several years, the thinning of annual layer thicknesses (λ) is due to strain, that is, the weight of the overlying snow is compressing the layers and making them thinner. By plotting the depth versus the raw annual layer thicknesses, obtained from the 'age vs. depth' file, one can make a linear regression to determine the rate of thinning (the strain) as the slope of the regression, and the present day accumulation is the intersection of the regression with the y-axis (assuming constant accumulation and interpreting the profile like a the Dansgaard-Johnsen-model (Dansgaard and Johnsen [1969])). From the deep drilling, NG96, the strain is calculated to be $-6.8 \cdot 10^{-5}$ and the present day accumulation is $0.193 \frac{m_{iceq}}{yr}$,

as seen in fig. 3.6.

The constant strain is used to correct the annual layer thicknesses to merely represent the accumulation, and thus the strain corrected λ are being used further on.

Since the accumulation does not have a seasonally cycled distribution, as the stable water isotopes do, it is not possible to calculate annual means from July to July. If doing so, it would be the same as calculating the mean of two subsequent years, which would only enhance noise. Therefore the accumulation data is only presented as an annual mean, thought to be running from January to January.

Chapter 4

Temperature analysis - observational data from Greenland

A way of testing how well the reanalysis is performing is to compare the parameter output with actual observations and this is performed here for the 2m temperature extracted from the 20CR and 2m temperature observations along the coast of Greenland.

In advance I have corrected the reanalysis according to sec.3.3 and the following results are therefore not the raw reanalysis data but a corrected version to fit the observational stations as best as possible.

In the following sections I will start by presenting the results of the comparison of the 20CR with coastal stations and its associated correlation values. Then the results of a large scale comparison will be shown, that is how well the observations match the 20CR for a larger area covering the Northern Hemisphere. Then a discussion of the results will be conducted and finally a summary of the conclusions found is made.

4.1 Results

4.1.1 Comparison of the 20CR with coastal stations

In fig. 4.1 the observations from the ten stations along the coast of Greenland are plotted as the red curve. Years with missing observations are not plotted. The nine closest grid cell temperature profiles from the 20CR are also plotted, the blue indicating that the grid cell is denoted as water, the green being land. Only the July-to-July annual mean is shown here but the analogous for January can be found in the appendix, fig. A.3 and A.4. The reason why only the July annual mean is shown is that the difference between them is difficult to see with the naked eye from the plots but the correlations are in fact higher for the July annual mean, as seen in the coming correlation tables.

The nine closest grid cells have been averaged to obtain a mean from where a correlation value can be calculated. Fig. 4.2 shows the observations from the stations (red) and the mean calculated 20CR temperature profile (cyan).

4.1.2 Correlation tables

The profiles seen in fig. 4.2 have been correlated according to eq. 2.6 and the resulting r can be seen in table 4.1 (column 2). The column denoted "January" is the correlation between the observations and the 20CR, where annual mean temperatures are calculated from and

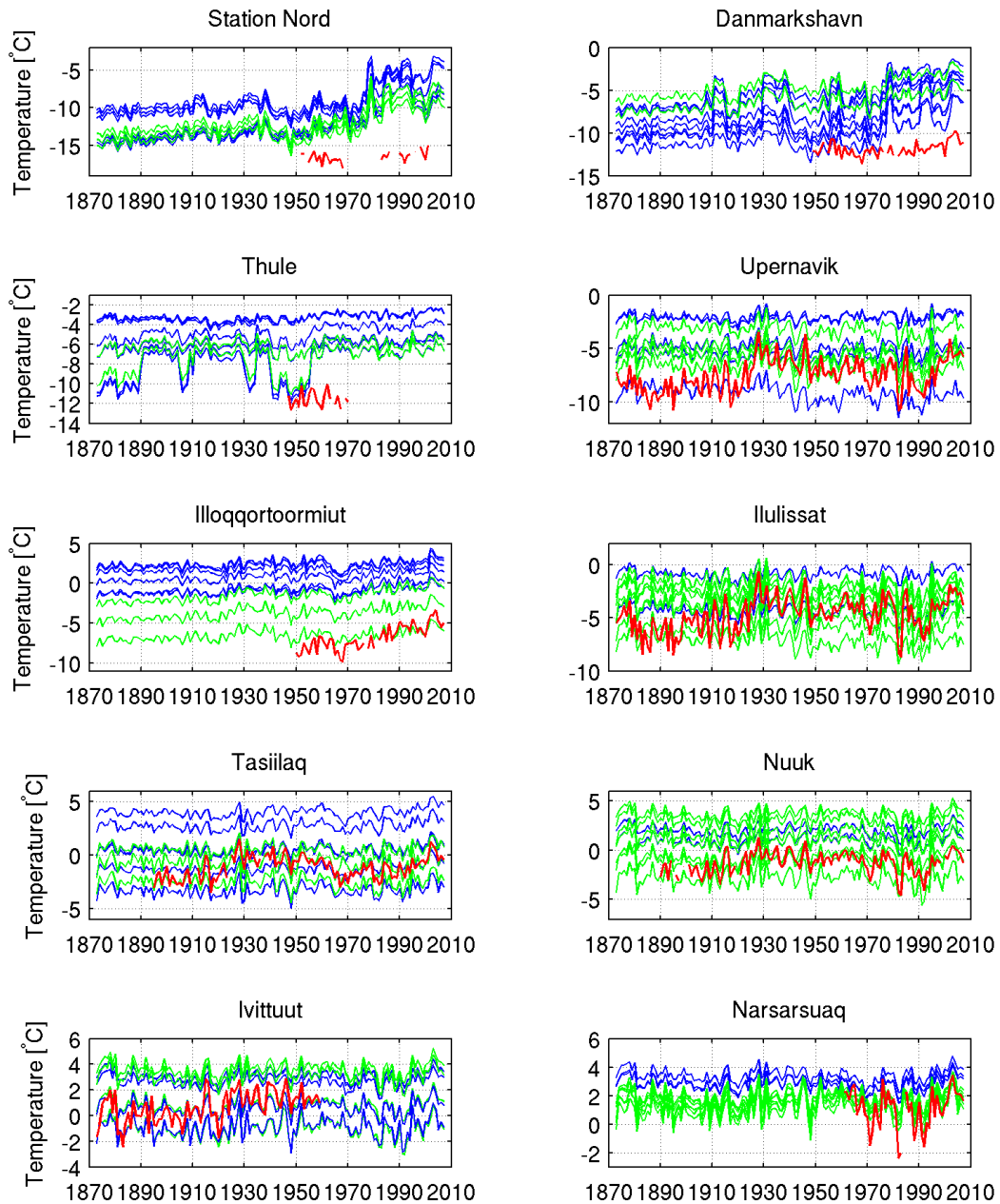


Figure 4.1: July annual mean 2m temperature for all stations. The data is elevation-corrected. The nine closest grid cells from the 20CR (land grids; green, water grids; blue) and observations (red) are shown.

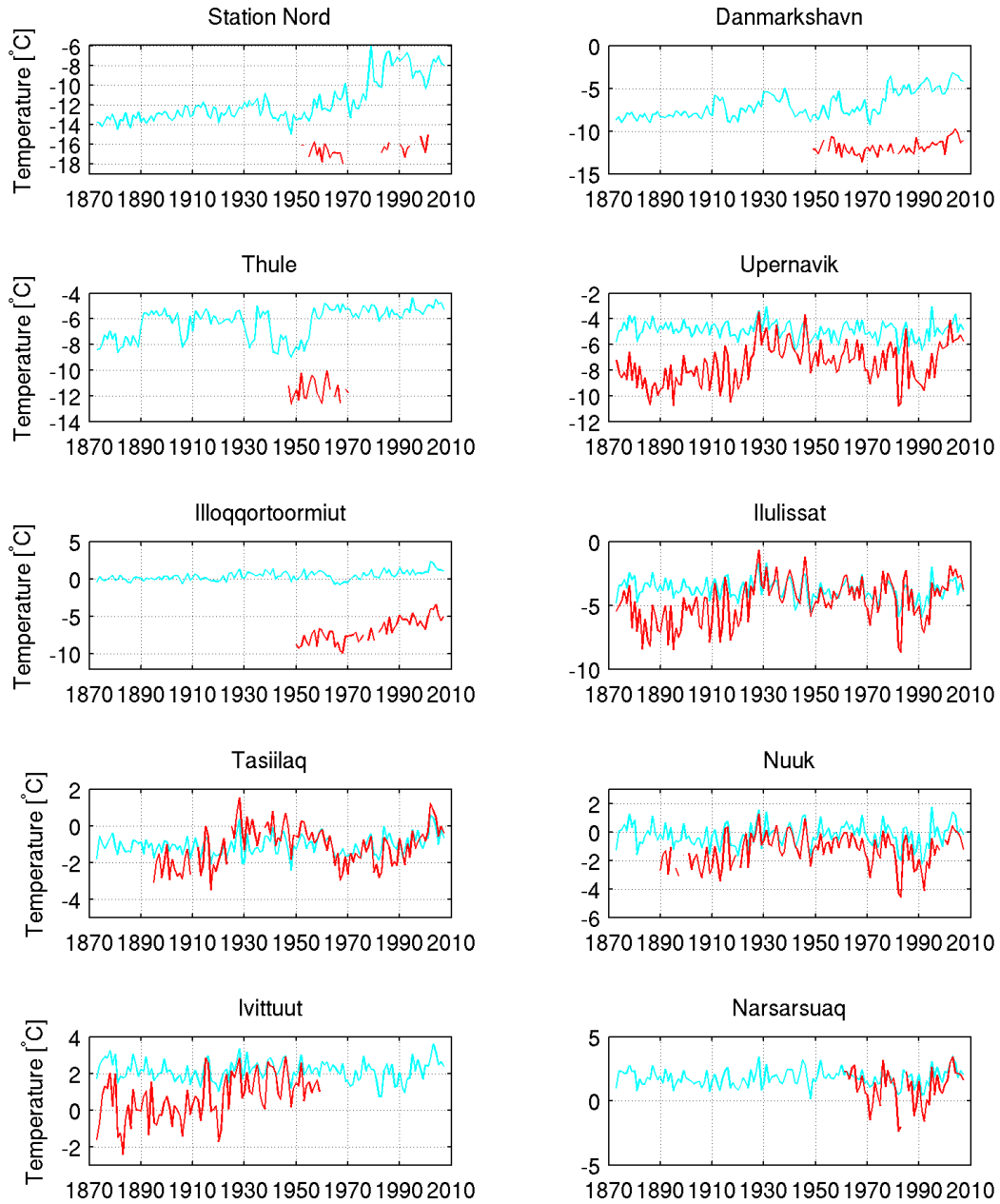


Figure 4.2: July annual mean surface temperature for all stations. The data is position- and elevation-corrected. The mean 20CR 2 m temperature for the nine closest grid cells (cyan) and observations (red) are shown.

to January. The profiles corresponding to the given correlation value is seen in fig. A.4 (appendix).

The significance level is indicated by the superscripts and a one-tailed probability is chosen. The reason for choosing a one-tailed probability is that the correlation is a priori known to be positive. Had it been negative something must have been wrong, either within the reanalysis or the observational data. The correlations obtained between the 20CR and the observations

Table 4.1: Table of correlations between observational temperature and temperature obtained from the 20CR, January and July annual mean, respectively.

	January	July
Station Nord	0.3932 ^a	0.3315 ^a
Danmarkshavn	0.5265 ^b	0.5337 ^b
Thule	0.1601	0.3485
Upernavik	0.4502 ^b	0.4916 ^b
Illoqqortoormiut	0.7955 ^b	0.7776 ^b
Ilulissat	0.5095 ^b	0.5734 ^b
Tasiilaq	0.6396 ^b	0.6960 ^b
Nuuk	0.7963 ^b	0.7972 ^b
Ivittuut	0.7048 ^b	0.6992 ^b
Narsarsuaq	0.7899 ^b	0.8746 ^b
Mean correlation	0.5766 ^b	0.6123 ^b

^a Significant correlation ($p \leq 0.05$, onetailed)

^b Highly significant correlation ($p \leq 0.005$, onetailed)

for period 1 and 2 can be seen in table 4.2. The mean correlation seen in the bottom row of both tables is the mean of the five-ten station correlations above. The significance levels are based on the lowest number of data points, that is, for instance, the mean correlation of period 2, July (0.6730) is significant ($p \leq 0.05$, onetailed) for $N = 22$ years of comparison

Table 4.2: Table of correlations between observational temperature and temperature obtained from the 20CR, January and July annual mean. The full period have been split into two, period 1 (before 1946) and period 2 (after 1946).

	Before 1946		After 1946	
	January	July	January	July
Station Nord	No data	No data	0.3932 ^a	0.3315 ^a
Danmarkshavn	No data	No data	0.5265 ^b	0.5337 ^b
Thule	No data	No data	0.1601	0.3485
Upernavik	0.3684 ^b	0.4063 ^b	0.7122 ^b	0.7482 ^b
Illoqqortoormiut	No data	No data	0.8063 ^b	0.7806 ^b
Ilulissat	0.4757 ^b	0.5581 ^b	0.8002 ^b	0.8400 ^b
Tasiilaq	0.5586 ^b	0.7246 ^b	0.7168 ^b	0.7371 ^b
Nuuk	0.7069 ^b	0.7001 ^b	0.8485 ^b	0.8606 ^b
Ivittuut	0.7233 ^b	0.7205 ^b	0.7751 ^b	0.6750 ^b
Narsarsuaq	No data	No data	0.7899 ^b	0.8746 ^b
Mean correlation	0.5666 ^b	0.6219 ^b	0.6529 ^b	0.6730 ^b

^a Significant correlation ($p \leq 0.05$, onetailed)

^b Highly significant correlation ($p \leq 0.005$, onetailed)

(Thule). The length of observation period for each station can be found in table 3.3.

4.1.3 Large scale correlation maps

To determine how well the reanalysis performs on a larger scale I have correlated the temperature observations with each grid point in the reanalysis. This provides me with colorcoded maps of the entire globe for each Greenland station and when looking at the Northern Hemisphere certain features are evident which will be discussed later on. The area shown here is from 50°N to 86°N and 130°W to 50°E and the stations are plotted in order from north to south (same order as in the correlation tables).

In fig. 4.3 the correlation from the five stations with data from period 1 (Upernavik, Ilulissat, Tasiilaq, Nuuk and Ivittuut) is shown. The annual mean is here calculated from July to July and the corresponding plot for January can be found in the appendix as fig. A.5. Period 2 can be seen in fig. 4.4, here every station is represented. Again only the July annual mean is shown, and the January annual mean plot is found in the appendix, fig. A.6.

The large scale figures only indicate significant correlation values ($p \leq 0.05$, two-tailed), the non-significant values have been set to NaN.

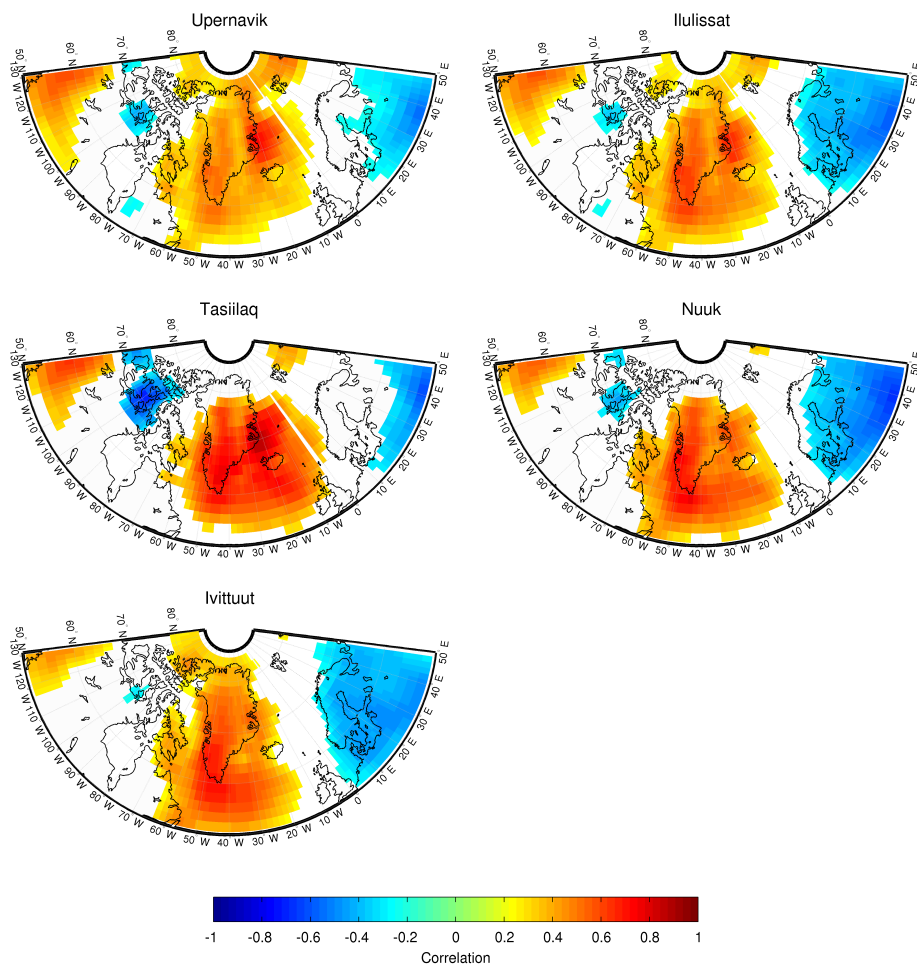


Figure 4.3: Correlation maps of temperature between each station and 20CR. July annual mean, period 1. Only significant correlations are shown ($p \leq 0.05$, two-tailed).

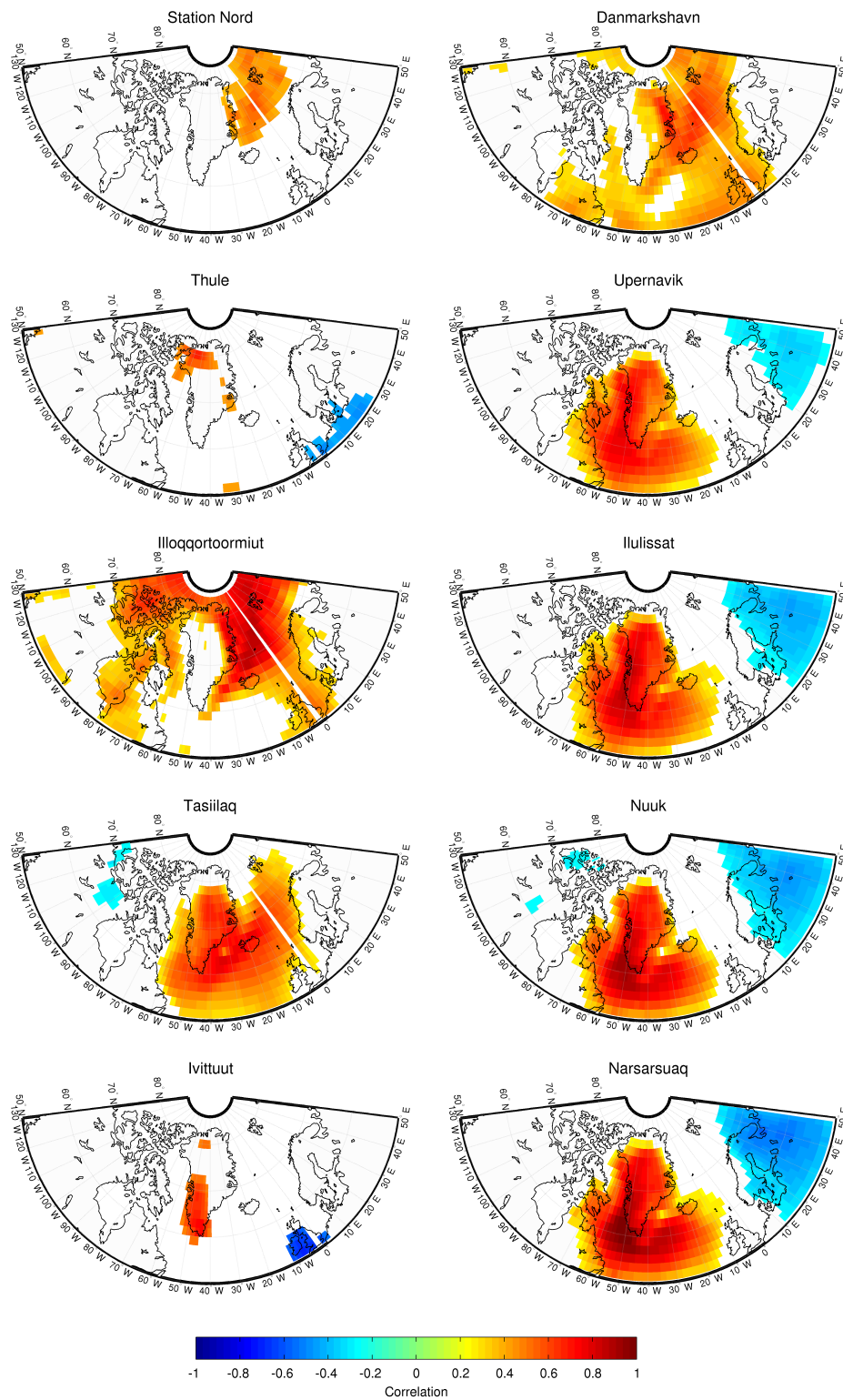


Figure 4.4: Correlation maps of temperature between each station and 20CR. July annual mean, period 2. Only significant correlations are shown ($p \leq 0.05$, two-tailed).

4.2 Discussion

4.2.1 Comparison of the 20CR with coastal stations

The reanalysis data from the grid cell where the observation station is situated and the surrounding eight grid cells are used to calculate a 20CR weighted mean to compare with the observations. This is seen in fig. 4.2 where the red curves show the observations for each station and the cyan curves is a mean of the nine closest grid cells, weighted by distance so that the center of the grid cell closest to the observation site is giving the largest contribution to the weighted mean. The reason for calculating a weighted mean instead of just using the cell data from where the station is situated, is to make sure that both a water grid cell and a land grid cell is represented, since using only a land grid cell would make the modeled temperatures too high and vice versa when using only a water grid cell (even when correcting for the height). This is also seen in fig. 4.1, which shows the temperature profiles for all Greenland stations (red) alongside the temperature profiles from the nine surrounding grid points of 20CR. Here it is obvious how the sea grid cells (blue) are warmer than the land (green), for instance with Narsarsuaq, Tasiilaq and Illoqqortoormiut. If they are not, then the latitudinal lapse rate must be larger than the altitudinal lapse rate, such as at Upernavik or Thule, for instance.

From fig. 4.2 it is in general seen that the 20CR is overestimating the temperatures for the northern stations (Station Nord, Danmarkshavn, Thule, Upernavik and Illoqqortoormiut) but is catching the correct level of temperature for the remaining five stations (Ilulissat, Tasiilaq, Nuuk, Ivittuut and Narsarsuaq). A different result was found for E. Hanna et al. [2011] who also have used the temperature obtained from the 20CR in calculating a parameter for the surface mass balance. Here the 20CR temperature have been compared to observations obtained from DMI (Cappelen [2011]), and similarly have been height- and position-corrected. A constant lapse rate for the coastal area of $-0.6 \frac{\text{°C}}{\text{km}}$ have been used. The average lapse rate used for my corrections was for comparison $-0.64 \frac{\text{°C}}{\text{km}}$. The average difference between available summer (June, July and August) temperature observations and the corrected 20CR output for the period 1948-2008 was found to be -0.6°C with the extremes being Tasiilaq (-2.9°C) and Nuuk (2.5°C) while Thule only differed by -0.6°C . This is a significant difference to my findings which indicate that at high latitudinal stations the temperatures are grossly overestimated ($>5 \text{°C}$) even after height- and position-corrections whereas the more southern stations such as Tasiilaq hardly indicate any difference in mean temperature. The fact that Hanna et al. only used summer temperatures for the study would indicate that the winter temperatures produced for the 20CR at high latitudes are highly underrated resulting in too high annual mean temperatures. The fact that they only used data from 1948 and onward could also explain the differences made. As seen in fig. 4.1 the coherences between the 20CR and observations seem to improve when considering the period after 1948. Further information concerning the approaches used by E. Hanna et al. are needed to fully determine if inconsistencies between my study and theirs are present.

It is also seen that only Station Nord, Danmarkshavn and Thule exhibit large shifts in temperature from the 20CR. The remaining stations have a constant level throughout the entire period only varying a maximum of $\pm 2 \text{°C}$ but the three most northern stations seem to experience higher variability. This is supported by the calculation of the variance seen in table 4.3. The 20CR has a considerably larger variance for the three most northern stations than for the remaining. The opposite is seen for the observations where the smallest variances are found for the three stations mentioned. This may be an indication that the 20CR is unable to capture the conditions of the stations situated in areas of higher temperatures, where the air is more humid and the wind patterns are causing a larger variability in temperature. It is also seen that the water grid cell are less variable compared to the land grid cells as expected. The two most northern stations, however, are showing lower variance at land, perhaps because of the changing sea ice distribution causing large albedo (and hence temperature) changes above

Table 4.3: Table of mean and variance for the 20CR and observational temperature data, corresponding to fig. 4.1. Only the values for the July-to-July annual mean calculations are shown. The mean and variance for both water and land grid cells from the 20CR are calculated.

	Mean [$^{\circ}\text{C}$]			Var. [$^{\circ}\text{C}^2$]		
	Obs.	20CR		Obs.	20CR	
		Water	Land		Water	Land
Station Nord	-16.50	-10.68	-12.22	0.46	5.20	3.81
Danmarkshavn	-11.88	-7.85	-5.54	0.65	3.07	1.31
Thule	-11.59	-5.16	-6.78	0.60	0.56	1.04
Upernavik	-7.51	-5.43	-4.60	2.40	0.31	0.55
Illoqqortoormiut	-6.86	0.90	-3.95	2.34	0.30	0.62
Ilulissat	-4.74	-4.13	-3.36	2.86	0.40	0.76
Tasiilaq	-1.14	0.53	-0.89	1.11	0.25	0.46
Nuuk	-1.29	1.59	-0.73	1.27	0.32	0.53
Ivittuut	0.67	2.96	1.05	1.45	0.25	0.46
Narsarsuaq	1.04	3.06	1.58	1.98	0.24	0.47

water whilst the land is constantly covered by snow thus keeping the temperatures constant as well.

As seen in fig. 2.3 assimilation data for the west side of Greenland were not available until 1921. This can be seen in fig. 4.2 where both Upernavik, Ilulissat, Nuuk and Tasiilaq (all being stations at the west coast of Greenland) shows a better coherence with observations around 1920 and forward. Hence it is indicated that more assimilation data from the earliest period would improve the 20CR output significantly.

The shift in temperature happening during the 1970s, noted at Station Nord and Danmarkshavn, is most likely caused by the larger amount of data assimilated by the model, rather than a climatological signal. The use of satellite data from the period must be influencing the model, even though the temperatures now become higher and thus further from the observations. None of the observations can confirm a shift, although it is difficult to say anything conclusive from the few years of observations at Station Nord.

The large peaks seen in the reanalysis data at Thule throughout the period is most likely also an effect caused by the dynamics of the model at high latitudes since it looks quite random and none of the other stations, neither north or south, experience the same pattern at any time. As seen in fig. 4.1 it is only the three most northern grid cells creating the two-level pattern at Thule, indicating that the model somehow creates the shifts internally. Another explanation for the seemingly two levels of output could be the existence of assimilation data for the model. The sea ice is measured from satellites from the late 1970s, prior to this reconnaissance aircrafts and marine vessels provided the data but not continuously. This could explain the dips in temperature if no observations of sea ice or sea level pressure were reported. However, this should then also affect the six other surrounding grid cells which it does not.

4.2.2 Correlation tables

In table 4.1 the correlation, r , between temperature observations and the weighted mean of 20CR have been calculated (correlation of profiles in fig. A.4 and 4.2) and the correlations show a wide spread of values (0.1601-0.8746). There are several reasons for this but in general it is seen that when moving north the reanalysis performs worse. The four stations with the lowest correlations are the four most northern ones, being Station Nord, Danmarkshavn,

Thule and Upernavik. Another factor is the time period of observations; the best correlation is found in Narsarsuaq due to both the southern location but also due to the 50 years of only modern time observation. Illoqqortoormiut is another example of the same. The reanalysis performs best in modern time since the amount of observations have increased heavily within the 20th Century and especially during the 1960s when the satellite era began (Compo et al. [2011]) (see sec. 2.3). The amount of assimilation data used for the old period and the young can be seen in fig. 2.2 and the location of them is seen in fig. 2.3. As seen the reanalysis have a large amount of data points to spin up to during period 2 compared to period 1 and this limits the reanalysis not to produce outputs that are too far away from the reality. But even though Ilulissat, Tasiilaq, Nuuk and Ivittuut all have a record going more than 110 years back, the correlation is still relatively high, 0.5095-0.7972, hence on most of Greenland the reanalysis performs well for the entire period (1873-2008) when considering the temperature parameter. Another thing to be noted is the difference in correlation when using the annual mean from July to July instead of from January to January. In general the correlations increase when the years split in July instead of January. The reason for this is that it is primarily the winter temperatures in the arctic that determine whether a year is cold or warm, since the summer temperatures have a more constant level throughout the time period considered (Persson et al. [2011]). When using annual mean from January to January the cold years are being mixed with the following year and hence are diffusing the signal. By splitting in July the interannual variability is seen more clearly and a better correlation is then obtained.

In table 4.2 the correlation for each Greenland station and the 20CR can be seen split up into the two periods. The mean correlation is also calculated and it is seen that the youngest period, from 1946 and onwards, performs better than the older period, even though the three most northern stations, which gave the worst correlations throughout the period (see table 4.1), are not represented in period 1. The station that drags down the mean in period 2 is Thule, not being data obtained from DMI but from NASA GISS. The quality of the data set here may be questioned. It is also difficult to obtain significant correlations when the number of data points are as low as for Thule (23 years) and this has of course an influence as well. There is obviously a large uncertainty when looking at observations near the boundary between land and sea, due to both topography changes and transition from water grid cells to land grid cells, since the different types of grid cells use different boundary conditions for the parameter calculations (G. Compo, pers. comm. [2011]). But by taking the height and the location of the stations into consideration, the reanalysis is very good at capturing the observed temperatures. In general the correlations are quite high, especially in period 2 but also in period 1, in fact all being highly significant for period 1, and all but Thule being at least significant for period 2. This is a very good indication that the reanalysis is being reliable all the way back to 1871.

4.2.3 Large scale correlation maps

Fig. 4.3 and 4.4 show the northern hemispheric correlation between 20CR and each station for period 1 and 2, respectively, with an annual mean calculated from July to July. The corresponding figures for the January annual mean is found in the appendix. Generally it is seen in both figures that the highest correlations are found in the areas closest to the observation site and anticorrelations are seen when moving towards Northern Europe. This is good as it is a testament of the North Atlantic Oscillation (NAO), resulting in warm temperatures in Europe whilst being cold in Greenland, and vice versa. It was expected to observe this since the 20CR is assimilated by pressure data and thus parameters with a strong NAO forcing should be evident. But larger differences occur when comparing the annual mean from period 1 to period 2. To maintain an overview, Greenland may be parted into three areas,

a northwestern part (Thule, Upernavik and Ilulissat), a northeastern part (Station Nord, Danmarkshavn and Illoqqortoormiut) and a southern part (Nuuk, Ivittuut, Narsarsuaq and Tasiilaq).

If we first consider period 1 versus period 2, July annual mean, it is obvious how the correlation improves when looking at the younger period. For all stations the correlation not only gets higher but also intensifies around the actual observation site.

When looking at the northwestern part of Greenland during period 1, containing Upernavik and Ilulissat, it seems as though the reanalysis is having trouble reproducing the signal of both Upernavik and Ilulissat. The area with the highest correlation is placed at the east coast of Greenland rather than on the west side where Upernavik and Ilulissat are situated. But when considering period 2 the reanalysis is able to correlate with the right areas. The plot for Thule, however, shows a rather low correlation for period 2, and the area of significant correlation is not very widespread. But all three large scale plots show a correlation with Greenland and an anticorrelation with Northern Europe which was expected.

The northeastern part of Greenland is only represented in period 2 but here the correlation for Illoqqortoormiut and Danmarkshavn is quite good as the observations correlate well (> 0.6) with a large part of the Arctic area. Even at Station Nord the correlation is still significant (> 0.35) over a large area but, as with Thule, one of the lower correlations is at the area closest to the observation site. This explains the low correlation seen in table 4.2 but on a larger scale the reanalysis seems to perform better when moving north than initially assumed.

During period 1 the southern part of Greenland is very well described by the reanalysis with a high correlation over a large area of Greenland with maximum in the vicinity of the observation site. And when looking at period 2 the picture is the same but with a higher maximum correlation, especially Nuuk and Narsarsuaq are displaying very high correlations (> 0.8) for a large area around the southern part of Greenland.

To say a few words on the January annual mean, it is seen in fig. A.5 and A.6 that roughly the same patterns can be found as the corresponding figures, 4.3 and 4.4 where the annual mean is calculated from July to July, but when looking closely some minor differences occur. In general the correlations over Greenland and the anticorrelations over Northern Europe and to some extent North America decrease throughout the Northern Hemisphere both during period 1 and 2 and especially in the higher latitudes such as at Station Nord, Danmarkshavn and Thule during period 2. This is in accordance with the previous statement that a July annual mean produces better correlations.

4.2.4 The influence on correlations of a warming of the Arctic

Since the 1980s the Arctic region has experienced a general warming [(Chylek et al. [2006]), (Vinther et al. [2006])] seen by infrared satellite images of the surface of the Earth. This warming most likely will influence the correlation values found for the large scale maps to some extent. By splitting the second period (1946-present) into two, 1946-1980 and 1981-present, a large scale correlation plot of the Northern Hemisphere can be made. In fig. 4.5 the correlation plot from one station from each area (northwest, northeast and south Greenland) is shown, more precisely Upernavik, Danmarkshavn and Nuuk. It is seen that the large scale plots from 1946-1980 (top row) are significantly different than the plots from 1980-present (bottom row). The correlation for all three sites increases throughout the Northern Hemisphere and this is a sign that the mean temperature is rising, since the long term trend is overriding the smaller variations and thus drives up the correlation. The same picture can be seen for the remaining stations and the correlations values are thus influenced by the warming. Since the 20CR is able to capture the rising temperatures for all stations, it is operating well throughout the entire Greenland area for the second period.

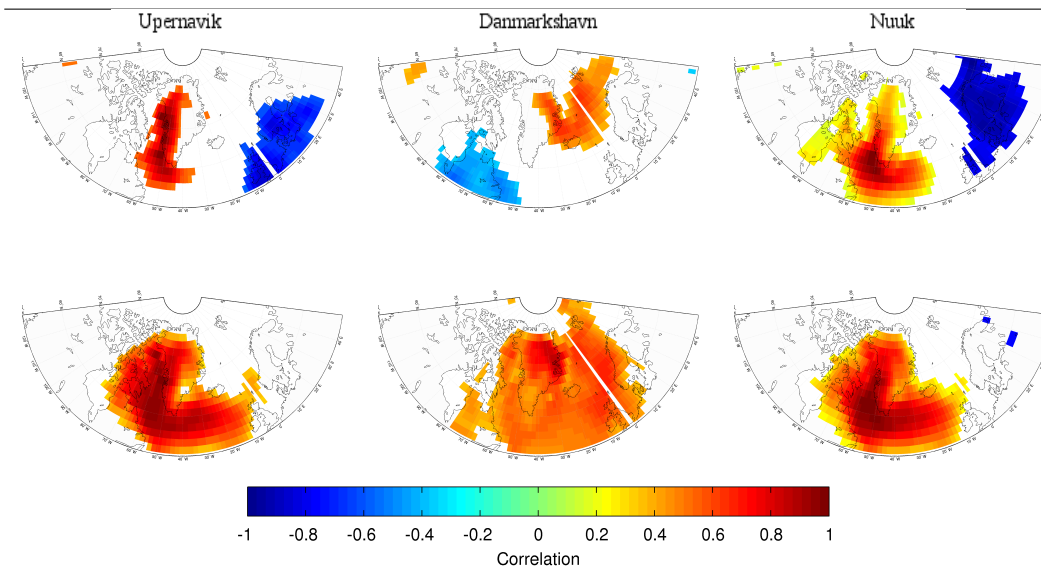


Figure 4.5: A large scale correlation map of two different periods: Top; 1946-1980, bottom; 1980-present. Left; Upernavik, middle; Danmarkshavn, right; Nuuk. Only significant correlations are shown ($p \leq 0.05$, two-tailed).

4.3 Summary

As stated in the "Review Article" by G. Compo et al. [2010], the 20CR is performing extremely well when compared to previous reanalyses, such as ERA-40. The correlation between the two reanalyses mentioned is more than 0.99 when considering the NAO index, and is higher than 0.90 at the Northern Hemisphere for the 300 hPa geopotential height fields for the period 1958-1978. The fidelity of ERA-40 has been widely tested and it is found to be highly reliable. Thus a correlation this high strengthens the view that the 20CR is capable of constructing usable parameter fields.

From the temperature analysis performed using observations along the coast of Greenland I observed that the 20CR temperatures were positively correlated with actual temperature observations throughout the period considered (1873-2008), e.i. mean correlation values of 0.6123, but it did, however, improve considerably when only looking at the modern period, since the amount of observation data used in the 20CR to compute the temperature profiles increased significantly, see fig. 2.2. The mean correlation then rose to 0.6730 for period 2. The 20CR seemed to perform best in the southern part of Greenland with a worsening in performance when moving on to higher latitudes, both in terms of correlation and absolute values. But the length of the observation period was important as well and unfortunately the most northern situated stations did not have any observations from period 1 and a more decisive evaluation of the 20CR back to 1873 was difficult at the northern part of Greenland. The correlations obtained when looking at individual station observations were significant or highly significant for most stations. Only correlations from Thule was not but the observational data, obtained from NASA GISS, might be the reason for this. It was seen that calculating the annual mean from July to July increased the mean correlation values for both periods.

The large scale correlation maps further strengthened the credibility of the 20CR since it was seen that a high correlation for a large area of Greenland was found for each station, both in period 1 and 2. The anti-correlation with Northern Europe due to the NAO was also evident. Only Thule and Ivittuut were not depicting the same but the length of observation period could be the reason for this, not necessarily the performance of the 20CR.

Chapter 5

Precipitation analysis - observational data from Greenland

Another test which would help determine the capability of the 20CR, is to compare the 20CR with precipitation observations. Since precipitation is an especially difficult parameter to both measure and predict (see sec.2.3.3), it would be a big achievement if the 20CR would be able to produce significant correlations at all. Even though the reanalysis seems to be capable of calculating the correct amounts of precipitation on a global, latitudinal scale (see sec.2.2.2) it has not been tested how well it captures the precipitation on local scales, especially for the polar region, all the way back to 1871.

The procedure is conducted as with the temperature analysis in the previous chapter, hence the results will be presented, followed by a discussion and a summary.

5.1 Results

5.1.1 Comparison of the 20CR with coastal stations

In fig.5.1 the observations from the ten stations along the coast of Greenland are plotted as the red curve. Years with missing observations are not plotted. The nine closest grid cell precipitation profiles from the 20CR are also plotted, the blue indicating that the grid cell is denoted as water, the green being land. Only the July annual mean is shown here but the analogous for January can be found in the appendix, fig.A.7 and A.8. The nine closest grid cells have been averaged to obtain a mean from where a correlation value can be calculated. Fig.5.2 shows the observations from the stations (red) and the mean calculated 20CR precipitation rate profile (cyan).

5.1.2 Correlation tables

The profiles seen in fig5.2 have been correlated according to eq.2.6 and the resulting r can be seen in table 5.1. The depiction resulting in correlations for the January annual mean can be found in the appendix, fig. A.8.

The significance level is indicated by the superscripts and a one-tailed probability is chosen, analogous to the temperature analysis.

The same split of observations into two periods, period 1 and 2, has been done, as with the temperature analysis. The correlations obtained between the 20CR and the observations for the two periods mentioned can be seen in table 5.2.

The mean correlation seen in the bottom row of both tables is the mean of the five-eight

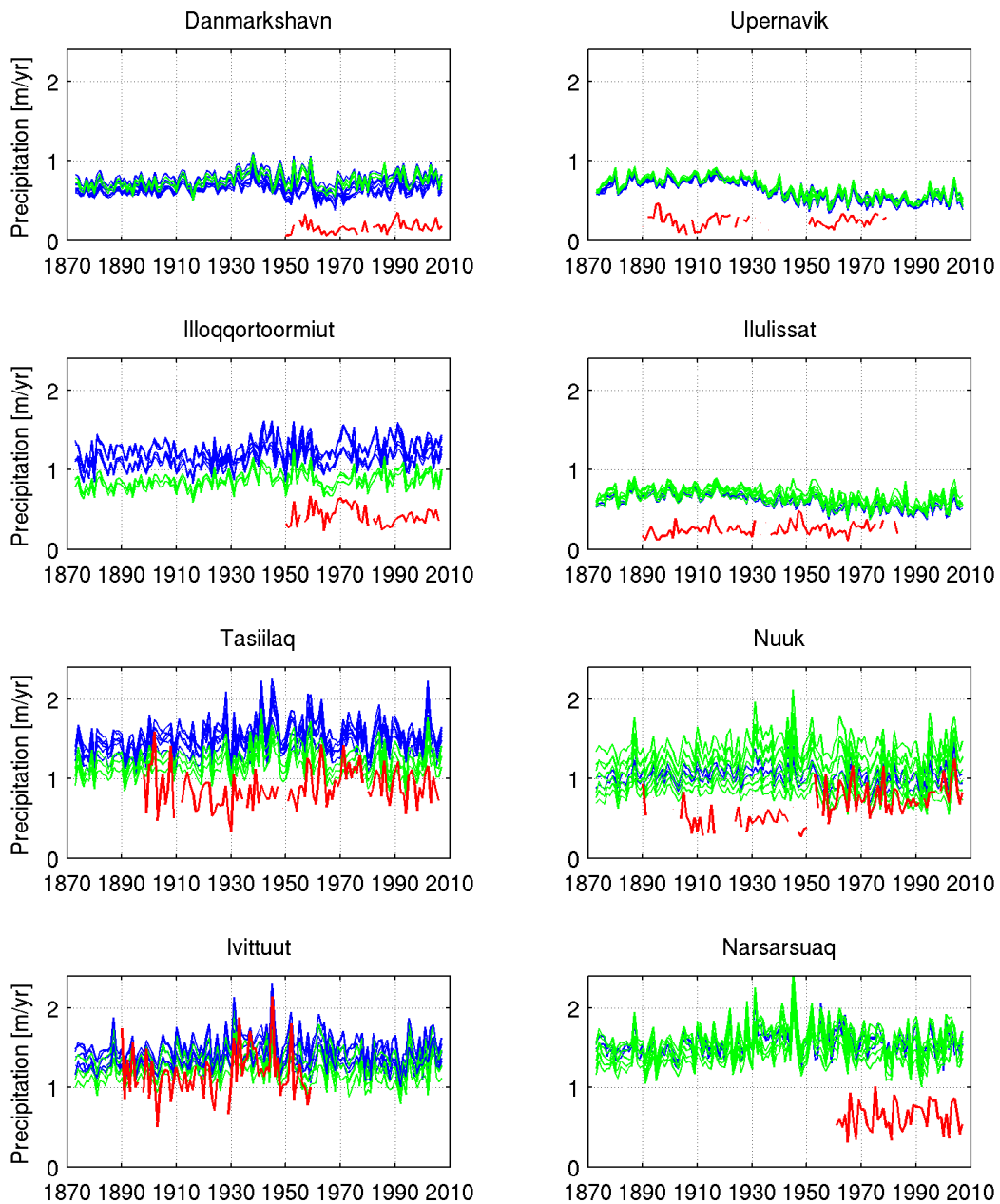


Figure 5.1: July annual mean precipitation rate for all stations. The nine closest grid cells from 20CR (land grids; green, water grids; blue) and observations (red) are shown.

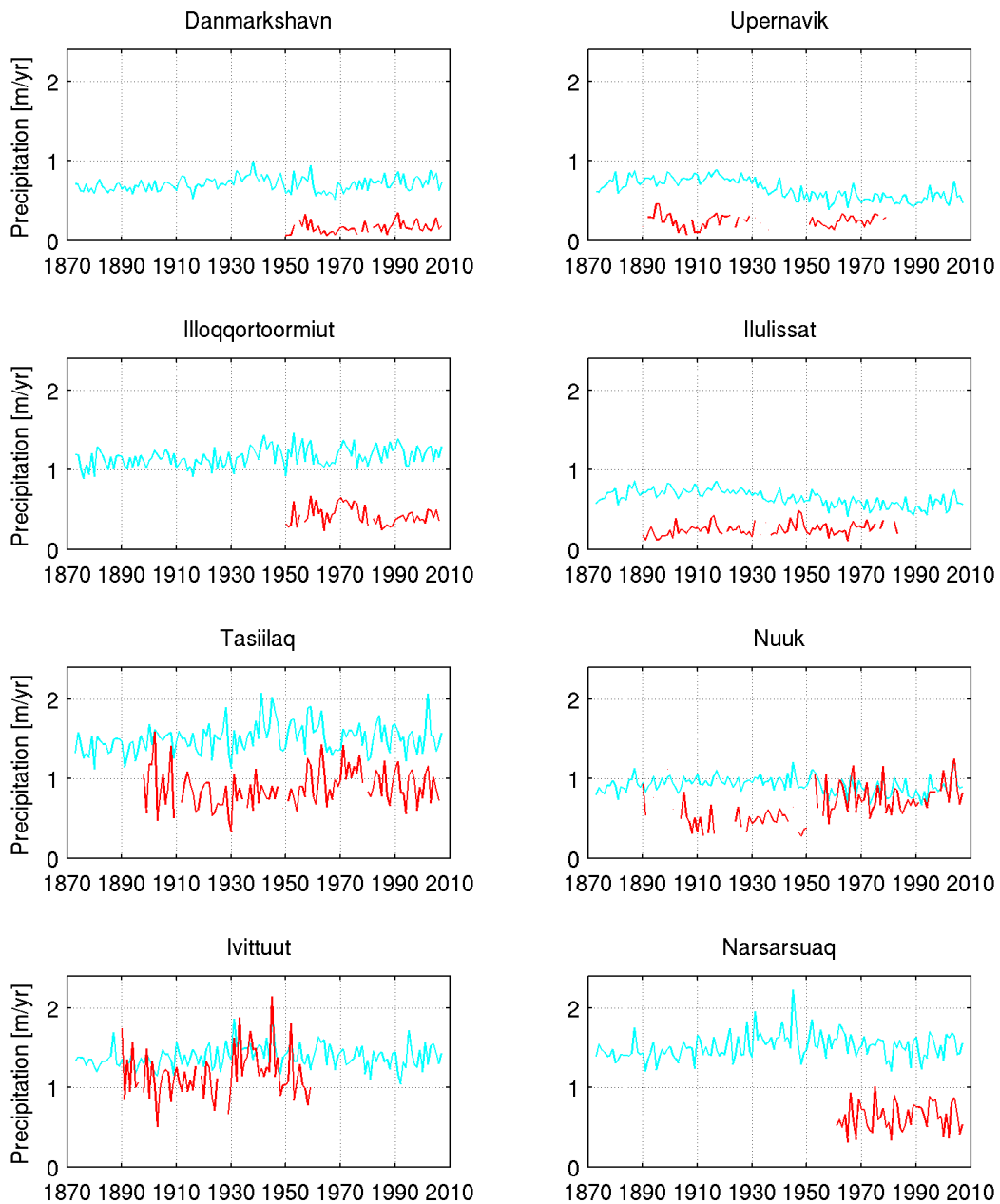


Figure 5.2: July annual mean precipitation rate for all stations. The data is position-corrected. The mean 20CR precipitation rate for the nine closest grid cells (cyan) and observations (red) are shown.

Table 5.1: Table of correlations between observational precipitation rate data from DMI and mean precipitation rates obtained from the 20CR, January and July annual mean.

	January	July
Danmarkshavn	0.7151 ^b	0.7346 ^b
Upernavik	0.1313	0.1567
Illoqqortoormiut	0.4488 ^b	0.3500 ^b
Ilulissat	0.0171	0.0459
Tasiilaq	0.4972 ^b	0.5117 ^b
Nuuk	0.1304	0.2038 ^a
Ivittuut	0.6740 ^b	0.6589 ^b
Narsarsuaq	0.2914 ^a	0.3853 ^a
Mean correlation	0.3632 ^a	0.3809 ^a

^a Significant correlation ($p \leq 0.05$, onetailed)

^b Highly significant correlation ($p \leq 0.005$, onetailed)

station correlations above. The significance levels are based on the lowest number of data points, that is, for instance, the mean correlation of period 2, July (0.4975) is significant ($p \leq 0.05$, onetailed) for $N = 14$ years of comparison (Ivittuut).

Table 5.2: Table of correlations between observational precipitation rate data from DMI and mean precipitation rates obtained from the 20CR, January and July annual mean. The time series are split into two periods, one prior to 1946 and on from 1946 and onwards.

	Before 1946		After 1946	
	January	July	January	July
Danmarkshavn	No data	No data	0.7151 ^b	0.7346 ^b
Upernavik	0.1651	0.1343	0.4493 ^a	0.4264 ^a
Illoqqortoormiut	No data	No data	0.4488 ^b	0.3500 ^b
Ilulissat	0.1907	0.1102	0.3285 ^a	0.4071 ^a
Tasiilaq	0.3981 ^b	0.4531 ^b	0.5506 ^b	0.5864 ^b
Nuuk	0.1120	0.1964	0.4500 ^b	0.5702 ^b
Ivittuut	0.7150 ^b	0.7124 ^b	0.7924 ^b	0.5199 ^a
Narsarsuaq	No data	No data	0.2914 ^a	0.3835 ^b
Mean correlation	0.3162 ^a	0.3213 ^a	0.5033 ^a	0.4975 ^a

^a Significant correlation ($p \leq 0.05$, onetailed)

^b Highly significant correlation ($p \leq 0.005$, onetailed)

5.1.3 Large scale correlation maps

To determine how well the reanalysis performs on a larger scale I have correlated the precipitation observations with each grid point in the reanalysis, as was done for the temperature. The area shown here is from 50°N to 86°N and 130°W to 50°E and the stations are plotted in order from north to south (same order as in the correlation tables).

In fig. 5.3 the correlation maps from the five stations with data from period 1 (Upernavik, Ilulissat, Tasiilaq, Nuuk and Ivittuut) are shown. The annual mean is here calculated from July to July and the corresponding plot for January can be seen in fig. 5.5. Period 2 can be seen in fig. 5.4 and fig. 5.6, which correspond to a July and January annual mean, respectively.

The reason for presenting both annual mean calculations will be obvious later on. The large scale figures only indicate significant correlation values ($p \leq 0.05$, two-tailed), the non-significant values have been set to NaN.

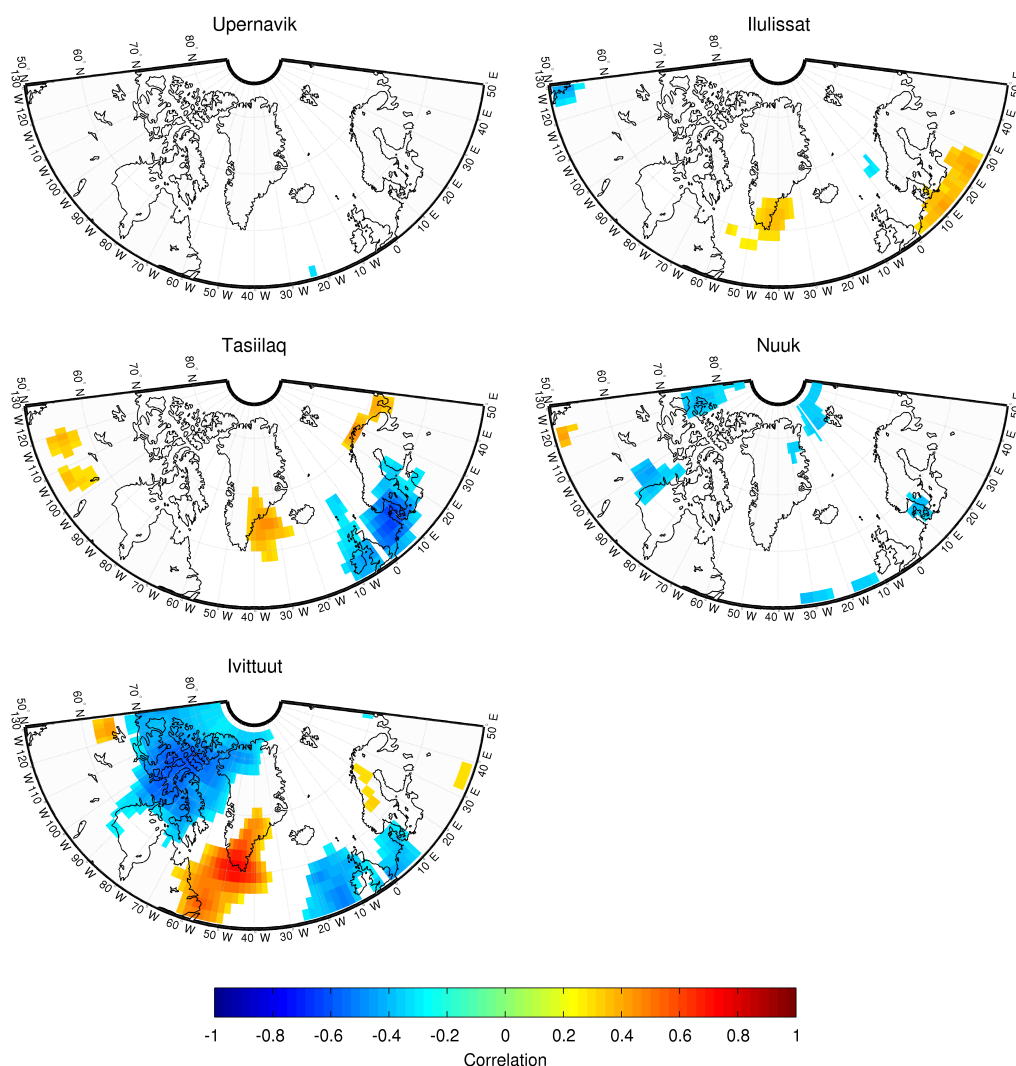


Figure 5.3: Correlation maps of precipitation rates between each station and 20CR. July annual mean, period 1. Only significant correlations are shown.

5.2 Discussion

5.2.1 Comparison of the 20CR with coastal stations

The reanalysis has obvious difficulties for modelling the correct absolute values of precipitation. In general the 20CR is overestimating the precipitation all over Greenland, as seen in fig. 5.2. But this was expected from previous reanalysis experiences, it is rather normal for reanalyses to overestimate precipitation at the coast and to underestimate it when moving inland (Hanna et al. [2006]). From fig. 5.1 it is seen that the differences in water grid cells (blue) and land grid cells (green) are not as pronounced as for the temperature difference. Only Illoqqortoormiut and Tasiilaq indicate that the water grid cells receive more precipitation than land grid cells. This is a bit odd since the topography changes would cause a

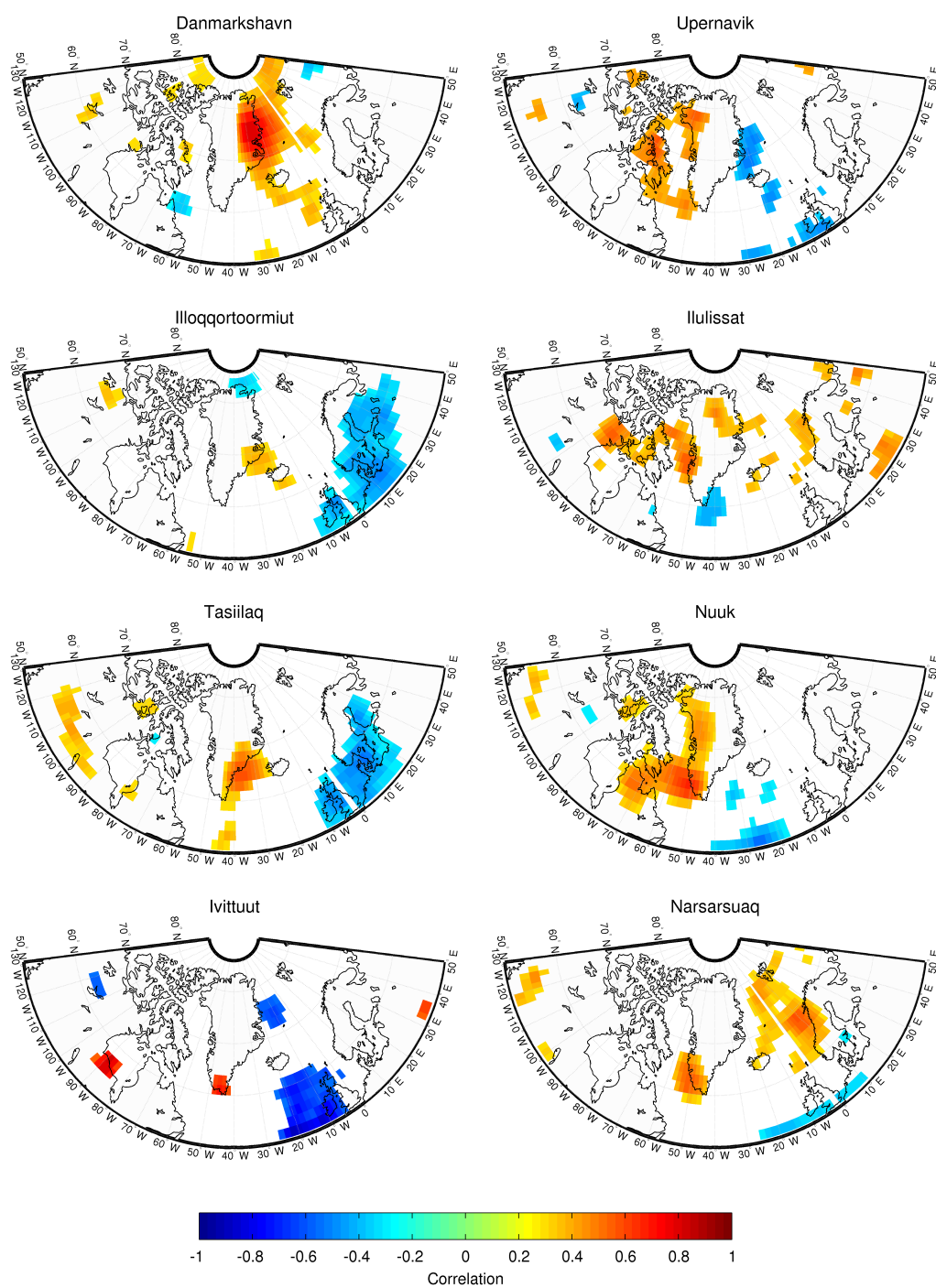


Figure 5.4: Correlation maps of precipitation rates between each station and 20CR. July annual mean, period 2. Only significant correlations are shown.

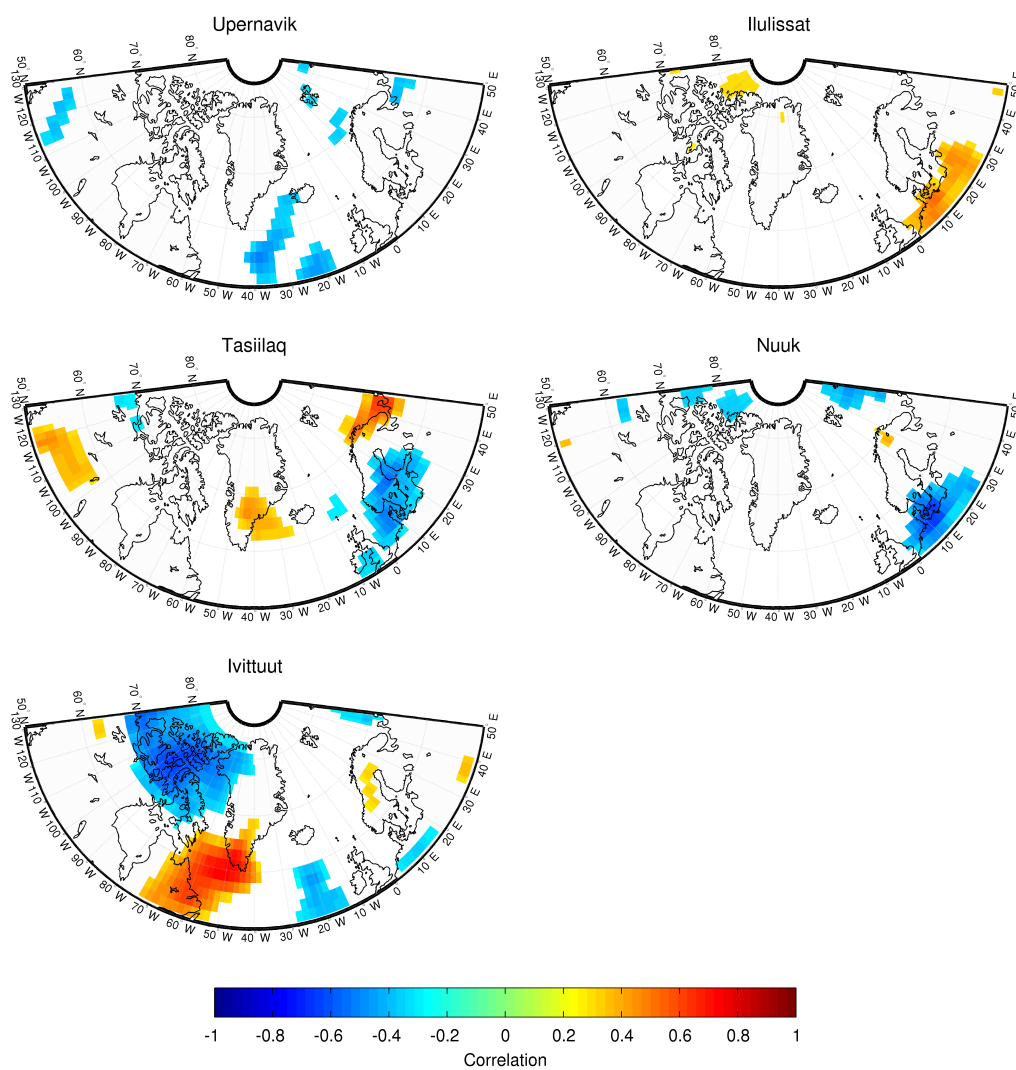


Figure 5.5: Correlation maps of precipitation rates between each station and 20CR. January annual mean, period 1. Only significant correlations are shown.

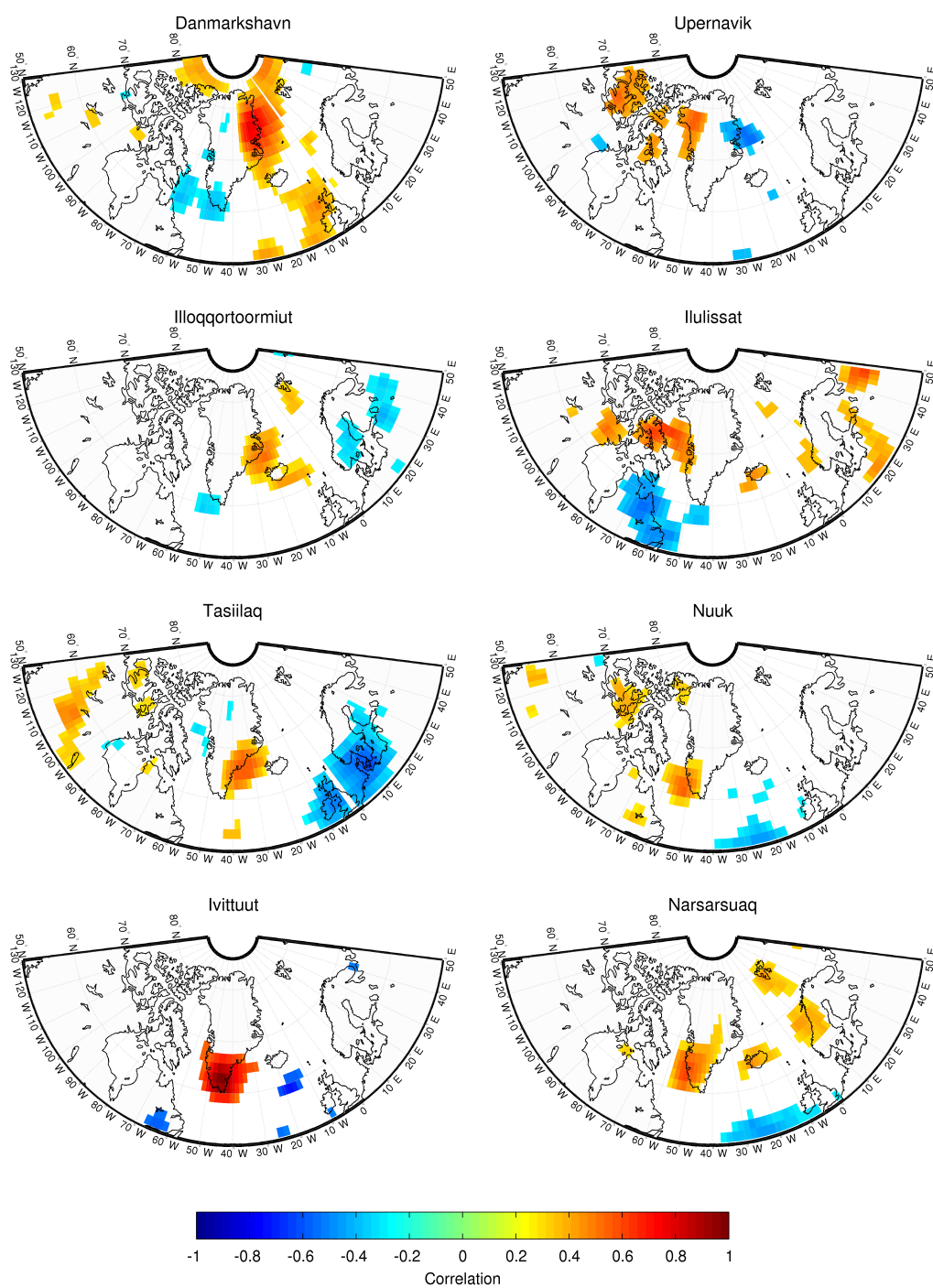


Figure 5.6: Correlation maps of precipitation rates between each station and 20CR. January annual mean, period 2. Only significant correlations are shown.

larger precipitation rate over land. But the latitudinal lapse rate must be stronger, if not the reanalysis is producing false outputs.

When looking at the precipitation rate profiles for two closely situated stations, Ivittuut and Narsarsuaq (150 km apart), it seems as though the observational data may be questioned. The mean value at Ivittuut is $1.16 \frac{m_{ieq}}{yr}$ whilst Narsarsuaq is only measuring half that amount ($0.62 \frac{m_{ieq}}{yr}$). This is probably due to changes in the apparent circumstances (station relocation, change in observing times, changes in averaging methods, changes in design of gauge, replacement of instruments) rather than a real change in climate or weather patterns.

On the west coast of Greenland (Upernavik, Ilulissat and Nuuk) it is seen that during the 1930s-1950s a slight decrease in annual precipitation occurs. Only the observations at Nuuk clearly rejects this pattern but perhaps an actual decrease in precipitation rate did occur for the west coast of Greenland.

The southernmost stations (Tasiilaq, Nuuk, Ivittuut and Narsarsuaq) are observing the highest mean values and the largest variability, see table 5.3. This is also found by the 20CR and is in accordance with the precipitation map constructed by R. Bales et al. [2009], see fig. 2.10.

As mentioned in sec. 2.4.2 the measured precipitation have an uncertainty of 20%. However, for the found absolute values it does not have an influence, since the discrepancies between model output and observations are so large. In the appendix (fig. A.9) a plot of the January annual mean precipitation rate with an uncertainty of 20% can be found for comparison.

Table 5.3: Table of mean and variance for the 20CR and observational precipitation data, corresponding to fig. 4.2. Only the values for the July annual mean calculations are shown. The mean and variance for both water and land grid cells from the 20CR are calculated.

	Mean [$\frac{m}{yr}$]			Var. [$(\frac{m}{yr})^2$]		
	Obs.	20CR		Obs.	20CR	
		Water	Land		Water	Land
Danmarkshavn	0.16	0.68	0.75	0.005	0.006	0.010
Upernavik	0.24	0.62	0.65	0.006	0.014	0.016
Illoqqortoormiut	0.42	1.19	0.87	0.013	0.015	0.011
Ilulissat	0.25	0.61	0.65	0.006	0.010	0.009
Tasiilaq	0.88	1.49	1.20	0.054	0.030	0.022
Nuuk	0.66	1.03	1.10	0.049	0.015	0.014
Ivittuut	1.16	1.40	1.32	0.088	0.021	0.020
Narsarsuaq	0.62	1.56	1.52	0.031	0.028	0.025

The reason for the changing precipitation rates is found when examining the wind patterns over Greenland. A. Ohmura et al. [1991] found that the resultant wind stream lines at the 850 hPa level for January and July were quite different, resulting in areas of Greenland receiving large amounts of precipitation in summer and little during winter, and vice versa.

As seen in fig. 5.7 (left) the winter air mass patterns are mainly caused by two atmospheric lows; the Baffin Bay low to the west and the stronger Icelandic low to the southeast. The water vapour content of the Icelandic low is relatively high and due to the stream lines being perpendicular to the coast line of southeastern Greenland, the air mass is forced up following the surface of the ice sheet. This results in large amounts of precipitation being deposited on the eastern flanks of southern Greenland. The summit of the ice sheet is also dominated by the air masses from the Atlantic Ocean.

On the west side during winter, the air is of continental origin and the water vapour content is here much lower than on the eastern side (Ohmura and Reen [1991]). It is only possible to absorb moisture from the small area of Baffin Bay. Therefore the amount of precipitation

is quite low for the west coast of Greenland, as seen in fig. 2.10.

For the summer months the circulation over Greenland changes (see fig. 5.7 (right)). The wind pattern is now dominated by the pressure ridge stretching from the northeast towards the center of the ice sheet. The southern east coast of Greenland receives less precipitation due to a pressure low at the polar basin which changes the streamlines to run parallel to the elevation slope. The west coast receives its majority of annual precipitation during the summer since the air mass reaching the west coast originates from the warm Atlantic Ocean and contains a large amount of water vapour. During the summer the northwestern part of Greenland also receives some precipitation due to an up-slope advection arriving from the west (Ohmura and Reen [1991]). The remaining part of the year the topography of Greenland ensures that the Northern Greenland remains precipitation poor since the air masses have dried out when lifted above the more than 2 km high ice sheet.

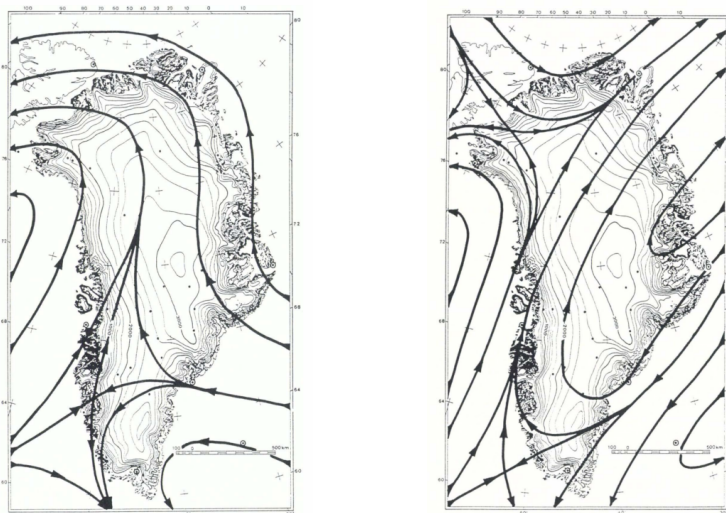


Figure 5.7: Monthly resultant wind stream lines at 850 hPa for January (left) and July (right) (Ohmura and Reen [1991]).

5.2.2 Correlation tables

Since the eastern coast stations (Danmarkshavn, Illoqqortoormiut, Tasiilaq and Narsarsuaq) mainly receive their precipitation during the winter it should be evident in the correlation tables as a higher correlation for the calculation of an July annual mean since a split in January will diffuse the high precipitation signal into two years (analogous to the cold winter temperatures justifying a split in July). The stations receiving their main precipitation during summer (Upernavik, Ilulissat, Nuuk) should then obtain larger correlations with the January annual mean calculations. Ivittuut is situated at the border of both regimes and a clear difference in correlations due to seasonal wind patterns may be difficult to see. As seen in table 5.1 the difference in main precipitation season can in fact be read from the correlations. Three of the four stations with significant correlations exhibit a higher value for the appropriate annual split. The same is seen when splitting the observation period into two, as for table 5.2. Here four (five if Ivittuut is considered to be dominated by summer precipitation) out of seven stations show higher correlations for the appropriate annual split for period 2. Period 1 only have two stations producing significant correlations but for Tasiilaq the highest is found when splitting the year in July which again fits the assumption that the season of most precipitation can be seen from the correlation, dependent on when the annual mean is calculated from.

When looking a bit closer on the absolute correlation values for period 1 and 2 (table 5.2) the results are rather uplifting. For period 1 both Upernavik, Ilulissat and Nuuk are producing insignificant correlation values but Tasiilaq and Ivittuut are capturing the precipitation variations nicely. This, however, does not strengthen the credibility of the 20CR since only two out of five stations, both being in the southern part of Greenland, are performing well. When looking at period 2 the picture changes significantly. Now the correlation values for every station are significant, even at the relatively northern stations, Danmarkshavn and Upernavik, which consists of 56 and 29 years of data, respectively. Danmarkshavn even being highly significant. Also at Ivittuut, which number of correlation years is as low as 15, the correlation found is statistically significant. Hence the reanalysis is certainly reliable for period 2 throughout most of the Greenland area.

5.2.3 Large scale correlation maps

When calculating a correlation map of the Northern Hemisphere the same conclusions are reached. For period 1 of the July annual mean (fig. 5.3) Upernavik, Ilulissat and Nuuk are very bad at capturing the correct precipitation profiles, not only at the station but also for the area around which on an annual mean is expected to show the same precipitation patterns. Upernavik is only capable of producing one single cell of significant (anti-)correlation for the entire northern area considered. Only 38 years are used at Upernavik with no observations for 1930-1950 and hence only very old and probably unreliable data are used for the large scale plot for period 1. Ilulissat is producing a statistically significant positive correlation but only for the area at the east coast of Greenland and also with Europe. This is a bit odd, since the precipitation patterns are driven by low pressure systems, hence the NAO is forcing the precipitation events as well as temperature. The NAO usually causes the meteorological conditions at Greenland to be opposite as for the Northern Europe, as seen for the large scale correlation plots from the temperature analysis. The 20CR may not be that good at modelling the dynamics resulting in precipitation events for this old period at the west coast of Greenland. For the eastern and southern coast during period 1 the result is much better, since both Tasiilaq and Ivittuut are producing significant correlations for the site of observation and anticorrelations for the Northern Europe, and for Ivittuut also at Nunavut. When looking at Ivittuut it seems as though the station here receives its main precipitation during winter because of the high correlation with the area extending up along the eastern coast which as earlier mentioned is dominated by winter precipitation. It could also just be explained by postulating that when it rains a lot during winter, the summer will be wet as well. Then the found correlation may just be a result of this.

It is seen from fig. 5.3 that the one (maybe two if Ivittuut is counted in) station receiving winter precipitation (Tasiilaq) is the one with the best large scale correlation. This is thus a result of the annual mean being calculated from and to July. However, when looking at fig. 5.5 to discover if the three other stations (Upernavik, Ilulissat and Nuuk) are producing better correlations when using an annual mean from January to January, the conclusion is that even though Upernavik and Nuuk are better at capturing the anticorrelation around Europe, a positive correlation at Greenland is still not found. Ilulissat is perhaps doing even worse since the positive correlation for the east coast of Greenland has moved and is now located close to the North Pole. Therefore the credibility of the 20CR for the west coast of Greenland, when considering period 1, is highly questionable. An explanation for the poor result at the west coast is the lack of SLP assimilation data available for the 20CR at this part of the Northern Hemisphere. SLP data are provided from Ammassalik/Tasiilaq back to 1894 and Stykkisholmur (Iceland) back to 1874 but no data is available on the west coast until 1921 where a Canadian station is providing data. From 1949 and 1952 the stations at Upernavik and Thule, respectively, also provide data for the 20CR (2012f).

For period 2 the correlations appear more clear, see fig. 5.4. Every station observation now has an area around the station where the highest correlations are found, even Upernavik which had effectively none significant correlations for the previous period. The three stations

with primary precipitation during winter (Danmarkshavn, Illoqqortoormiut and Tasiilaq) are also the ones producing the highest correlations in Greenland and anticorrelations around Europe, and when looking at fig. 5.6 the correlations for the remaining stations with summer precipitation maximum, also get better. For the 20CR data set both sides of Greenland seem to be correlating well with observations during period 2 mainly because of the reanalysis having significantly more assimilation data (see fig. 2.3) but also due to the better ways of observing precipitation.

For Ivittuut only 14 years of observation is available (July-to-July annual mean), hence the significance level is quite high ($r \geq 0.532$) compared to the remaining stations which ranges between 28 and 57 years of observations ($r \geq 0.317$ and $r \geq 0.235$, respectively). And for the reanalysis to be able to produce significant correlations this high from only 14 data points is very good and it shows that the 20CR is capturing the right dynamics for calculating precipitation throughout the Greenland area from 1946 and onwards.

5.3 Summary

Compared to the temperature parameter, it is much harder to obtain precipitation, both during measuring and when modelling. This was also expressed in the considerably lower correlation values that generally was found for the precipitation, compared to the temperature analysis results in the previous chapter.

Overall the 20CR produces too high precipitation rates at the coast but this is not uncommon for reanalyses in general (Hanna et al. [2006]). The dynamics of the atmospheric circulation transporting moist air to Greenland is very difficult to model, and in combination with the change from water grid cells to land grid cells and the imposed topography the model is overestimating precipitation rates along the coast line. As a result the precipitation at the center of the ice sheet is expected to be estimated too low.

Even though the precipitation data were sparse, compared to the availability of temperature data, and some stations did not provide any data, the 20CR is producing positive and significant correlations with observations throughout the entire Greenland area during period 2 (mean correlation of 0.5033, January annual mean). The correlations found for period 1, however, show that the conditions for the west and north coast of Greenland is poorly captured by the 20CR. This is most likely due to the lack of published SLP data from the west coast of Greenland. The southern and eastern parts are, on the other hand, more trustworthy when using precipitation data from period 1 due to the pressure data available from Tasiilaq since 1894 (2012f)(mean correlation of 0.3213, January annual mean).

It was noticed that the difference in seasonality was seen in the correlation values calculated and in the large scale correlation maps. Stations receiving its main precipitation during winter correlated better with the reanalysis when the annual mean was calculated from July to July, whilst the stations dominated by summer precipitation showed better correlations with 20CR when the annual mean was calculated from and to January.

Observations from the most northern stations are missing for both periods and therefore the conclusion on whether or not the reanalysis is usable at very high latitudes is difficult to decipher. But from the data available it seems as though no deterioration when moving north is seen, since both Danmarkshavn and Upernavik produce high correlations from 1946-present. A few stations, Danmarkshavn and Ivittuut, is performing exceptionally well with correlations above 0.65 and it is very uplifting that a high latitude station as Danmarkshavn (76.8°N, 18.7°W) is producing this high correlation values, since that indicates that the 20CR is capable of capturing the correct precipitation patterns (but not the correct absolute values) when moving far north as well.

Chapter 6

Ice core analysis - measurements from NGRIP

In the years 1996-2004 the major deep drilling project of NGRIP was carried out. The construction of the camp started in 1996 and in 1999 the actual drilling began which lasted until the bedrock was reached July 17th 2003. A large number of international institutions participated financially, as well as scientifically, in the research program and thus both Germany, Japan, Sweden, Switzerland, France, Belgium, Iceland and the US were represented at the Greenland inland ice, where the project was coordinated by the Glaciology Group at the Department of Geophysics, Niels Bohr Institute, University of Copenhagen (2004a).

The NGRIP project was aimed at retrieving and analysing a continuous ice core drilled through the Greenland ice sheet at a place selected to give the longest reliable record. This would give the best conditions for obtaining ice from the previous warm period, the Eemian. From radio echo soundings the location of NGRIP was selected since the bedrock here was flat and without undulations that could corrupt the annual layers. Therefore there was founded hope of retrieving Eemian ice. But what was later discovered as the bedrock was reached, was an unforeseen melting at the bottom due to the thermal heat of the Earth and the huge pressure of the 30084.99 m of overlying ice. This had melted a large part of the Eemian ice and the ultimate goal of the project was therefore unreachable. Still a large amount of new discoveries has been made and the deep drilling is most certainly considered a succes (2012b). In connection with the deep drilling a number of shallow cores have been obtained. They vary in depth of 100-140 meters. The oldest ones had the purpose of obtaining information on the drill site chosen; to determine the accumulation rate, the borehole temperature, the density profile, if any summer melting had occurred, to test the new and improved drilling equipment, and so on. The subsequent shallow cores were recovered in order to perform scientific experiments that needed a seasonal, or better, resolution, but didn't need a time frame going thousands of years back. The cost and time effort put into a shallow core drilling are only a fraction of that of a deep drilling project, therefore it is possible to obtain several shallow cores in combination with a deep drilling project [(2004a), (2012b)].

The shallow cores drilled at NGRIP provide a data set to which the 20CR can be compared. Since the accumulation can be deduced from the stable isotope profile (see sec. 3.4.2) it is possible to compare the precipitation data obtained from the 20CR with a data point situated at the center of the Greenland ice sheet. The shallow cores provide a data set from the central part of Greenland, almost covering the full 20CR period starting in 1871.

In the following chapter I will start by conducting a noise level analysis on the shallow cores from NGRIP, to determine if the signal within the cores is strong enough to overcome the noise found in ice cores (see sec. 2.4.3). Both the isotopic profile and the accumulation will be evaluated. Then the accumulation data at NGRIP will be compared to the precipitation data from the 20CR as another test of the credibility of the 20CR.

6.1 Noise level analysis

Since a relatively large number of shallow cores from the same site is available, all assumed to contain the same signal but with different amounts of noise, it is possible to conduct a noise level analysis on them. But first the cores must be checked for any major errors, such as errors occurred during measurements. Therefore I have intercorrelated the cores which is seen in table 6.1. The correlation for all cores are significant or highly significant. It indicates that the data obtained from the cores are correct and are not containing any noticeable errors and can thus be used in further investigations.

Table 6.1: Table of correlations between ice core data based on accumulation calculations, annual mean January to January

	NG04S1	NG03S1	NG03S2	NG97S1	NG97S2	NG96
NG04S1	1	0.6506 ^b	0.4200 ^b	0.6506 ^b	0.6982 ^b	0.5259 ^b
NG03S1	...	1	0.5313 ^b	0.4869 ^b	0.6395 ^b	0.2377 ^a
NG03S2	1	0.4304 ^b	0.4489 ^b	0.2588 ^b
NG97S1	1	0.6955 ^b	0.4518 ^b
NG97S2	1	0.3577 ^b
NG96	1

^a Significant correlation ($p \leq 0.05$, twotailed)

^b Highly significant correlation ($p \leq 0.01$, twotailed)

As described in sec. 2.4.3 the signal-to-noise ratio is a method to determine if the cores are consisting primarily of a common signal or if noise is dominating the measurements. The equation used is shown below, as well as in sec. 2.4.3 (eq. (2.5)), where \bar{s} and \bar{n} are the mean signal and noise variances, respectively, v_A is the variance of the record obtained by averaging all the $N = 6$ data series (stacking) and \bar{v} is the mean variance of the six cores. The derivation can be found in sec. 2.4.3.

$$SNR = \frac{\bar{s}}{\bar{n}} = \frac{v_A - \frac{1}{N}\bar{v}}{\bar{v} - v_A}$$

When calculating the variance for each core the results for the isotope profiles lie between 1.73-2.13 ‰². The variance for the average annual isotopic profile, v_A , is 1.18 ‰². This results in a SNR of 1.11. Similarly for the noise level analysis for the annual accumulation, the variance for the cores was found to be $0.78-1.84 \cdot 10^{-3} m^2$, while the average annual accumulation was $0.61 \cdot 10^{-3} m^2$, and the SNR then becomes 0.90. These are both reasonable values, cf. values of 0.9 for annual $\delta^{18}O$ in GRIP cores (Johnsen et al. [1997]) and 2.4 for cores originating in the relatively high accumulation area of DYE-3 (Fisher et al. [1985]). H. C. Steen-Larsen [2011] has recently obtained SNR for NEEM of 2.7 and 1.6 for annual $\delta^{18}O$ and accumulation, respectively. As seen in table 3 of D. Fisher et al. [1985] the station of North Central is situated close to NGRIP and therefore experiences similar atmospheric conditions. The SNR for annual averages of accumulation are here found to be 1.1, which is a bit higher than the SNR at NGRIP found in this thesis but considering the low accumulation at both NGRIP and North Central ($< 20 cm_{ieq}/yr$) the agreement is satisfactorily.

The above SNR calculations were all obtained from an annual mean, where the year was defined to run from January 1st to December 31st. The seasons were here determined from the maximum (July) and minimum (January) of the isotopic profiles. But the annual mean could also be calculated using the maximum (July) as a starting point, hence calculating an annual mean where the year was defined to run from July 1st to June 30th. This can only be done for the isotopic profile since the accumulation does not experience the same continuous seasonal cycle.

The SNR for the annual mean of isotope values calculated from July to July is 0.95. This is still in the same range as with a January annual mean and a shift of six month does not seem to amplify the signal at all for this parameter.

Since I have chosen to split the analysis into two periods, period 1 (1871-1945) and period 2 (1946-present) throughout the thesis, the same may be done for the SNR . The results can be seen in table 6.2.

Table 6.2: Table of SNR for period 1 and 2, calculated for isotopes (annual mean from January and July) and accumulation.

SNR		
	Period 1	Period 2
Accumulation	1.05	0.72
$\delta^{18}O$ - Jan	1.60	0.61
$\delta^{18}O$ - July	1.37	0.55

As seen the noise is largest in the top part of the ice sheet, ie. the youngest snow. This is not surprising since the noise from sastrugi and other shortwaved noise patterns will eventually get smoothed out due to diffusion. This will remove the largest deviations from the mean and cause the variance of each core to decrease, resulting in a smaller value in the denominator in eq. (2.5) and thus a larger SNR .

Table 6.3: Table of correlations between ice core data for period 1 and 2 based on accumulation calculations, annual mean January to January. The correlations for period 1 (1871-1945) are seen at the upper right triangle of the table and the values for period 2 (1946-1993) is seen at the lower left triangle of the table.

Period 2 \ Period 1	NG04S1	NG03S1	NG03S2	NG97S1	NG97S2	NG96
NG04S1	—	0.7331 ^a	0.4200 ^b	0.6506 ^b	0.6982 ^b	0.5259 ^b
NG03S1	0.5682 ^b	—	0.6705 ^b	0.5890 ^b	0.5734 ^b	0.2768 ^a
NG03S2	0.2171	0.4122 ^b	—	0.4304 ^b	0.4489 ^b	0.2588 ^a
NG97S1	0.5682 ^b	0.3957 ^b	0.2677	—	0.6955 ^b	0.4518 ^b
NG97S2	0.6592 ^b	0.6824 ^b	0.3364 ^a	0.6339 ^b	—	0.3577 ^b
NG96	0.4996 ^b	0.1848	0.1600	0.3928 ^b	0.2897	—

^a Significant correlation ($p \leq 0.05$, twotailed)

^b Highly significant correlation ($p \leq 0.01$, twotailed)

The difference in SNR for period 1 and 2 is also evident when intercorrelating the individual cores for the two periods. The result is seen in table 6.3 where the correlations for the accumulation calculation is shown. Period 1 is seen in the upper right triangle of the table while period 2 is seen in the lower left triangle. A clear worsening in the correlation values is noticed when going from period 1 to 2. This is due to the larger amount of noise in the top part of the ice core which has not been smoothed out by diffusion yet. The same is noticed for the isotopic profiles for the two periods (table 6.4). The annual mean is here calculated from July to July and an intercorrelation between the cores is calculated as with the accumulation above. Also here the correlations are best for period 1 due to the lesser amount of noise. The January annual mean is not shown here but the result is similar.

The two time periods are believed to have experienced the same climatic variability and are thus comparable in terms of SNR . If the climate in general had been different for the two periods, it could also have been a reason for the different SNR . Another factor that affects the calculations is the length of period used. Analysing too short a period could result in false interpretations, since a few consecutive years of low annual temperature and/or accumulation could significantly lower the mean or cause large variances that may not depict the true general climate. But when considering periods of 74 and 48 years, respectively, this will not be an issue. Therefore the only reason for the change in SNR for the two periods

considered is the smoothing of the noise due to diffusion.

The noise in the cores is of a normal level, compared to previous studies and hence it does not dominate the signal. Thus the core data are therefore usable for further investigation.

Table 6.4: Table of correlations between ice core data for period 1 and 2 based on isotope profiles, annual mean July to July. The correlations for period 1 (1871-1945) are seen at the upper right triangle of the table and the values for period 2 (1946-1992) is seen at the lower left triangle of the table.

Period 2 \ Period 1	NG04S1	NG03S1	NG03S2	NG97S1	NG97S2	NG96
NG04S1	—	0.6411 ^b	0.5277 ^b	0.5762 ^b	0.4921 ^b	0.5849 ^b
NG03S1	0.4775 ^b	—	0.4992 ^b	0.5731 ^b	0.6326 ^b	0.6186 ^b
NG03S2	0.4502 ^b	0.2062	—	0.4882 ^b	0.3826 ^b	0.5387 ^b
NG97S1	0.4775 ^b	0.2959 ^a	0.3938 ^b	—	0.4245 ^b	0.5188 ^b
NG97S2	0.4946 ^b	0.2269	0.2217	0.2643 ^a	—	0.4118 ^b
NG96	0.4656 ^b	0.3766 ^b	0.4314 ^b	0.4446 ^b	0.2892 ^a	—

^a Significant correlation ($p \leq 0.05$, twotailed)

^b Highly significant correlation ($p \leq 0.01$, twotailed)

6.2 Results

6.2.1 Comparison of the 20CR with accumulation at NGRIP

The accumulation, λ , at NGRIP has been calculated for each shallow core and the result is seen in fig. 6.1 (a blowup can be found in the appendix, fig. A.10). Here the top plot shows a profile for each core (multi-coloured lines) along with the 20CR precipitation rate (cyan). The bottom plot shows the same but a mean accumulation from the six cores have been calculated (red). The precipitation rate from the 20CR is presented in units of $[\frac{m_{ieq}}{yr}]$ to match the ice core calculations.

As seen in the figure the ice core data end before the 20CR. This is a consequence of the different drilling periods (see table 3.4). The oldest core (NG96) ends in 1993 and thus the data from the remaining cores have been cut in 1993 as well to calculate a stacked accumulation profile.

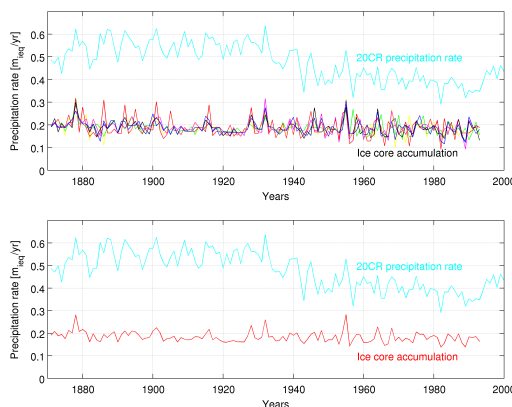


Figure 6.1: Top: The precipitation from the 20CR (cyan) and the accumulation data from the shallow cores at NGRIP (multi-coloured lines). Bottom: Same as above but the stacked accumulation data from the shallow cores at NGRIP (red) is seen instead.

6.2.2 Correlation tables

In table 6.5 the correlation between ice core accumulation and precipitation rates obtained from the 20CR are shown. The stacked (mean) profile for the ice cores are seen as well. The correlation between the stacked λ from the ice cores and the reanalysis is for the full timeseries (1871-1993) 0.4147, which is highly significant ($p \leq 0.01$, twotailed). The significance level is based on a twotailed probability distribution since, as previously mentioned, the correlation between cores of short distance in between is seen to anticorrelate at times due to the sastrugi formations at the surface. A year of high accumulation is often followed by a year with low accumulation since the sastrugi "valley" created one year is filled up the following. Cores within short distance may experience the same but shifted one year.

Table 6.5: Table of correlations between ice core data, based on accumulation calculations, and reanalysis data, January to January

	1871-1945	1946-1993
NG04S1	0.3664 ^b	0.5150 ^b
NG03S1	0.3655 ^b	0.5485 ^b
NG03S2	0.2659 ^a	0.0436
NG97S1	0.4457 ^b	0.5112 ^b
NG97S2	0.3762 ^b	0.4563 ^b
NG96	0.3179 ^b	0.4537 ^b
Mean of above correlations	0.3563 ^b	0.4214 ^b
Stacked λ	0.4245 ^b	0.5957 ^b

^a Significant correlation ($p \leq 0.05$, twotailed)

^b Highly significant correlation ($p \leq 0.01$, twotailed)

6.2.3 Large scale correlation maps

The correlation between the stacked accumulation and individual grid points in the reanalysis have been calculated as well, as was done for the coastal stations analysis. The area shown here is from 50°N to 86°N and 130°W to 50°E and the annual mean precipitation rate from the 20CR has been calculated from January to January. Fig. 6.2 (left) shows the correlations for the older period (1871-1945) and to the (right) the younger period is seen (1946-1993).

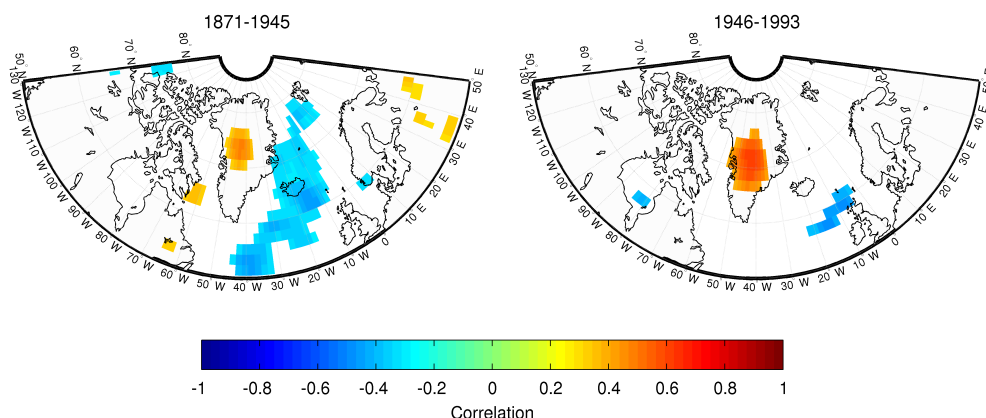


Figure 6.2: Correlation maps of precipitation profiles from 20CR and mean accumulation profiles from the ice cores. January annual mean, period 1 (left) and period 2 (right). Only significant correlations are shown ($p \leq 0.05$, two-tailed).

6.3 Discussion

6.3.1 Comparison of the 20CR with accumulation at NGRIP

The absolute values for the precipitation rate at NGRIP is seen to be approx. 2.5 times as high as the actual accumulation rate from the stacked core up until the 1940s (see fig. 6.1). From here on it seems as if the reanalysis is shifting to another level which is "only" twice as high as the observations. The shift in 20CR precipitation rate is most likely due to the availability of observational assimilation data, such as regular pressure observations and sea ice distribution. The too high absolute precipitation rates from the 20CR are in disagreement with earlier reanalyses (ERA-40 and NNR) where the precipitation rate is being estimated too high at the coast but conversely was estimated too low above land far from the coast (Hanna et al. [2006]). The 20CR is clearly estimating the precipitation rate too high everywhere above the Greenland area, as seen when comparing fig. 2.10 and 3.3 (right). It is obvious that the reanalysis is having trouble predicting the correct annual precipitation rates inland and thus one must assume that the daily precipitation rate values probably are wrong as well. However, as with the temperature parameter E. Hanna et al. [2011] found a much better coherence between precipitation rates from the 20CR and accumulations rates determined from a large number of cores at Central Greenland (see E. Hanna et al. [2011] (figure 6)) The annual accumulation rate averaged over the entire Greenland area was approx. 0.4 m while the reanalysis produced almost the same level of precipitation (0.45 m). It did not seem as though the reanalysis was overestimating any precipitation rates in their study even though the result seen for both coastal stations and the data from the center of the ice sheet found in my study is giving a different view of the situation. However, the mean precipitation found in E. Hanna et al. fig. 8, does indicate that the total precipitation at Greenland shifts from one level to another during the 1940s. Since this is not seen for the modelled precipitation rate at the coastal stations (see sec. 5.1.1, fig. 5.2) it is assumed that this is a phenomenon only present at the ice sheet and not for the coastal areas. Again, further investigation is needed to determine any irregularities between studies.

6.3.2 Correlation tables

It is seen from the noise analysis that the signal within the ice cores seems to be highest for the oldest period. This is not the case for coastal observations of precipitation and temperature where the reliability were assumed to decrease when going back in time due to the difficulties when measuring the parameter and the unstandardised methods used. The inconsistencies between reanalysis and coastal observations could therefore be a result of both unreliable observations and model failure, whereas the reliability of the annual accumulation rate from the ice core improves when going back in time, hence creating optimal conditions for a comparison with the reanalysis for period 1. However, as seen in table 6.5 the correlation is still highest for period 2. The only exception is seen for NG03S2, for which the period 2 correlation indicates a noise-filled profile (with the close-to-zero correlation). This is supported by the intercorrelation values seen in table 6.3, where the mean correlation for NG03S2 in period 2 is by far lower than the mean intercorrelation values for the remaining cores (not shown). Hence the noise level for NG03S2 is higher than those for the remaining cores. In spite of the inclusion of the noise-filled core the stacked profile is highly significantly correlated with the 20CR for both periods. The lower correlation for period 1 indicates that it is the reanalysis that is producing incorrect values when going back in time, and the lower correlation values found for period 1 both for the temperature analysis as well as with the precipitation (the previous two chapters) can not be explained by poor observational data alone. The reanalysis is clearly not performing as well during period 1 as during period 2 in general (due to the nature of the coupled models).

The two levels noticed in fig. 6.1 are splitting during the 1940s, where also period 1 and 2 split. Therefore it is expected that the correlations for the full time period are lower than the

correlations for the two periods individually. This is also the case since the full time series produce a value of 0.4147, whilst period 1 and 2 are 0.4245 and 0.5957, respectively.

6.3.3 Large scale correlation maps

As seen in fig. 6.2 the 20CR precipitation rate is positively correlated with the NGRIP stacked accumulation rate for a large area of the inland ice for both periods considered. An anticorrelation is seen for an area southeast of Greenland in accordance with the NAO, however, the area is extending far north for period 1 which is not seen in the correlation plots for the precipitation at the coast (fig. 5.3, 5.4, 5.5 and 5.6). The lower number of grid cells producing significant correlations seen in fig. 6.2 (right) is a consequence of the larger amount of noise present for period 2 in the ice cores. Compared to the coastal stations the correlations are of same order of magnitude for both periods.

It is interesting to notice the change in performance when moving across the Greenland ice sheet. For period 1 the station at Tasiilaq is positively correlated to 20CR (see fig.5.3), when moving north to NGRIP the correlation is still positively correlated but when reaching Upernavik the correlation is insignificant everywhere. The central part of Greenland must be influenced by the pressure observed at Ammassalik/Tasiilaq which is the only ones available this far back in time to be used in the 20CR at present (2012f), and hence the precipitation rate at NGRIP is correlating well with the observational accumulation. This also fits the seasonal wind systems seen in fig.5.7. Here the precipitation reaching Central Greenland is transported by the wind systems originating from the east side of Greenland.

6.4 Summary

As seen from the noise level analysis the *SNR* within the shallow cores (and deep core) was found to be 1.05 for period 1 and 0.72 for period 2, when considering annual mean of accumulation. Thus the signal is clearest for the old period due to diffusion smoothing out the noise when the ice is being compressed.

The results from the comparison between observed accumulation rates and precipitation obtained from the 20CR is close to what was discovered for the precipitation analysis for the coast stations (chapter 5), that is the 20CR is overestimating the amount of precipitation. This was not expected since previous reanalyses have shown an underestimation inland (Hanna et al. [2006]).

The reanalysis is still performing best during period 2 even though the accumulation data at NGRIP is better (less noise) for period 1. The correlation values for period 1 and 2 are both positive and highly significant, 0.4245 and 0.5957, respectively. This is better than the mean correlations for precipitation found at the coastal stations which was 0.3231 and 0.5033 for period 1 and 2, respectively. The stations dragging down the mean correlation for the stations around the coast are the stations located on the west side of Greenland and this indicates that the NGRIP area is affected by the atmospheric conditions on the east side of Greenland where assimilation data is available back to 1894 (SLP at Ammassalik/Tasiilaq). This is supported by the large scale correlation maps where it is seen that the correlation for each grid cell between accumulation observations at NGRIP and the 20CR precipitation rate is producing positive and significant correlations values at the area around NGRIP for period 1. Had NGRIP accumulation been correlated with the west coast atmospheric conditions, the reanalysis would have had difficulties producing a positive correlation as was seen for the west coast stations (Upernavik, Ilulissat and Nuuk) for the precipitation analysis. The contrary is seen at NGRIP which must indicate that the central part of Greenland is heavily influenced by the atmospheric conditions at the east side.

Even though the reanalysis is capable of producing a significant and positive correlation the absolute amount of precipitation at NGRIP is highly overrated and the daily amounts are thus expected to be unreliable as well.

Chapter 7

Using the 20CR for comparison with ice core proxy data

The parameters obtained from the 20CR can be used for a variety of purposes. For instance it is possible to compare meteorological parameters with proxy parameters to discover or reject correlations not fully uncovered or understood. As an example the isotopes found in ice cores are to first order determined by the temperature at the deposition site (Paterson [1994]). The relationship can be tested by the data obtained from a reanalysis since observations for the inland ice only recently (the last 50 years) have been carried out on a continuous basis. Furthermore the reanalysis data can be combined so that a combination of several parameters may be able to better explain the proxy parameters in question. For instance a problem for ice core data is the fact that a recording is only done when it precipitates. But since a reanalysis can provide both temperature data along with precipitation rates on a synoptic scale, the temperature may be weighted by precipitation and hence a better correlation between isotope data and meteorological features may be found. Other parameters such as changing pressure fields may also affect the isotopic profiles and such parameters are also provided by the 20CR. Hence the data provided by reanalyses can be very useful for more advanced studies of proxy parameters.

In the following sections I will present the isotope measurements from the shallow cores drilled at NGRIP along with isotope measurements from the deep core. I will be comparing the isotopic profiles of the cores with the temperature history for NGRIP obtained from the 20CR. Both the actual temperature and the precipitation-weighted temperature will be considered.

7.1 Temperature vs. isotope profiles

The annual $\delta^{18}\text{O}$ values for the cores drilled at NGRIP is calculated as described in sec. 3.4.1 and an annual mean from January to January along with an annual mean to and from July is found. Only the annual means from July to July are considered in the following due to the higher correlation with annual temperatures found in the temperature analysis. The $\delta^{18}\text{O}$ is a proxy parameter for the temperature at the deposition site (see sec. 3.4.1) and thus a significant correlation with the temperature calculated by the 20CR is expected.

7.1.1 Results

The temperature from the 20CR has been position-corrected to fit the location of the scientific deep drilling, NGRIP. On fig. 7.1 the temperature profile (blue) is seen along with the stacked $\delta^{18}\text{O}$ profile (red). The correlation between the temperature and the isotope profiles have

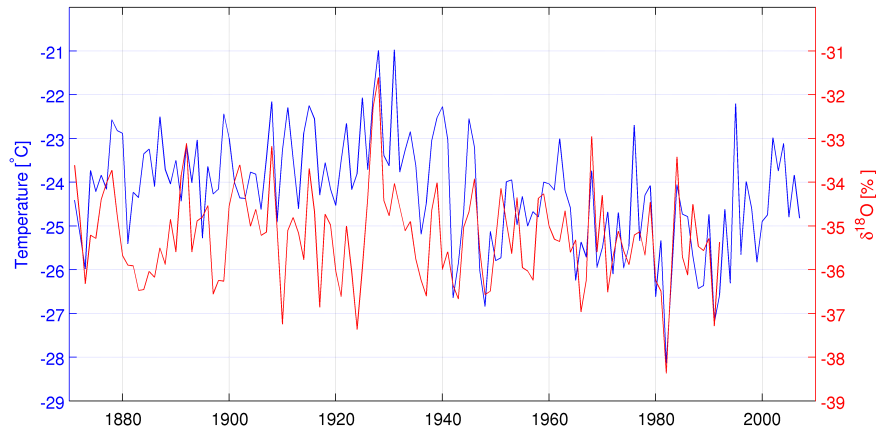


Figure 7.1: Temperature profile obtained from the 20CR (blue) and stacked $\delta^{18}\text{O}$ profile (red) from shallow cores at NGRIP. Annual mean is calculated from July to July.

been calculated and the result is seen in table 7.1. The correlation values between the stacked isotope profile and the 20CR for the full period is 0.4564 (highly significant, $p \leq 0.005$, onetailed) for the January annual mean and 0.4452 (highly significant $p \leq 0.005$, onetailed) for the July annual mean. The stacked ice core data end in 1993, thus the correlations for period 2 are based on the time span 1946-1993.

Table 7.1: Table of correlations between ice core data, based on isotope measurements of $\delta^{18}\text{O}$, and reanalysis temperature data, January-to-January and July-to-July annual mean.

	1871-1945		1946-1993	
	Jan	July	Jan	July
NG04S1	0.3506 ^b	0.4350 ^b	0.3623 ^a	0.4062 ^b
NG03S1	0.3119 ^b	0.3144 ^b	0.5478 ^b	0.4600 ^b
NG03S2	0.2221 ^a	0.1963	0.5443 ^b	0.4210 ^b
NG97S1	0.4372 ^b	0.3966 ^b	0.3190 ^b	0.3215 ^a
NG97S2	0.4478 ^b	0.3884 ^b	0.1140	0.1346
NG96	0.2362 ^a	0.2639 ^a	0.4645 ^b	0.4890 ^b
Mean of above correlations	0.3343 ^a	0.3324 ^b	0.3920 ^b	0.3721 ^a
Stacked $\delta^{18}\text{O}$	0.4030 ^b	0.4193 ^b	0.5707 ^b	0.5468 ^b

^a Significant ($p \leq 0.05$, onetailed)

^b Highly significant ($p \leq 0.005$, onetailed)

Also in this analysis a large scale comparison between the stacked isotope profile and every grid cell from the 20CR has been conducted. The result is seen in fig. 7.2, where the oldest period (1871-1945) is seen to the left and the youngest period (1946-1993) to the right. Only statistical significant correlations are shown ($p \leq 0.05$, two-tailed).

7.1.2 Discussion

Since the isotope profiles are only proxy parameters for the site temperature a direct comparison can not be conducted. Thus to determine to which degree the variability of the $\delta^{18}\text{O}$ profiles is explained by the variability in site temperatures, it is crucial that the 20CR is

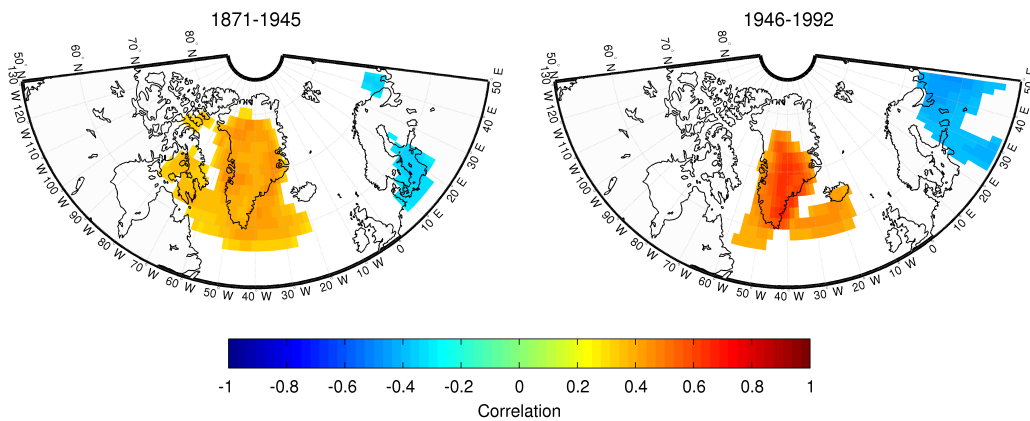


Figure 7.2: Correlation maps of temperature from 20CR and stacked isotope profiles from the ice cores. July annual mean, period 1 (left) and period 2 (right). Only significant correlations are shown ($p \leq 0.05$, two-tailed).

producing the correct temperature profiles. As seen previously the 20CR is having difficulties when calculating temperatures far back in time, especially when moving north. But the processes determining the 20CR temperature are explaining between 17% and 50% of the variability seen in the observations for period 1 along the coast, and up to 65% for period 2. It is justified to use the 20CR for correlations with isotope profiles, when keeping in mind the limitations in performance when moving far back in time and also towards the north.

As seen in fig. 7.1 the annual isotope record is varying in phase and with the same variance as the temperature at NGRIP. Especially after 1940 the two profiles are coinciding nicely. This is also noted when looking at the correlation values for period 1 and 2 for each core (table 7.1). The stacked $\delta^{18}\text{O}$ profile and the 20CR are correlating best for period 2, despite the fact that the ice cores are containing more noise closest to the surface (see sec.6.1). This again points toward the performance of the 20CR being best in the younger period where assimilation data is vastly available at the Greenland area (see fig. 2.3). The correlations are, however, still positive and highly significant ($p \leq 0.005$, onetailed) for both periods, and 18-30% of the variability in the isotope observations is explained by the 20CR site temperature. The differences seen for calculating the annual means from January or July are not pronounced, in fact the January annual mean is for period 2 providing the best correlations (stacked $\delta^{18}\text{O}$). This could be a result of the fact that the ice core proxy data is only recording when it snows and thus the coldest temperatures are not recorded within the isotopes. An annual mean from July to July will hence not make much of a difference since the largest fluctuations for the winter temperatures will be uncaptured by the isotopes. And as seen in the table (7.1) the correlation even worsens for the July annual mean but this is probably just a coincidence due to the uncertainties within the model as well as for the isotope measurements rather than an actual signal.

The large scale plots of the correlation is showing a wide area from where the isotopes are significantly correlated with temperature. For both periods the positive correlation at Greenland and the negative correlation at Europe, caused by the NAO, are clearly seen. These plots look like the plots obtained during the temperature analysis (chapter 4) and it was expected that the 20CR was capable of producing positive correlations over Greenland since both the east coast and the west coast were producing positive correlations over a large area of Greenland. Thus there was no reason why the area at NGRIP should not produce the same positive significant correlations. Even though the correlations increase for period 2 compared to period 1, the area of significant correlations over Greenland also diminish. This may be due to the lower number of data points for period 2 and thus the correlation needs to be higher to be significant.

7.2 Precipitation-weighted temperature vs. isotope profiles

To address the problem of seasonal timing of precipitation events, the data from reanalyses can be used to produce a precipitation-weighted temperature field to which the isotopic profiles from the ice cores can be compared. Since the temporal resolution of reanalyses is very high (6 hours) it is possible to study the atmospheric condition on a synoptic scale or shorter. A weather system usually has a temporal extent of a few days and thus it is possible to link certain precipitation events with the simultaneous temperature at site. A simple mathematical weighting is shown in eq. (7.1).

$$T_{pw} = \frac{\sum_{i=1}^N T_i p_i}{\sum_{i=1}^N p_i} \quad (7.1)$$

Here N denotes the number of time-equidistant samples used per year, and T_i and p_i denote the average temperature and precipitation rate, respectively, for the i th time interval (Persson et al. [2011]). It should be sufficient to consider the daily averages of temperature and precipitation for computing the precipitation-weighted annual mean temperature, T_{pw} , due to the synoptic time scales of a passing weather system [pers. comm. Peter Langen, 2012]. A. Persson et al. [2011] have made a more sophisticated model for precipitation-weighted temperatures but due to the difficulties when modelling the precipitation already seen for the 20CR when operating in the Greenland area (see sec. 6.3), I have chosen to stick with the simple weighting method to ease the computational effort.

In the following subsections a similar analysis as for the temperature vs. isotope profiles (sec. 7.1) will be performed. The expected result of precipitation-weighting the temperature is an improvement of correlations, both locally and globally.

7.2.1 Results

The temperature from the 20CR have been weighted by precipitation rates according to eq. (7.1) and a position-correction to match the location of NGRIP have been conducted. On fig. 7.3 the precipitation-weighted temperature profile (cyan) is seen along with the stacked $\delta^{18}\text{O}$ profile (red). The ordinary temperature profile (seen in fig. 7.1 (blue)) is also seen (blue).

The correlation between the precipitation-weighted temperature and the isotope profiles have been calculated and the result is presented in table 7.2. The correlation values between the stacked isotope profile and the 20CR for the full period is 0.3933 (highly significant, $p < 0.005$, onetailed) for the January annual mean and 0.3853 (highly significant $p < 0.005$, onetailed) for the July annual mean.

The large scale correlation maps are seen in fig. 7.4. As with the previous maps period 1 is seen to the left, while period 2 is placed to the right.

7.2.2 Discussion

The exact same procedure as for the previous comparison of pure annual 2 m temperature with isotope data was conducted, only now the temperature was weighted by the amount of precipitation falling the same day. As seen in fig. 7.3 the annually averaged precipitation-weighted temperatures are higher than the ordinary temperatures due to the fact that precipitation events typically occur in warmer weather. But as seen in table 7.2 the correlations decrease compared to table 7.1. This was not according to the hypothesis, however, it was perhaps expected due to the poor precipitation profile produced at NGRIP where more than a doubling of the measured amount were modelled (see sec. 6.3). The only change made in

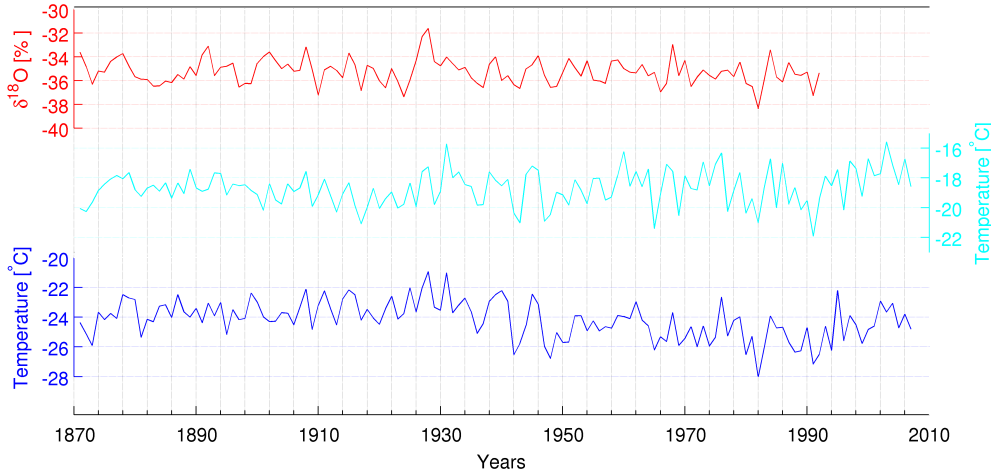


Figure 7.3: Precipitation-weighted temperature profile (T_{pw} - cyan) and ordinary temperature profile (T - blue) from 20CR extracted at NGRIP, and stacked $\delta^{18}\text{O}$ profile (red), all July annual means.

Table 7.2: Table of correlations between ice core data, based on isotope measurements of $\delta^{18}\text{O}$, and reanalysis daily precipitation-weighted temperature data, January and July annual mean.

	1871-1945		1946-1993	
	Jan	July	Jan	July
NG04S1	0.2292 ^a	0.2655 ^a	0.3329 ^a	0.2583 ^a
NG03S1	0.3351 ^b	0.3330 ^b	0.3963 ^b	0.3203 ^a
NG03S2	0.2708 ^a	0.2715 ^a	0.4527 ^b	0.3249 ^a
NG97S1	0.3390 ^b	0.3869 ^b	0.2646 ^a	0.2048
NG97S2	0.4045 ^b	0.4186 ^b	0.0607	0.1032
NG96	0.2191 ^a	0.2987 ^a	0.4696 ^b	0.3839 ^b
Mean of above correlations	0.2996 ^a	0.3290 ^b	0.3295	0.2659
Stacked $\delta^{18}\text{O}$	0.3620 ^b	0.4602 ^b	0.4809 ^b	0.3909 ^b

^a Significant ($p \leq 0.05$, onetailed)

^b Highly significant ($p \leq 0.005$, onetailed)

this setup compared to the actual temperature correlations, was an adding of the precipitation parameter, which clearly made the correlation worse. Thus the reanalysis most likely is predicting the daily precipitation wrong. Also here period 1 seems to be doing worse than period 2 even though the noise within the stacked July annual mean profile is lowest for period 1. It is interesting to notice the difference in mean correlation and the correlation obtained for the stacked profile. Here the reduction of noise when stacking clearly is seen, resulting in a higher stacked correlation.

The discouraging result for the local precipitation-weighted temperatures are also seen in the large scale correlation maps. Fig. 7.4 is showing a reanalysis performing worse both during period 1 and 2, compared to when considering the original 2 m temperature alone. For both periods it is seen that the anticorrelations over Europe have vanished and the positive correlations above Greenland have also been diminished heavily.

According to previous studies of precipitation-weighting using ERA-40 data (Persson et al. [2011]) the correlation between temperature and $\delta^{18}\text{O}$ increases for the Greenland area, but as seen in this study the opposite is the case for the 20CR. This indicates that there are limitations for the capabilities of the 20CR in the Greenland area. Most likely the problem

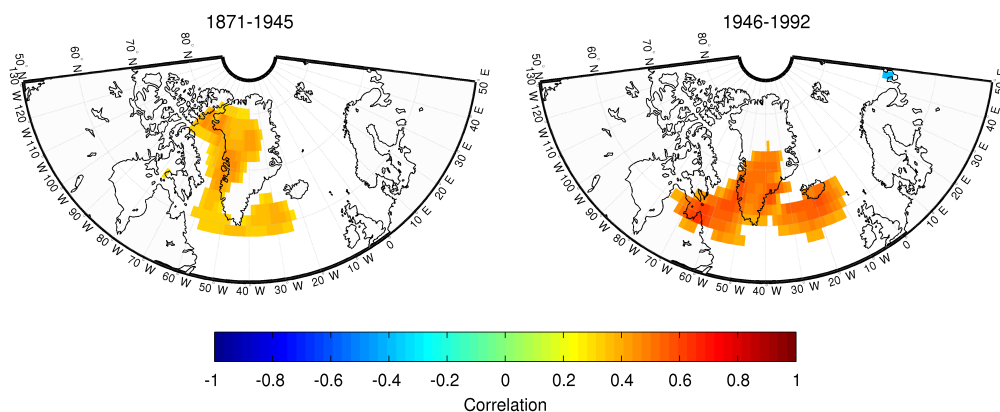


Figure 7.4: Correlation maps of precipitation-weighted temperature from 20CR and mean isotope profiles from the ice cores. July annual mean, period 1 (left) and period 2 (right).

lies within the precipitation parameter, being the most difficult parameter to predict as discovered in the previous analyses (chapter 4 and 5). To discover whether or not the 20CR is relatively better or worse than the ERA-40 in the Greenland area, the exact same comparison done by A. Persson et al. [2011] with respect to time period considered and method used must be executed. This is beyond the scope of this thesis but could be an interesting project for further research.

7.3 Summary

T vs. $\delta^{18}O$

NGRIP is situated in the northern central part of the Greenland ice sheet some distance away from any stations producing assimilation data used within the 20CR. As such the comparison between the proxy parameter $\delta^{18}O$ and temperature from the 20CR was expected to be worse compared to the correlation analyses made for the coastal stations. This was also the case, however, the reanalysis was producing highly significantly positive correlations for period 1 as well as period 2. A difference in correlation when considering the January and July annual mean was not noticed, most likely since the coldest temperatures are not captured by the precipitation and thus the noise created when calculating a January annual mean is not recorded by the isotopes due to the seasonality of precipitation events. Even though the signal in the ice cores is clearest for period 1 the best correlation was still found for period 2 due to the larger amount of assimilation data. The large scale maps (fig. 7.2) do show the significant and positive correlation with a large area of Greenland and the negative correlation with Europe, indicating the influence of the NAO.

T_{pw} vs. $\delta^{18}O$

When considering the precipitation-weighted temperature obtained from the 20CR a better correlation with $\delta^{18}O$ was expected (Persson et al. [2011]) but unfortunately this was not the case. The correlations were still significant and positive at NGRIP but the correlations for all individual cores were lower than if using original temperature, and so was the stacked profile. The large scale maps (fig. 7.4) showed a noticeable difference. Now the anticorrelation over Europe disappeared and the area of significant correlation over Greenland had for period 1 moved further south and was spread out around the 60°N latitude. For the older period the positive correlations were now situated along the west coast of Greenland rather than on both coastal sides. Since previous analyses in this thesis tell that period 2 is the most trustworthy

period, it is seen that the isotope records are more likely to correlate with the southern coast of Greenland. But unlike previous studies reporting the temperatures at the southwest coast to correlate best with isotopes at Central Greenland [(Werner and Heimann [2002]), (Vinther et al. [2010])] it is seen for both precipitation-weighted and original temperature analyses that the area of significant correlations is extending both east and west as far as Iceland and Canada with the same level of correlation. For the original temperature comparison the southern east coast even seems to correlate better with the stacked isotope record, than the southern west coast.

Chapter 8

Conclusion

In this thesis a detailed examination of the correlations between actual observations of temperature and precipitation and the parameter output produced by the 20th Century Reanalysis Project (20CR) has been performed. Furthermore shallow ice cores drilled at the North Greenland Ice Core Project (NGRIP) has been used as another comparison point for actual observations of accumulation. The 20CR was then used to obtain correlations between a stacked isotopic profile and site temperature as well as precipitation-weighted site temperature at NGRIP.

The correlations found between observed and modelled temperatures for observations along the coast of Greenland were significant and positive throughout the period considered (1873-2008), e.i. a mean correlation value of 0.6123 (July). When split into two periods the correlation did, however, improve considerably. The old period (1871-1945, period 1) now produced a value of 0.6219 (July) while the young period (1946-2008, period 2) gave a mean correlation value of 0.6730 (July). This was thought to be due to the amount of assimilation data used in the 20CR to compute the temperature profiles, which increased significantly (see fig. 2.2) for period 2, resulting in better predictions. It was seen that calculating the annual mean from July to July increased the mean correlation values for both periods, as expected (Persson et al. [2011]).

The 20CR seemed to perform best in the southern part of Greenland with a worsening in performance when moving towards higher latitudes for the entire period. This was seen both in the correlation values (table 4.1) as well as in the absolute values (fig. 4.2) where the temperature was highly overestimated at the northern stations (Station Nord, Danmarkshavn, Thule, Illoqqortoormiut and period 1 at Upernavik). From the correlation values for the two periods it was difficult to recognise a worsening when going north for period 1 due to the lack of available observational data. Though from the four stations providing data a trend toward lower correlations when moving north was found.

Most individual stations did produce significant or highly significant correlation values for both periods. Thule was the only station producing insignificant correlations which indicated that this observational data might be poor. It was also the only station not owned and maintained by DMI, suggesting different measuring protocols and thus perhaps unreliable data. The large scale correlation maps strengthened the credibility of the 20CR since it was seen that a high correlation for a large area of Greenland was found for each station, both in period 1 and 2. The anti-correlation with Northern Europe due to the North Atlantic Oscillation (NAO) was also evident. Only Thule and Ivittuut did not depict the same pattern but the length of their observation period could be a reason for this; not necessarily the performance of the 20CR.

The precipitation rate was predicted too high by the 20CR at all coastal stations, as expected (Hanna et al. [2006]). The correlations found between observed and modelled precipitation

rates for observations along the coast of Greenland were significant and positive throughout the period considered (1895-2008), e.i. a mean correlation value of 0.3809 (July). However, a few individual stations did not produce significant correlations for the full time period, e.i. Upernavik, Ilulissat and Nuuk. All of those are situated at the west and north-west side of Greenland which indicated that the lack of published SLP data from the west coast of Greenland had a large influence on the performance of the 20CR. The correlations found for period 1 showed the exact same, e.i. the three stations mentioned produced insignificant correlation values. The southern and eastern parts were, on the other hand, more trustworthy when considering the precipitation rate data from period 1, thus the mean correlation resulted in being significant 0.3213. However, for period 2 all station observations showed significant or highly significant correlation with the 20CR (mean correlation of 0.5033), which was clearly due to the increase in assimilation data.

The difference in seasonality was seen in the correlation values calculated and the large scale correlation maps. Furthermore the effect from the NAO was recognised in the large scale correlation maps as well for period 2, when the appropriate annual mean calculation (January for Upernavik, Ilulissat, Nuuk and Narsarsuaq, and July for Danmarkshavn, Illoqqortoormiut and Tasiilaq, perhaps Ivittuut as well) was chosen. For period 1 only Tasiilaq and Ivittuut produced an image where both the correlation for a large area over Greenland was significant and positive, and an area over Northern Europe was significant and negative, independently of the annual mean calculation being from January or July.

Since the most northern stations (Thule and Station Nord) did not provide any observations of precipitation it was difficult to determine whether or not the 20CR was performing worse when moving north. However, from the relatively high correlations seen at Danmarkshavn and Upernavik for period 2, no indication of a worsening in performance with respect to precipitation rates when moving north was seen.

When moving onto the ice sheet, the comparison between the accumulation rate found in shallow cores and the precipitation rate obtained from the 20CR showed that the 20CR was overestimating the absolute amounts here as well, which was unexpected (Hanna et al. [2006]). Furthermore the precipitation obtained from the 20CR made a shift from one level of approx. $0.55 \frac{m_{ieq}}{yr}$ prior to 1940 to a lower level of approx. $0.4 \frac{m_{ieq}}{yr}$ from the 1940s and onwards. From the *SNR* it was also seen that the accumulation signal within the stacked core was highest for period 1 (1.05 compared to 0.72 for period 2). However, the correlation values with the 20CR were still highest for the youngest period, indicating that the performance of the 20CR was in fact worse during period 1, rather than poor and unreliable observations being part of the cause, as was seen for previous lower correlation values.

The correlation values for the stacked profile for period 1 and 2 were both positive and highly significant, 0.4245 and 0.5957, respectively. These values resembled those found for the precipitation analysis at the east coast of Greenland, which indicated that the NGRIP area is affected by the atmospheric conditions dominating the east side of Greenland where assimilation data is available back to 1894.

This was supported by the large scale correlation maps where the correlation for each grid cell between the stacked accumulation profile and the 20CR precipitation rate was giving positive and significant correlation values at the area around NGRIP both for period 1 and 2.

The correlation between stacked accumulation and 20CR precipitation rates for the full time series was 0.4147, which was less than the correlations for either period. This was due to the shift in precipitation rate seen for the 20CR during the 1940s (also found in (Hanna et al. [2011])). Even though the reanalysis was capable of producing a significant and positive correlation, the absolute amount of precipitation at NGRIP was highly overrated and the daily amounts was thus expected to be unreliable as well.

As a further step the reanalysis data were then used in a comparison with the proxy parameter, $\delta^{18}O$, found in the NGRIP ice cores. It was expected to find a positive correlation with

the site temperature (Paterson [1994]), and this was also achieved, with a correlation value for the full time series of 0.4564, and when split in two, the correlation value for period 1 was 0.4153 and 0.5707 for period two, at best. No significant change between January and July annual mean was noticed, due to the seasonality of the precipitation.

The *SNR* in the stacked profile for the annual $\delta^{18}\text{O}$ values was largest during period 1, as for the accumulation. The correlation, however, was largest for period 2, due to the larger amount of assimilation data. The better correlation for period 2 was also seen in the large scale maps where both the significant correlation above Greenland along with the anticorrelation above Northern Europe, caused by the NAO, were noticed. Previous studies have reported the temperatures at the southwest coast of Greenland to correlate best with isotopes at central Greenland [(Werner and Heimann [2002]), (Vinther et al. [2010])]. However, this was difficult to see from the large scale plots since the area of significant correlation was extending both west and east as far as Canada and Iceland with the same level of correlation, for both periods. One might argue that the southeastern coast of Greenland was correlating better with the stacked isotope record.

The result for the comparison between precipitation-weighted site temperature, T_{pw} , from the 20CR and the stacked isotope profile from NGRIP was worse than for the original temperature comparison above. This was somewhat expected due to the large difference between observations and model prediction found for the accumulation. However, the correlations between the stacked isotope profile and T_{pw} were 0.3933 for the full period, and 0.4602 for period 1 and 0.4809 for period 2, at best. The correlations for the individual periods were larger than for the full time series, due to the shift seen for the precipitation rate in the 20CR.

The worsening of the correlation when using T_{pw} rather than T , was clearly seen in the large scale correlation maps. The anticorrelation over Europe disappeared and the area of significant correlation over Greenland had for period 2 moved south and covered an area on both sides of Greenland, indicating that isotopes found at Central Greenland correlate with temperatures found at the southwest coast, as well as the southeast coast of Greenland. However, the unreliable precipitation data obtained from the 20CR made it impossible to conclude anything.

In summary, the 20CR was overall producing positive and significant correlations for the entire Greenland area for the full time period, when considering the temperature parameter. The calculation of an annual mean from July to July increased the correlation for both periods as well. A general decrease in correlation values and an increasing underestimation of absolute values were seen when moving north, both for period 1 and 2. A difference in performance from the east coast to the west for both periods was not noticed. The correlation pattern resulting from the NAO was evident in both periods, however, clearest for period 2. The precipitation rate from the 20CR was estimated too high along the coast, however it did produce significant and positive correlations for every station for period 2. The correlations for period 1 was not as good, since the stations at the west coast of Greenland were unable to produce significant correlation values. Only stations on the east and south (Tasiilaq and Ivittuut) coast of Greenland were giving a significant correlation value for period 1. A general decrease in correlation values when moving north was not seen, however the worsening in performance when comparing the east coast to the west for period 1 was clearly noticed. The difference in seasonality of precipitation events was recognised in the calculation correlations using an annual mean from January vs. July.

The precipitation rate modelled for the central ice sheet at NGRIP was also highly overestimated. Furthermore two levels for the profile was noticed, shifting in the 1940s. A highest correlation was found for period 2, despite the accumulation signal from the ice core stacking being clearest for period 1. However, a significant and positive correlation was found for both periods.

Finally the correlation between $\delta^{18}\text{O}$ and site temperature resulted in significant and positive correlations for the full time period. The large scale correlation pattern caused by the NAO was noticed as well. When calculating a precipitation-weighted annual mean temperature the correlation decreased for the full time period, due to the likely wrong daily precipitation rates modelled by the 20CR. This was clearly noticed in the large scale correlation maps as well as for the on-site correlation values.

Hence even though the 20CR was globally tested to perform well back to 1871, it does have some limitations, both spatially and temporally, when focusing on the Greenland area.

Chapter 9

Outlook

As discovered throughout the analyses made in the thesis, the 20CR is having difficulties producing the correct parameter values for the Greenland area when moving far back in time, e.i. back to 1871. This is mainly due to the low amounts of assimilation data available for the 20CR, as seen in fig. 2.3. However, many stations at the west coast of Greenland have been measuring the meteorological parameters needed for the 20CR for a lot longer than what is presently available. For instance did the stations in Upernavik, Ilulissat, Nuuk and Ivittuut began observations of both pressure and temperature in 1873-1875 (Lauersen [2003]) but the daily data have not been digitised and published yet. Today the stations mentioned does not provide data usable for the 20CR until 1948. Therefore only data from Tasiilaq is available back to 1894 (2012f), which clearly has large consequences for the performance of the 20CR in the Greenland area. It would be highly preferable if such data could become available for the International Surface Pressure Databank (ISPD) and hence be used within the 20CR.

The data produced from the 20CR can be used for a variety of purposes. As mentioned E. Hanna et al. [2011] have produced a surface mass balance model by the use of precipitation, temperature, surface latent heat and runoff obtained from the 20CR. It is of high interest at present to determine the state of the Greenland ice sheet and how it is responding to climate changes, due to the modelled projections for sea level rise. This can be done by examining how the ice sheet has behaved previously, for instance when coming out of the the late 19th Century cold period and also when reaching the very high level of temperatures at Greenland occurring during the 1930s and 1940s (2012g). However, an accurate precipitation rate is aquired and here the 20CR is not adequate yet.

As seen the reanalysis can also be used for correlating proxy parameters to meteorological features, which was done here for the precipitation-weighting of temperatures to match the isotopic profile (Persson et al. [2011]). Other proxy parameters may be correlated to reanalysis outputs, such as atmospherical content of CO₂, CH₄, dust and so forth found in ice cores, tree-ring widths, the North Atlantic ice berg flux, pollen measurements from sediment and ice cores and so on. They are all in some way correlated to the atmosphere-land system which is described by the reanalysis output.

Specifically it would be interesting to examine the temperature where the precipitation was formed and correlate this to the isotopic profiles found in ice cores. This can be done since the reanalysis provide 24 pressure levels along with temperature and precipitation on a sub-synoptic scale. If a method for determining in which level precipitation is formed can be formulated, it will be possible to both find and precipitation-weight the temperatures.

Also it could be worth investigating the change in pressure fields back in time and the possible effects on isotopes in ice cores. A correlation may be evident which could improve the understanding of the variability of the isotopes when considering other climatic regimes than the present. A possible effect might be unimportant for todays climate regime but could have a larger impact for a colder climate such as the previous ice age.

Bibliography

2004a.

http://www.gfy.ku.dk/www-glac/ngrip/index_eng.htm.
[Online; accessed 20-June-2012].

2005a.

<http://www.fgse.nova.edu/edl/secure/stats/lesson6.htm>.
[Online; accessed 5-July-2012].

2005b.

[http://faculty.fortlewis.edu/chew_b/documents/table of critical values for pearson correlation.htm](http://faculty.fortlewis.edu/chew_b/documents/table_of_critical_values_for_pearson_correlation.htm).
[Online; accessed 5-July-2012].

2005c.

http://www.dmi.dk/dmi/ny_vejrsatellit_op_i_nat.
[Online; accessed 9-July-2012].

2006a.

<http://www.oneonta.edu/faculty/vomsaaw/w/psy220/files/signifofcorrelations.htm>.
[Online; accessed 20-June-2012].

2009a.

<http://www.ua.nws.noaa.gov/factsheet.htm>.
[Online; accessed 9-July-2012].

2011a.

<http://www.mad.zmaw.de/projects-at-md/era40/remarks/index.html>.
[Online; accessed 3-July-2012].

2011b.

<http://cires.colorado.edu/science/groups/steffen/gcnet/aws.html>.
[Online; accessed 9-July-2012].

2011c.

http://www.weatherquestions.com/how_do_weather_satellites_work.htm.
[Online; accessed 9-July-2012].

2012a.

http://www.ats.ucla.edu/stat/mult_pkg/faq/general/tail_tests.htm.
[Online; accessed 20-June-2012].

2012b.

<http://www.iceandclimate.nbi.ku.dk>.
[Online; accessed 20-June-2012].

2012c.

<http://www.esrl.noaa.gov/psd/>.
[Online; accessed 4-July-2012].

- 2012d.
http://www.eso.org/public/images/img_4773-potw/.
[Online; accessed 9-July-2012].
- 2012e.
http://www.esa.int/specials/msg/semjrg2vw3h_0.html.
[Online; accessed 9-July-2012].
- 2012f.
http://reanalyses.org/sites/default/files/groups/users/gilbert.p.compo/ispd_history_v2.2.4.txt.
[Online; accessed 20-July-2012].
- 2012g.
http://www.dmi.dk/dmi/en/index/klima/klimaet_indtil_nu/temperaturen_i_groenland.htm.
[Online; accessed 25-July-2012].
- W. Ambach, W. Dansgaard, H. Eisner, and J. Moller.
The altitude effect on isotopic composition of precipitation and glaciers ice in alps.
Tellus, 20(4), 1968.
- R. C. Bales, Q. Guo, D. Shen, J. R. McConnell, G. Du, J. F. Burkhart, V. B. Spikes, E. Hanna, and J. Cappelén.
Annual accumulation for Greenland updated using ice core data developed during 2000-2006 and analysis of daily coastal meteorological data.
Journal of Geophysical Research - Atmospheres, 114, MAR 27 2009.
- L. Boas and P. R. Wang.
Weather and Climate Data from Greenland 1958-2010.
Technical Report 11-15, Danish Meteorological Institute, 2011.
- M. J. Brettle and J. F. P. Galvin.
Back to basics: Radiosondes: Part 1 - the instrument.
Weather, 57, SEP 2003.
- R. Brugge and M. Stuttard.
Back to basics: From sputnik to envisat, and beyond: The use of satellite measurements in weather forecasting and research: Part 1 - a history.
Weather, 58, 2003.
- J. Cappelén.
DMI monthly climate data collection 1768-2010, Denmark, The Faroe Islands and Greenland.
Technical Report 11-05, Danish Meteorological Institute, 2011.
- J. Cappelén, B. V. Jørgensen, E. V. Laursen, L. S. Stannius, and R. S. Thomsen.
The observed climate of Greenland, 1958-99 - with climatological standard normals, 1961-90.
Technical Report 00-18, Danish Meteorological Institute, 2001.
- C. D. Charles, D. Rind, J. Jouzel, R. D. Koster, and R. G. Fairbanks.
Glacial-interglacial changes in moisture sources for Greenland - Influences on the ice core record of climate.
Science, 263(5146):508-511, 1994.
- P. Chylek, M. K. Dubey, and G. Lesins.
Greenland warming of 1920-1930 and 1995-2005.
Geophysical Research Letter, 33(11), JUN 13 2006.

- H. B. Clausen and C. U. Hammer.
The Laki and Tambora eruptions as revealed in Greenland ice cores from 11 locations.
Annals of Glaciology, 10:16–22, 1988.
- A. M. Closter, R. M. Closter, J. Cappelen, J. H. Christensen, K. Christoffersen, and C. Kern-Hansen.
Temperature measurements in Copenhagen from 1767 to 1860.
Technical Report 06-13, Danish Meteorological Institute, 2006.
- G. P. Compo, J. S. Whitaker, and P. D. Sardeshmukh.
The 20th century reanalysis project.
American Meteorological Society, 2006.
- G. P. Compo, J. S. Whitaker, and P. D. Sardeshmukh.
The 20th century reanalysis project.
Unpublished, 2008.
- G. P. Compo, J. S. Whitaker, P. D. Sardeshmukh, N. Matsui, R. J. Allan, X. Yin, B. E. Gleason, Jr., R. S. Vose, G. Rutledge, P. Bessemoulin, S. Broennimann, M. Brunet, R. I. Crouthamel, A. N. Grant, P. Y. Groisman, P. D. Jones, M. C. Kruk, A. C. Kruger, G. J. Marshall, M. Maugeri, H. Y. Mok, O. Nordli, T. F. Ross, R. M. Trigo, X. L. Wang, S. D. Woodruff, and S. J. Worley.
The Twentieth Century Reanalysis Project.
Quarterly Journal of the Royal Meteorological Society, 137(654, Part a):1–28, JAN 2011.
- K. M. Cuffey and W. S. B. Paterson.
The physics of glaciers.
Elsevier, fourth edition edition, 2010.
- D. Dahl-Jensen and S. L. Buchardt.
Field Season Report 2001.
University of Copenhagen, 2001.
- D. Dahl-Jensen and S. L. Buchardt.
Field Season Report 2003.
University of Copenhagen, 2003.
- D. Dahl-Jensen and S. L. Buchardt.
Field Season Report 2004.
University of Copenhagen, 2004.
- D. Dahl-Jensen, S. J. Johnsen, C. Hammer, and J. Jouzel.
Past accumulation rates derived from the observed annual layers in the grip ice core from summit, central greenland.
Contribution to the Greenland Ice-core Project (GRIP), 1993.
- D. Dahl-Jensen, N. S. Gundestrup, K. Keller, S. J. Johnsen, S. P. Gogineni, C. T. Allen, T. S. Chuah, H. Miller, S. Kipfstuhl, and E. D. Waddington.
A search in north Greenland for a new ice-core drill site.
Journal of Glaciology, 1997.
- W. Dansgaard and Johnsen.
Stable Isotope Glaciology.
Tellus, 16(4):436–468, 1964.
- W. Dansgaard and S. J. Johnsen.
A flow model and a time scale for the ice core from camp century, greenland.
Journal of Glaciology, 8(53), 1969.

- W. Dansgaard, S. J. Johnsen, H. B. Clausen, and N. Gundestrup.
Stable Isotope Glaciology.
Kommisionen for Videnskabelige Undersøgelser i Grønland, 1973.
København, C. A. Reitzels Forlag.
- D. A. Fisher, N. Reeh, and H. B. Clausen.
Stratigraphic noise in time series derived from ice cores.
Annals of Glaciology, 7, 1985.
- P. Frich, H. Alexandersson, J. Ashcroft, B. Dahlström, G. R. Demarée, A. Drebs, A. F. V. van Engelen, E. J. Førland, I. Hanssen-Bauer, R. Heino, T. Jónsson, K. Jonasson, L. Keegan, P. O. Nordli, T. Schmidt, P. Steffensen, H. Tuomenvirta, and O. E. Tveito.
North atlantic climatological dataset (nacd version 1) - final report.
Technical report, Danish Meteorological Institute, 1996.
- N. Gundestrup.
Field Season Report 1997.
University of Copenhagen, 1997.
- E. Hanna, J. McConnell, S. Das, J. Cappelen, and A. Stephens.
Observed and modeled Greenland ice sheet snow accumulation, 1958-2003, and links with regional climate forcing.
Journal of Climate, 19(3):344–358, FEB 1 2006.
- E. Hanna, P. Huybrechts, J. Cappelen, K. Steffen, R. C. Bales, E. Burgess, J. R. McConnell, J. P. Steffensen, M. Van den Broeke, L. Wake, G. Bigg, M. Griffiths, and D. Savas.
Greenland Ice Sheet surface mass balance 1870 to 2010 based on Twentieth Century Re-analysis, and links with global climate forcing.
Journal of Geophysical Research - Atmospheres, 116, DEC 2011.
- C. S. Hvidberg, A. Svensson, and S. L. Buchardt.
Dynamics of the greenland ice sheet.
Elsevier B.V., 2007.
- S. J. Johnsen.
Stable isotope homogenization of polar firn and ice.
Proc. Symp. on Isotopes and Impurities in Snow and Ice, I.U.G.G. XVI, General Assembly, Grenoble, Aug. Sep., 1975, 1977.
- S. J. Johnsen.
Isotopes in natural waters, 1986.
Unpublished notes.
- S. J. Johnsen and B. M. Vinther.
Greenland stable isotopes.
Elsevier B.V., 2007.
- S. J. Johnsen, H. B. Clausen, K. M. Cuffey, G. Hoffmann, J. Schwander, and T. Creyts.
Diffusion of stable isotopes in polar firn and ice: the isotope effect in firn diffusion.
Physics of Ice Core Records, 2000.
- S. J. Johnsen, W. Dansgaard, and J. W. C. White.
The origin of Arctic precipitation under present and glacial conditions.
Tellus series B - Chemical and Physical Meteorology, 41(4):452–468, 1989.
- S. J. Johnsen, H. B. Clausen, W. Dansgaard, N. S. Gundestrup, C. U. Hammer, U. Andersen, K. K. Andersen, C. S. Hvidberg, D. Dahl-Jensen, J. P. Steffensen, H. Shoji, A. E. Sveinbjornsdottir, J. White, J. Jouzel, and D. Fisher.

-
- The delta O-18 record along the Greenland Ice Core Project deep ice core and the problem of possible Eemian climatic instability.
Journal of Geophysical Research - Oceans, 102(C12):26397–26410, NOV 30 1997.
- A. M. K. Jørgensen and J. Cappelen.
Klimaændringer de seneste 150 år.
Aktuel Naturvidenskab, 2007.
- E. Kalnay, M. Kanamitsu, R. Kistler, W. Collins, D. Deaven, L. Gandin, M. Iredell, S. Saha, G. White, J. Woollen, Y. Zhu, M. Chelliah, W. Ebisuzaki, W. Higgins, J. Janowiak, K. C. Mo, C. Ropelewski, J. Wang, A. Leetmaa, R. Reynolds, R. Jenne, and D. Joseph.
The NCEP/NCAR 40-year reanalysis project.
Bulletin of the American Meteorological Society, 77(3):437–471, MAR 1996.
- R. Kistler, E. Kalnay, W. Collins, S. Saha, G. White, J. Woollen, M. Chelliah, W. Ebisuzaki, M. Kanamitsu, V. Kousky, H. van den Dool, R. Jenne, and M. Fiorino.
The NCEP-NCAR 50-year reanalysis: Monthly means CD-ROM and documentation.
Bulletin of the American Meteorological Society, 82(2):247–267, 2001.
- E. V. Lauersen.
metadata, selected climatological and synoptic stations, 1750-1996.
Technical Report 03-24, Danish Meteorological Institute, 2003.
- A. Ohmura and N. Reen.
New precipitation and accumulation maps for Greenland.
Journal of Glaciology, 37(125):140–148, 1991.
- W. S. B. Paterson.
The physics of glaciers.
Butterworth-Heinemann, 1994.
Third Edition.
- A. Persson, P. L. Langen, P. Ditlevsen, and B. M. Vinther.
The influence of precipitation weighting on interannual variability of stable water isotopes in Greenland.
Journal of Geophysical Research - Atmospheres, 116, OCT 26 2011.
- E. M. Pugh and G. H. Winslow.
The Analysis of Physical Measurements.
Addison-Wesley, 1966.
- G. D. Quartly, T. H. Guymer, and K. G. Birch.
Back to basics: Measuring rainfall at sea: Part 1 - in situ sensors.
Weather, 57, 2002.
- S. O. Rasmussen, K. K. Andersen, A. M. Svensson, J. P. Steffensen, B. M. Vinther, H. B. Clausen, M. L. Siggaard-Andersen, S. J. Johnsen, L. B. Larsen, D. Dahl-Jensen, M. Bigler, R. Rothlisberger, H. Fischer, K. Goto-Azuma, M. E. Hansson, and U. Ruth.
A new Greenland ice core chronology for the last glacial termination.
Journal of Geophysical Research - Atmospheres, 111, 2006.
- N. A. Rayner, D. E. Parker, E. B. Horton, C. K. Folland, L. V. Alexander, D. P. Rowell, E. C. Kent, and A. Kaplan.
Global analyses of sea surface temperature, sea ice, and night marine air temperature since the late nineteenth century.
Journal of Geophysical Research - Atmospheres, 108(D14), JUL 17 2003.
-

- W. F. Ruddiman.
Earth's Climate.
W. H. Freeman and Company, third edition edition, 2008.
- J. Schwander, J. M. Barnola, C. Andrie, M. Leunberger, A. Ludin, D. Raynard, and B. Stauffer.
The age of the air in the firn and ice at Summit, Greenland.
Journal of Geophysical Research - Atmospheres, 98(D2):2831–2838, 1993.
- H. C. Steen-Larsen, V. Masson-Delmotte, J. Sjolte, S. J. Johnsen, B. M. Vinther, F. M. Breon, H. B. Clausen, D. Dahl-Jensen, S. Falourd, X. Fettweis, H. Gallee, J. Jouzel, M. Kageyama, H. Lerche, B. Minster, G. Picard, H. J. Punge, C. Risi, D. Salas, J. Schwander, K. Steffen, A. E. Sveinbjornsdottir, A. Svensson, and J. White.
Understanding the climatic signal in the water stable isotope records from the NEEM shallow firn/ice cores in northwest Greenland.
Journal of Geophysical Research - Atmospheres, 116, MAR 22 2011.
- K. Steffen and J. Box.
Surface climatology of the Greenland ice sheet: Greenland Climate Network 1995-1999.
Journal of Geophysical Research, 106(D24):33951–33964, 2001.
- D. Steinhage, O. Eisen, and H. B. Clausen.
Regional and temporal variation of accumulation around NorthGRIP derived from ground-penetrating radar.
In Dowdeswell, J and Willis, IC, editor, *Annals of Glaciology, VOL 42, 2005*, volume 42 of *Annals of Glaciology*, pages 326–330, 2005.
International Symposium on Arctic Glaciology, Geilo, Norway, Aug 23-27, 2004.
- D. Stockburger.
Introductory Statistics: Concepts, Models, and Applications.
Atomic Dog Publishing, second edition edition, 2001.
- P. Stott and J. Kettleborough.
Origins and estimates of uncertainty in predictions of twenty-first century temperature rise.
Nature, 416(6882):723–726, APR 18 2002.
- I. Strangeways.
Back to basics: The 'met. enclosure': Part 4 - temperature.
Weather, 54(9), SEP 1999.
- I. Strangeways.
Back to basics: The 'met. enclosure': Part 9(a) - automatic weather stations: Temperature, humidity, barometric pressure and wind.
Weather, 58, 2003a.
- I. Strangeways.
Back to basics: The 'met. enclosure': Part 9(b) - automatic weather stations: Radiation, evaporation, precipitation, ocean buoys and cold regions.
Weather, 58, 2003b.
- I. Strangeways.
Back to basics: The 'met. enclosure': Part 12 - telemetry by satellite.
Weather, 60(2), FEB 2005.
- J. R. Taylor.
Error Analysis.
University Science Books, second edition edition, 1997.

- S. M. Uppala, P. W. Kallberg, A. J. Simmons, U. Andrae, V. D. Bechtold, M. Fiorino, J. K. Gibson, J. Haseler, A. Hernandez, G. A. Kelly, X. Li, K. Onogi, S. Saarinen, N. Sokka, R. P. Allan, E. Andersson, K. Arpe, M. A. Balmaseda, A. C. M. Beljaars, L. Van De Berg, J. Bidlot, N. Bormann, S. Caires, F. Chevallier, A. Dethof, M. Dragosavac, M. Fisher, M. Fuentes, S. Hagemann, E. Holm, B. J. Hoskins, L. Isaksen, P. A. E. M. Janssen, R. Jenne, A. P. McNally, J. F. Mahfouf, J. J. Morcrette, N. A. Rayner, R. W. Saunders, P. Simon, A. Sterl, K. E. Trenberth, A. Untch, D. Vasiljevic, P. Viterbo, and J. Woollen.
The ERA-40 re-analysis.
Quarterly Journal of the Royal Meteorological Society, 131(612, Part b):2961–3012, OCT 2005.
- B. M. Vinther, P. D. Jones, K. R. Briffa, H. B. Clausen, K. K. Andersen, D. Dahl-Jensen, and S. J. Johnsen.
Climate Signal in Multiple Highly Resolved Stable Isotope Records from Greenland.
Quaternary Science Reviews, 29:522–538, 2010.
- B. M. Vinther, K. K. Andersen, P. D. Jones, K. R. Briffa, and J. Cappelen.
Extending Greenland temperature records into the late eighteenth century.
Journal of Geophysical Research - Atmospheres, 111(D11), JUN 6 2006.
- B. M. Vinther, S. L. Buchardt, H. B. Clausen, D. Dahl-Jensen, S. J. Johnsen, D. A. Fisher, R. M. Koerner, D. Raynaud, V. Lipenkov, K. K. Andersen, T. Blunier, S. O. Rasmussen, J. P. Steffensen, and A. M. Svensson.
Holocene thinning of the Greenland ice sheet.
Nature, 461(7262), 2009.
- M. Werner and M. Heimann.
Modeling interannual variability of water isotopes in Greenland and Antarctica.
Journal of Geophysical Research - Atmospheres, 107(D1-D2), JAN 2002.
doi: 10.1029/2001JD900253.
- J. W. C. White, L. K. Barlow, D. Fisher, P. Grootes, J. Jouzel, S. J. Johnsen, M. Stuiver, and H. Clausen.
The climate signal in the stable isotopes of snow from Summit, Greenland: Results of comparisons with modern climate observations.
Journal of Geophysical Research - Oceans, 102(C12):26425–26439, NOV 30 1997.
- Wonders, W.C.
Canada's Changing North.
McGill-Queen's University Press, 1971.

Appendix A

Figures

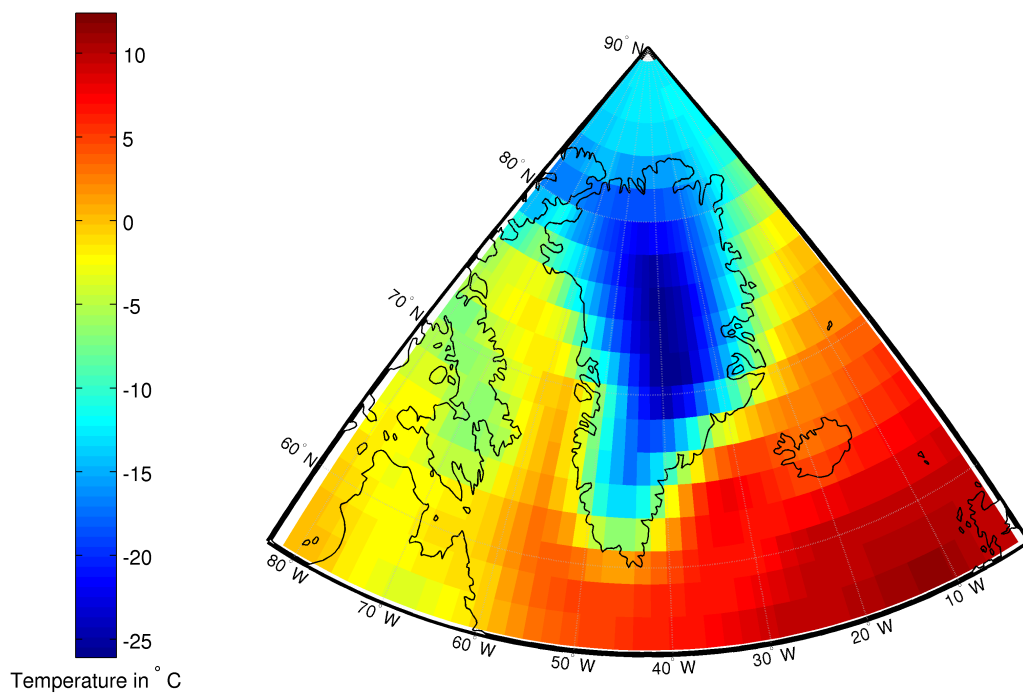


Figure A.1: Map of Greenland. Average temperature from the 20CR 1873-2008. Blowup of fig. 3.3 (left).

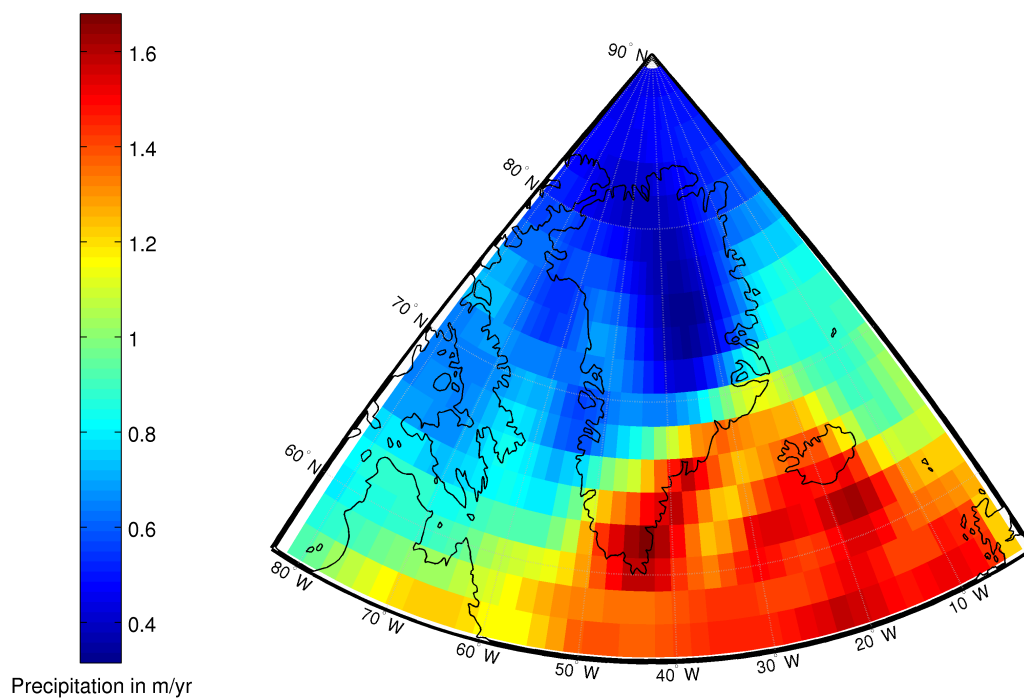


Figure A.2: Map of Greenland. Average precipitation from the 20CR 1873-2008. Blowup of fig. 3.3 (right).

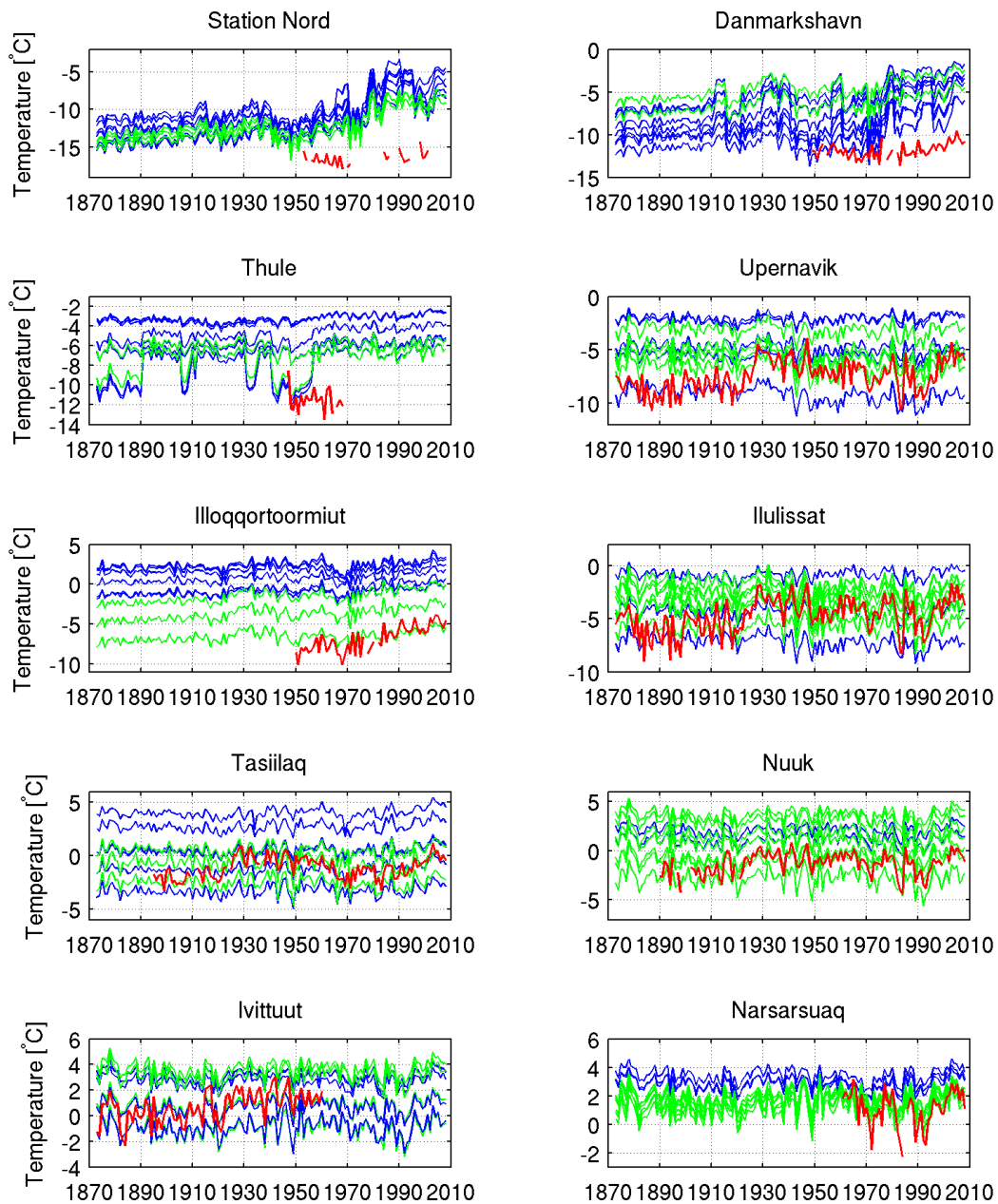


Figure A.3: January annual 2m temperature for all stations. Nine closest grid cells from 20CR (land grids; green, water grids; blue) and observations (red). The 20CR profiles have been height-corrected.

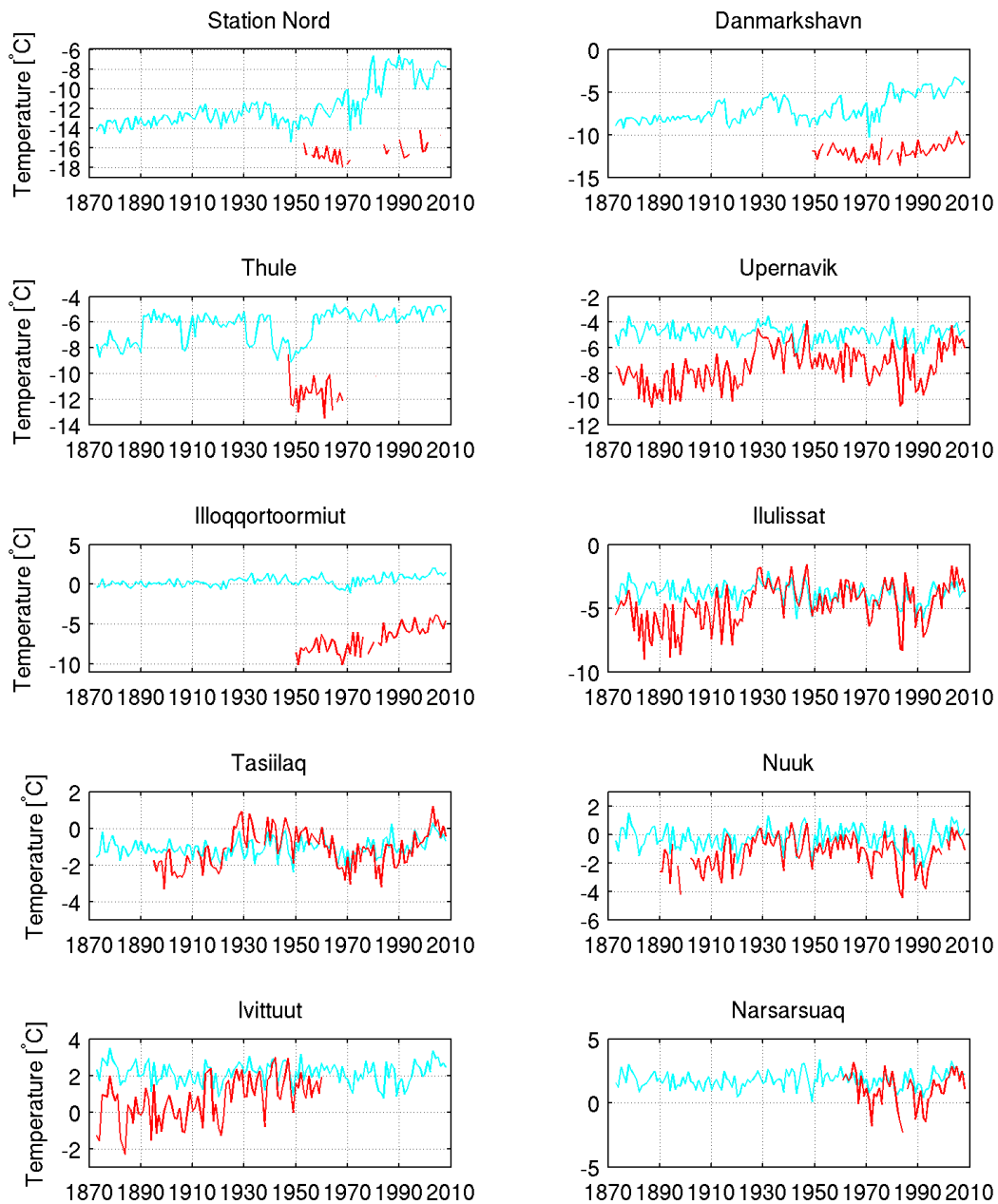


Figure A.4: January annual 2m temperature for all stations. Mean 20CR for nine closest grid cells (cyan) and observations (red). The 20CR profiles have been height- and position-corrected.

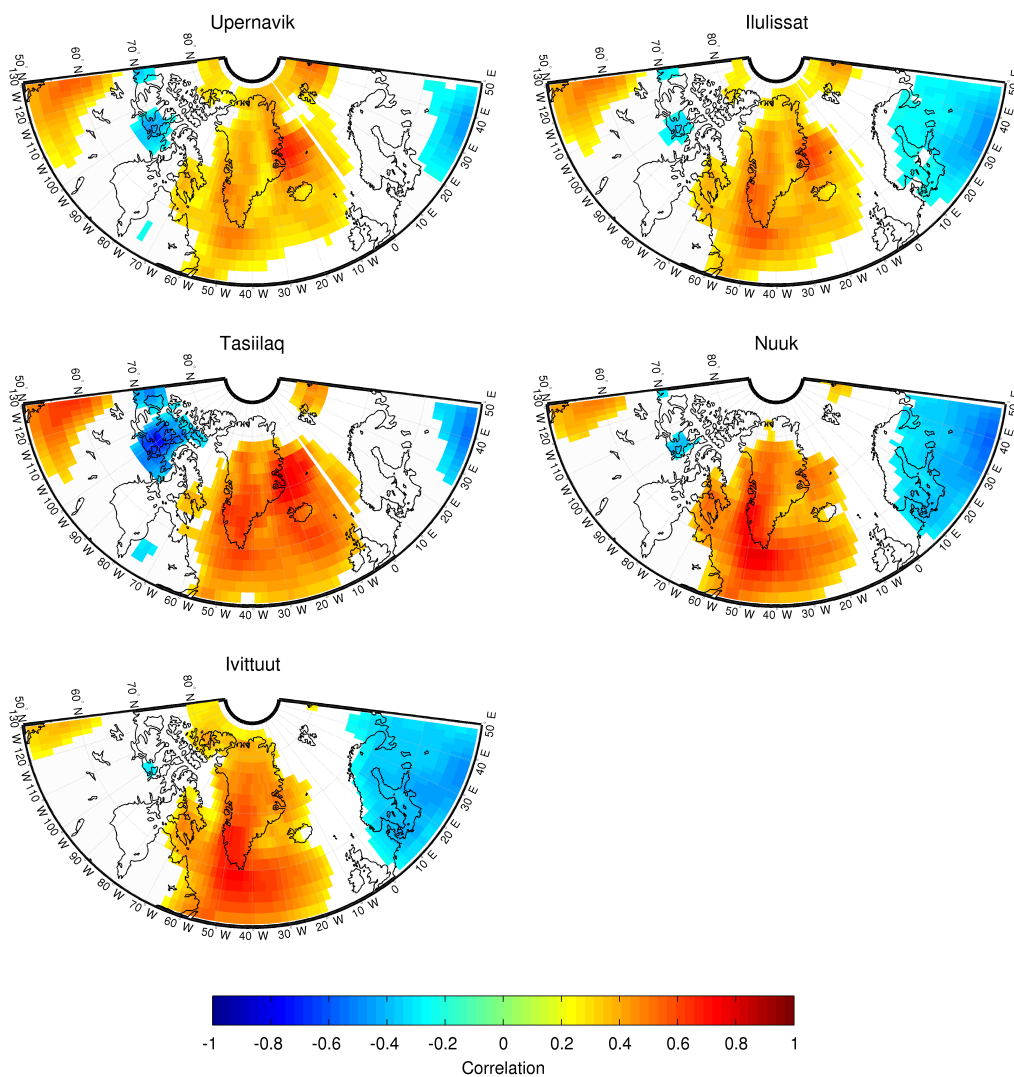


Figure A.5: Correlation maps of temperature between each station and 20CR. January annual mean, period 1. Only significant correlations are shown.

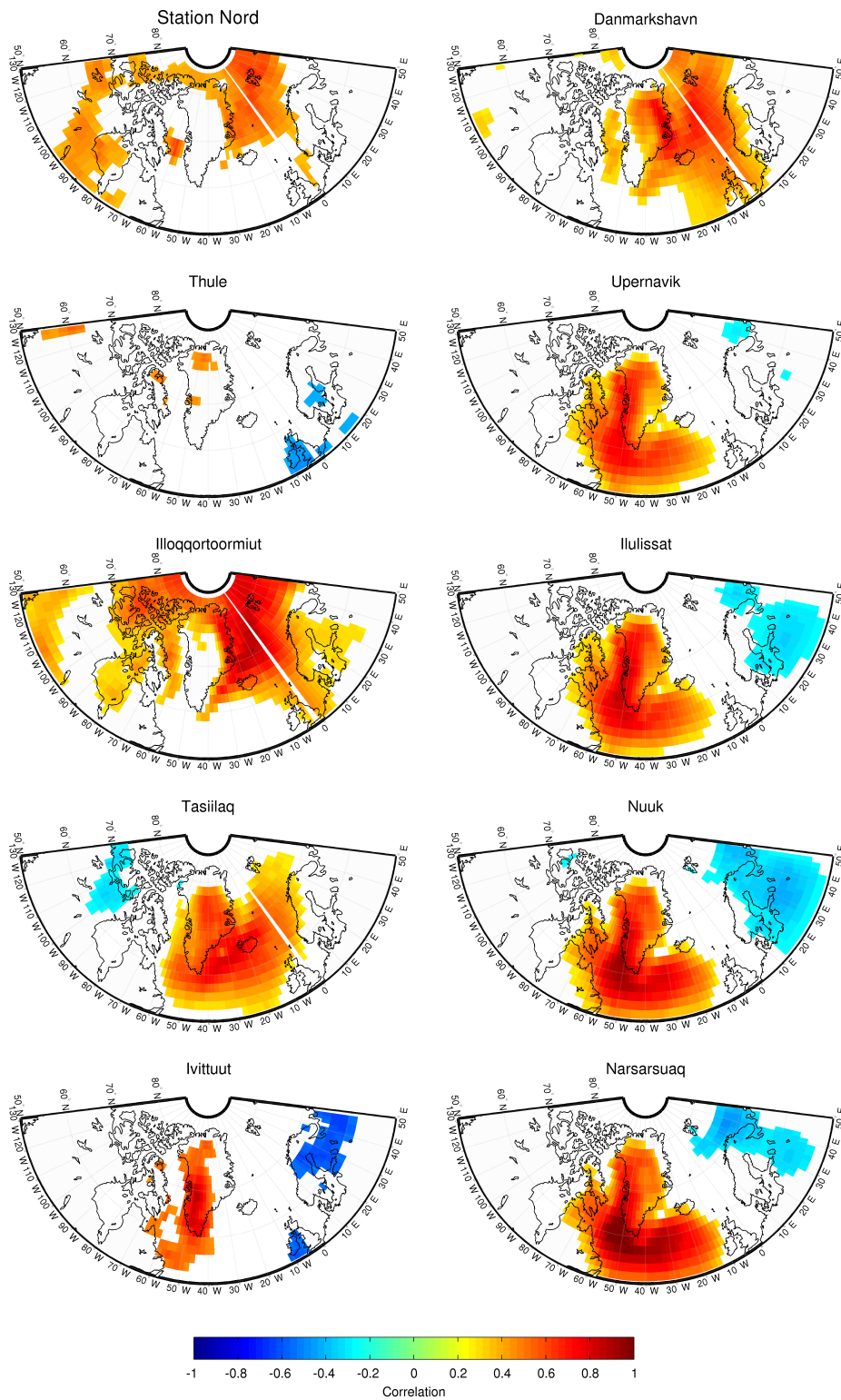


Figure A.6: Correlation maps of temperature between each station and 20CR. January annual mean, period 2. Only significant correlations are shown.

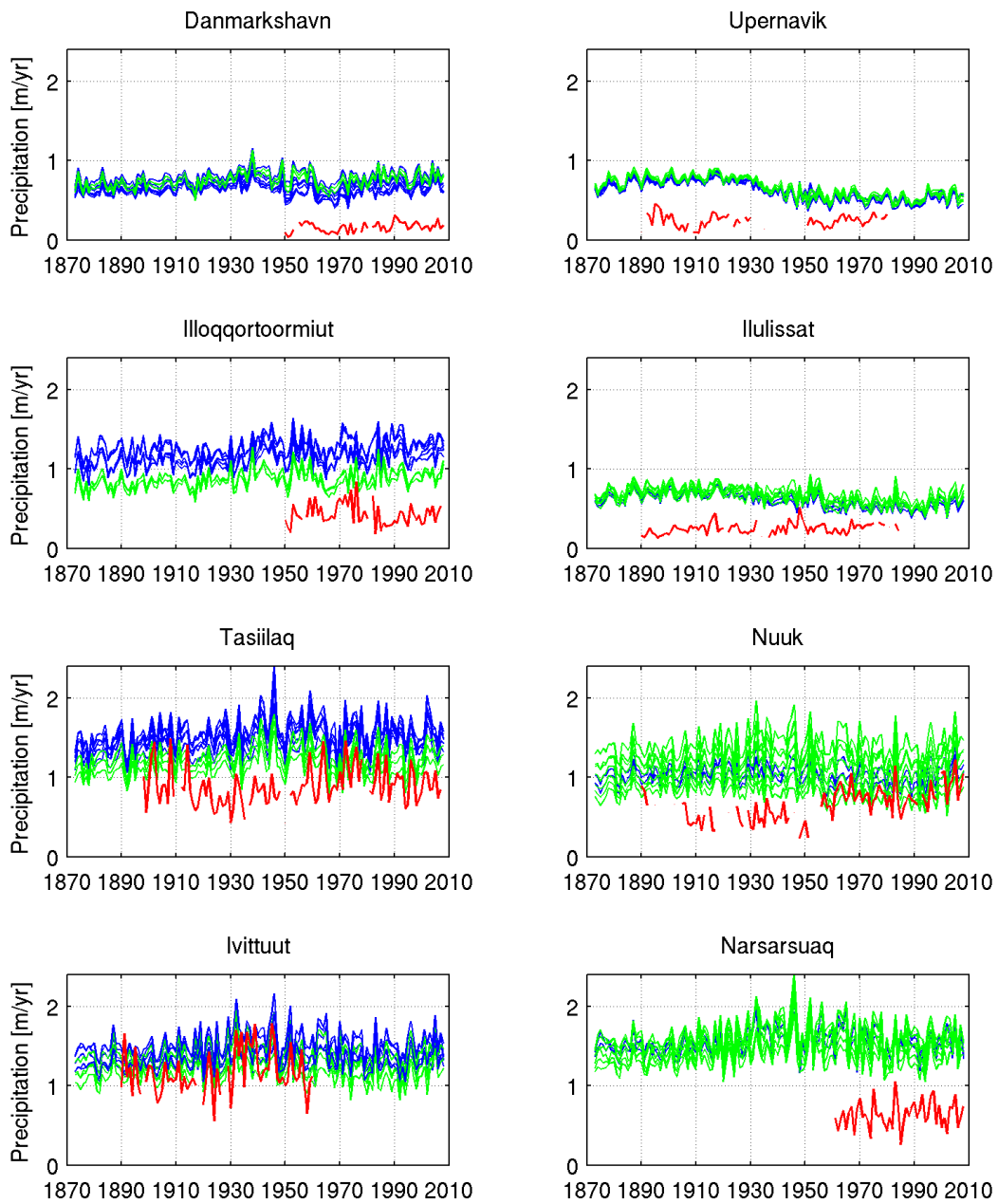


Figure A.7: January annual precipitation rates for all stations. Nine closest grid cells from 20CR (land grids; green, water grids; blue) and observations (red). The 20CR profiles have been height-corrected.

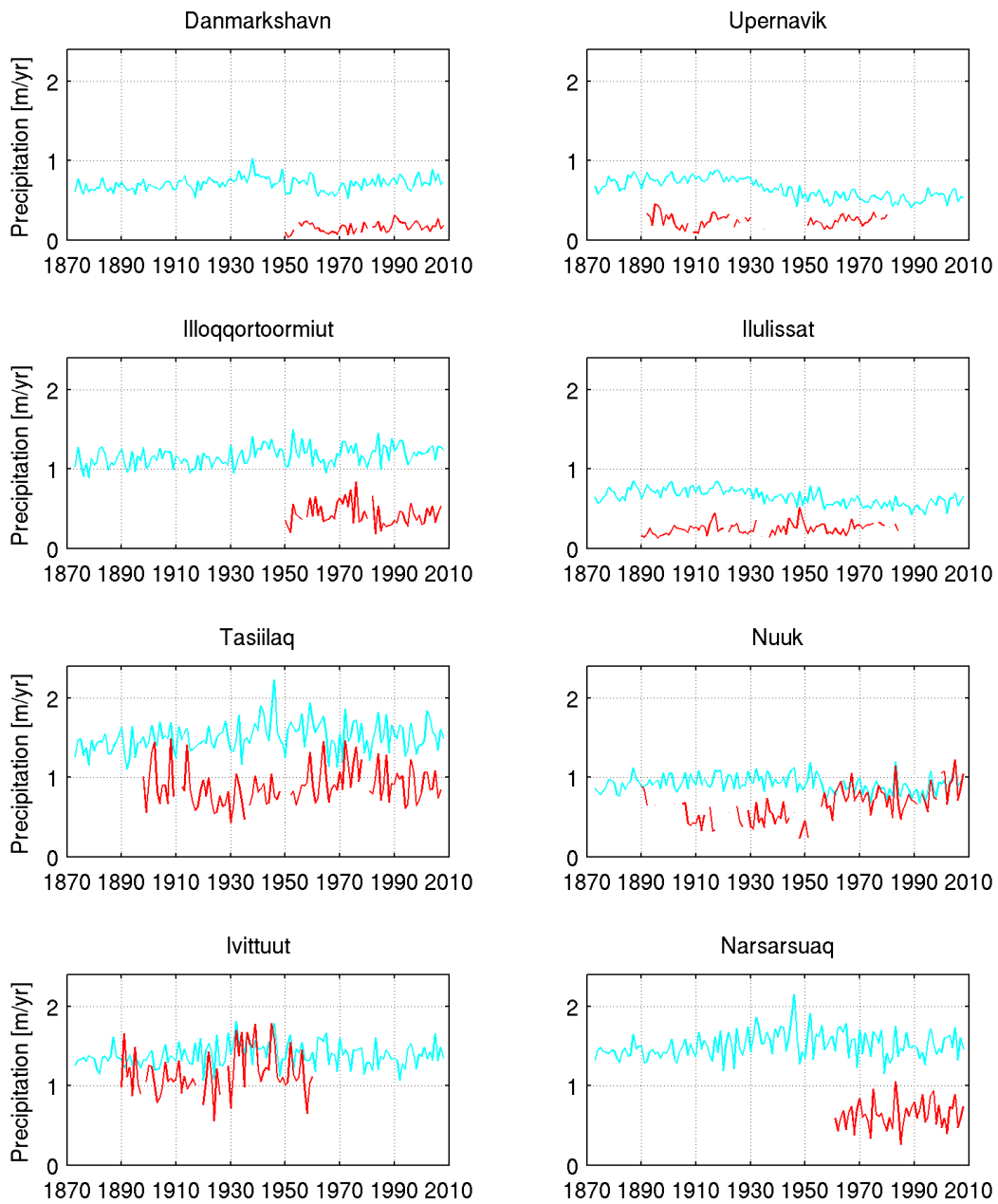


Figure A.8: January annual precipitation rates for all stations. Mean 20CR for nine closest grid cells (cyan) and observations (red). The 20CR profiles have been height- and position-corrected.

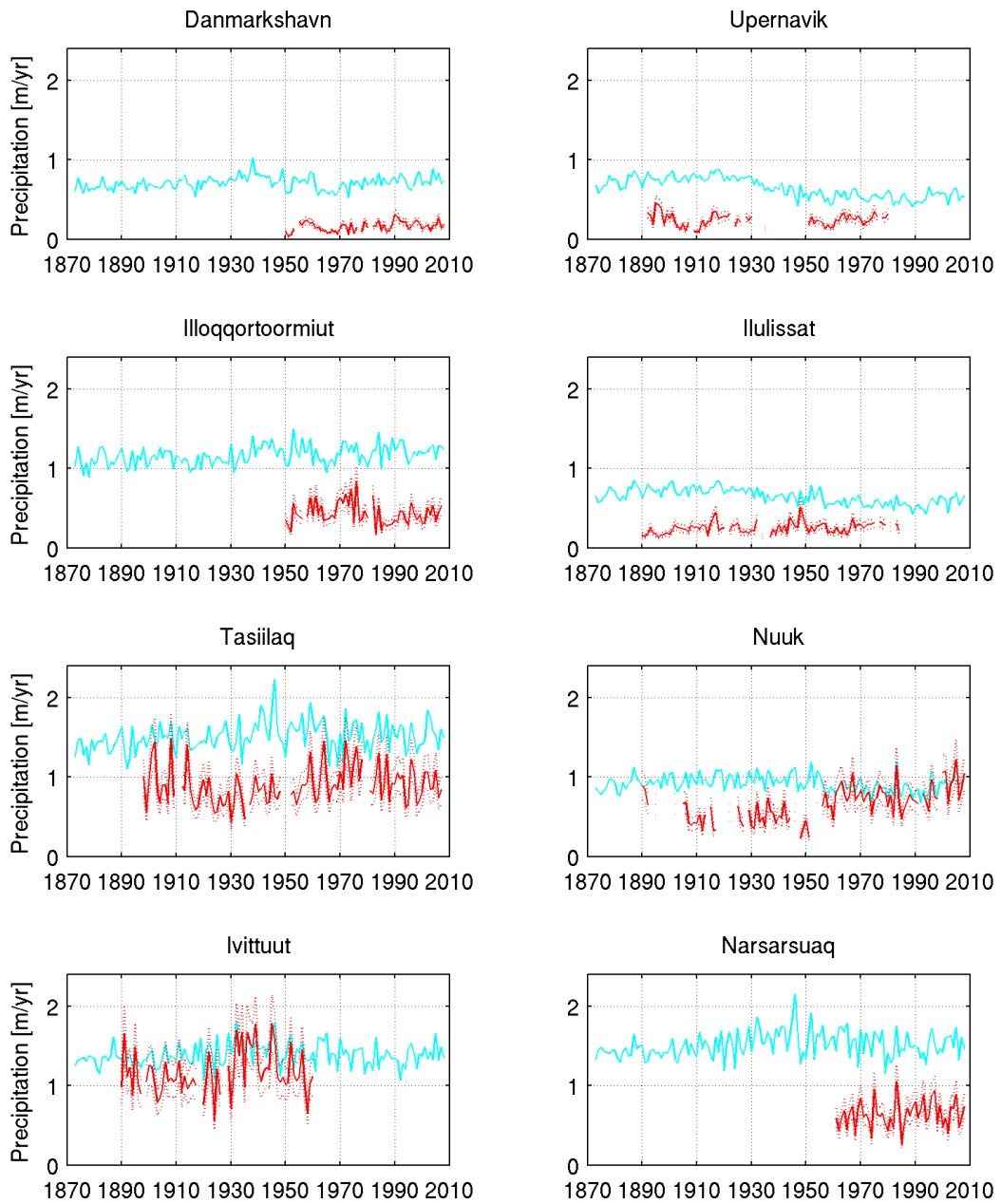


Figure A.9: January annual precipitation rates for all stations. Mean 20CR for nine closest grid cells (cyan) and observations (red) with an uncertainty of $\pm 20\%$. The 20CR profiles have been height- and position-corrected.

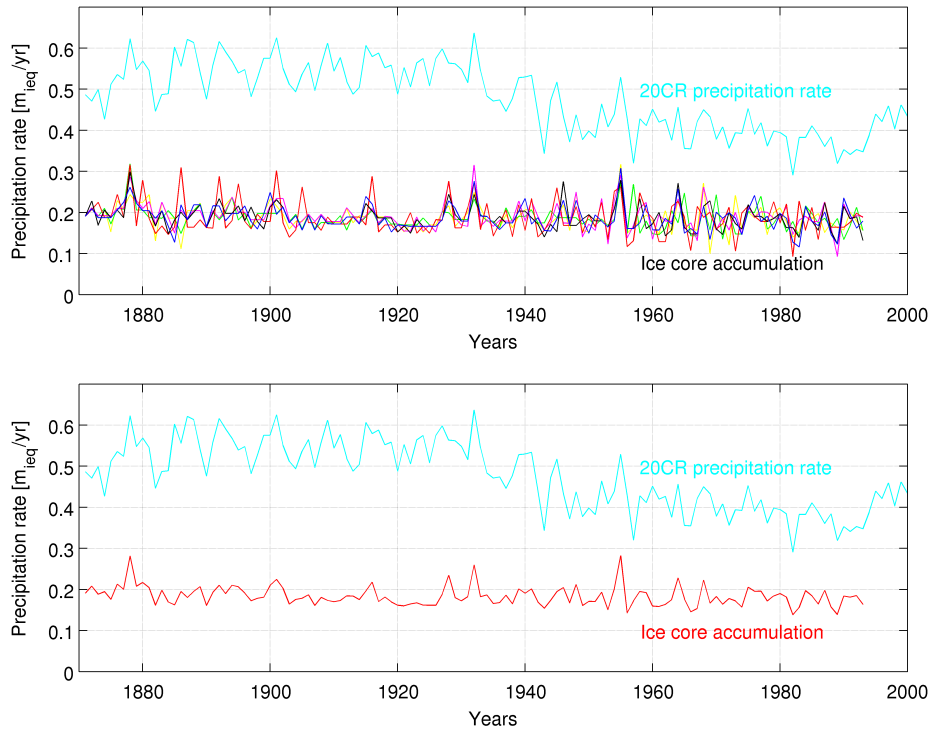


Figure A.10: Top: The precipitation from the 20CR (cyan) and the accumulation data from the shallow cores at NGRIP (multi-coloured lines). Bottom: Same as above but the stacked accumulation data from the shallow cores at NGRIP (red) is seen instead.

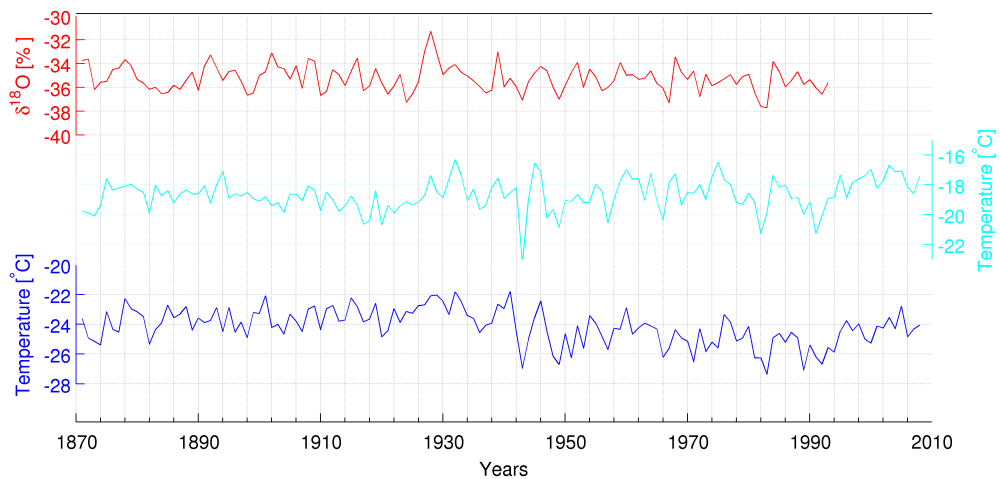


Figure A.11: Precipitation-weighted temperature profile (T_{pw} - green) and ordinary temperature profile (T - blue) from 20CR extracted at NGRIP, January annual mean, along with the stacked $\delta^{18}O$ profile (red). A significant one-tailed correlation of 0.4054 between $\delta^{18}O$ and T_{pw} is obtained.

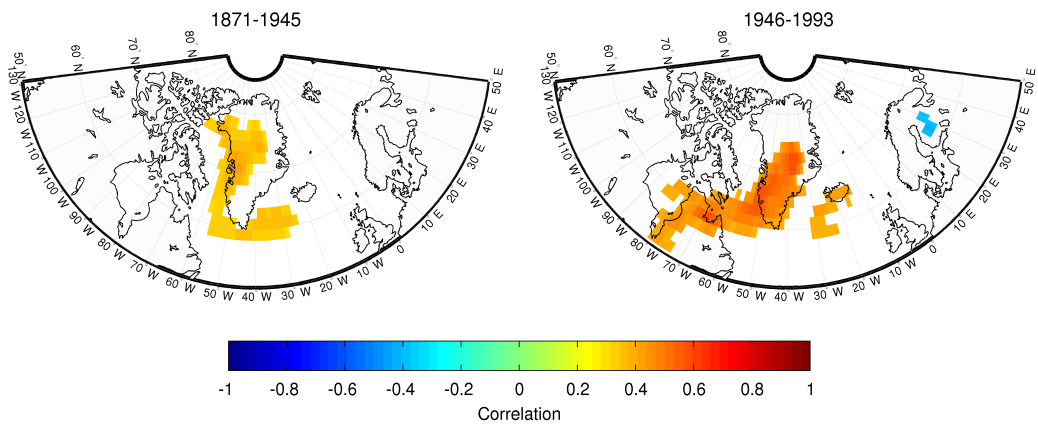


Figure A.12: Correlation maps of precipitation-weighted temperature from 20CR and mean isotope profiles from the ice cores. January annual mean, period 1 (left) and period 2 (right).